THE UNIVERSITY OF CHICAGO

BRWD1 ESTABLISHES EPIGENETIC STATES FOR GERMINAL CENTER INITIATION, MAINTENANCE, AND FUNCTION

A DISSERTATION SUBMITTED TO
THE FACULTY OF THE DIVISION OF THE BIOLOGICAL SCIENCES
AND THE PRITZKER SCHOOL OF MEDICINE
IN CANDIDACY FOR THE DEGREE OF
DOCTOR OF PHILOSOPHY

INTERDISCIPLINARY SCIENTIST TRAINING PROGRAM: IMMUNOLOGY

BY
NATHANIEL EDWIN WRIGHT

CHICAGO, ILLINOIS
AUGUST 2024

To my parents, who taught me to love learning

&

To Christine, who has been there for the good and bad times

TABLE OF CONTENTS

LIST OF FIGURES

LIST OF TABLES

LIST OF ABBREVIATIONS

AID activation-induced deaminase

ASCs antibody-secreting cells

ATAC-seq assay for transposase-accessible chromatin and sequencing

BCR B cell receptor

BRWD1 BROMO domain and WD repeat containing protein 1

ChIP-seq chromatin immunoprecipitation with sequencing

CSR class switch recombination

DZd dark zone differentiation

DZp dark zone proliferation

FDCs follicular dendritic cells

Fol follicular

GC germinal center

GSEA gene set enrichment analysis

Hi-C high-throughput sequencing and chromatin conformation capture

HOMER hypergeometric optimization of motif enrichment

LCMV lymphocytic choriomeningitis virus

LZ light zone

MFI median fluorescence intensity

MZ	marginal zone
PCA	principal component analysis
RNA-seq	RNA sequencing
SHM	somatic hypermutation
SRBCs	sheep red blood cells
TBMs	tingible body macrophages
tdT	tdTomato
TF	transcription factor
Tfh	T follicular helper
TUNEL	terminal deoxynucleotidyl transferase dUTP nick end labeling

ACKNOWLEDGMENTS

So many have supported me throughout my academic journey at the University of Chicago. Foremost, I thank my mentor, Dr. Marcus Clark, whose unwavering encouragement and excitement kept me going throughout this journey. He has always prioritized both my project and growth as a scientist, and he always finds time to help me when I need it most.

I would also like to thank the members of the Clark lab who have all contributed to my growth as a scientist. All of you make science fun! Dr. Malay Mandal believes every experiment I do will succeed, and always knows what experiment or analysis to do next. Margaret Veselits has been so reliable and generous to me in sharing her lab experience and continually working to keep our lab running. No experiments could be done without her. Dr. Junting Ai has been so generous with her microscopy expertise and patient with me as I was learning. Dr. Domenick Kennedy began this project and his preliminary data gave me the first pieces to know this would be a fun and interesting story to uncover. Mary Attaway rotated in the lab and worked tirelessly on the class switch recombination experiments. Dr. Madeleine Durkee and Dr. Deepjyoti Ghosh were essential in analyzing microscopy images. I am thankful for my fellow trainees past and present in the Clark lab who are very fun and continually support me: Dr. Young me Yoon, Dr. Gabriel Casella, Greer Gurewitz, Thao Cao, Jacob Veselits, Sarah Kim, and Dr. Jenna Guthmiller. Lastly, thank you to the BSLC third floor staff who are essential to our work: Angela Hayes, Greg Washington, and Gloria Davis.

I am thankful for Dr. Sandeep Gurbuxani, who helped with the analysis of H&E slides. Thank you to Eirinaios Gkika and Dr. Tatyana Golovkina who helped me with the LCMV infections and plaque assays.

I was fortunate to have great scientists on my thesis committee: Dr. Barbara Kee, Dr. Fotini Gounari, and Dr. Mark Maienschein-Cline. I am thankful for how they have contributed their time and expertise to guide me, and their belief in me keeps me going. Dr.

Mark Maienschein-Cline has been extremely generous in answering my computational questions, and the many workshops I took from him provided foundational training to complete this project.

I am thankful for the Medical Scientist Training Program for fostering an incredible learning environment. Thank you to the current and past deans, Dr. Alison Anastasio and Dr. Kristin McCann, as well as the many MSTP staff, who work so hard to make the MSTP an elite training environment. I also thank the Committee on Immunology and the many faculty I am fortunate to have learned from. They have made me a more critical scientist and a well-rounded immunologist.

Thank you to the following University of Chicago core facilities, which provided valuable training and equipment: the Animal Resources Center, the Cytometry and Antibody Technology Core Facility, the Genomics Facility, the Integrated Light Microscopy Core, the Human Immunologic Monitoring Core, the DNA Sequencing and Genotyping Facility, and the Human Tissue Resource Center.

This work was supported by National Institutes of Health grants T32 GM007281, F30 AI174324, R01 AI143778, and R01 AI150860.

I am thankful for my former mentors, Dr. Kristen Page at Wheaton College and Dr. Mark Connors at the National Institutes of Health. Their training was foundational to my growth and success during my graduate training.

So many communities have sustained me during the past five years: my MSTP cohort, Arpit, Brendan, Denis, Hagerah, Gabriel, Kyle, Mayuri, Sophie, and Tanner; my Greenwood roommates, David, Micah, AJ, Sam, Matthew, and Gabe; my New Community Church family; my Graduate Christian Fellowship friends; my T3 friends, my in-laws Jim, Lori, Caroline, Daniel, and Mary; and many more. I treasure our relationships, which make me who I am.

To my parents, Mark and Deborah, thank you for always loving and supporting me. So

much of how I think and learn is because of your parenting. Thank you for all the immunology you have studied to understand my project and for caring about every experiment and abstract submission.

To my wife, Christine, thank you for everything. You bring such joy to my life. You have been there for every celebration and challenge of graduate school. I owe this PhD to you.

Lastly, as a Christian, I thank my Creator for sustaining me throughout my training and for the beautiful biology I have been able to witness by studying BRWD1.

ABSTRACT

Germinal center (GC) B cells segregate into three subsets that compartmentalize the antagonistic molecular programs of selection, proliferation, and somatic hypermutation. In bone marrow, the epigenetic reader BRWD1 orchestrates and insulates the sequential stages of cell proliferation and *Igk* recombination. We hypothesized that BRWD1 might play similar insulative roles in the periphery. In *Brwd1*$^{-/-}$ follicular B cells, GC initiation and class switch recombination following immunization were inhibited. In contrast, in *Brwd1*$^{-/-}$ GC B cells there was admixing of chromatin accessibility across GC subsets and transcriptional dysregulation including induction of inflammatory pathways. This global molecular GC dysregulation was associated with specific defects in proliferation, affinity maturation, and tolerance. These data suggest that GC subset identity is required for some but not all GC-attributed functions. Furthermore, these data demonstrate a central role for BRWD1 in orchestrating epigenetic transitions at multiple steps along B cell developmental and activation pathways.

CHAPTER 1

INTRODUCTION

1.1 Proliferation and somatic mutation throughout the life of a B cell

Throughout[1] their lineage, mammalian B cells must balance their proliferation with the severe genomic stress associated with V(D)J recombination and somatic hypermutation (SHM). During B cell lymphopoiesis, B cell progenitors undergo sequential rearrangement of the locus encoding the immunoglobulin (*Ig*) heavy-chain (*Igh*), followed by rearrangement of the locus encoding the immunoglobulin light-chain (*Igk* followed by *Igl* if necessary) (Clark et al., 2014). Stages of proliferation proceed each rearrangement. These transitions are highly ordered, and each stage of proliferation or mutation is mutually exclusive (Clark et al., 2014). Similarly, germinal center (GC) B cells in peripheral lymphoid organs alternate between proliferation and SHM to drive adaptive humoral immunity (Figure 1.1) (Kennedy and Clark, 2021). Moreover, strict separation between proliferation and somatic mutation is necessary for proper B cell differentiation and to prevent oncogenesis (Zhang et al., 2011; Gostissa et al., 2013). The risk for off-target mutation is high. Indeed, whole-genome sequencing of memory B cells from healthy human controls has revealed that memory B cells experience 18 off-target mutations for every on-target *Ig* gene mutation during GC differentiation, and these mutation profiles mirror the mutation profiles of many B cell cancers (Machado et al., 2022). Indeed, the danger of mutation within the GC is exemplified by the many GC-derived cancers observed in humans, including diffuse large B cell lymphoma, follicular lymphoma, and Burkitt's lymphoma (Holmes et al., 2020; Milpied et al., 2018).

Recent mouse studies (unless otherwise noted) have described new mechanisms for how

1. Much of this chapter, including figures, is reproduced from Wright NE, Mandal M, and Clark MR. Molecular mechanisms insulating proliferation from genotoxic stress in B lymphocytes. *Trends in Immunology*, 44 (9):668-677, 2023.

B cell progenitors and GC B cells insulate proliferation from somatic mutation by cytokine signaling, by reordering epigenetic landscapes, and by regulating chromatin topology. In this dissertation, we propose a model in which GC B cells cycle between three unique populations and that the epigenetic reader BRWD1 maintains these distinct molecular programs to separate proliferation from selection and SHM. In this introduction, we propose a unified model for B cell development and the GC in which the molecular constraints operating during transitions between cell states within the bone marrow and GC are similar, as are the solutions.

1.2 A three-zone model of the GC

The molecular logic that proliferation and somatic mutation must be separated dictates GC organization. Traditionally, the GC has been subdivided into two zones. In the light zone (LZ), $CD83^+$ B cells undergo selection, whereas in the dark zone (DZ), $CXCR4^+$ B cells undergo proliferation and SHM (Victora and Nussenzweig, 2022). In the LZ, B cells capture antigens from follicular dendritic cells (FDCs) and present these antigens to cognate T follicular helper (Tfh) cells to receive help signals via CD40, IL-21, and IL-4 (Liu et al., 2015; Zotos et al., 2021; Duan et al., 2021). Signaling through the B cell receptor (BCR) following antigen binding, as well as reception of these selective help signals, induces B cells to express *Myc* and *Cxcr4* and to become primed for proliferation within the DZ (Long et al., 2022; Chen et al., 2023; Calado et al., 2012; Dominguez-Sola et al., 2012). This cyclical process between LZ and DZ drives affinity maturation.

A recent study demonstrated that this two-zone model obscures underlying transcriptional and chromatin accessibility differences within the DZ (Kennedy et al., 2020). Because the expression of CD83 and CXCR4 follows a gradient between the canonical LZ and DZ, the authors flow-sorted three GC B cell populations: $CD83^+CXCR4^-$ LZ cells, $CD83^+CXCR4^+$ dark zone proliferation (DZp) cells, and $CD83^-CXCR4^+$ dark zone differentiation (DZd)

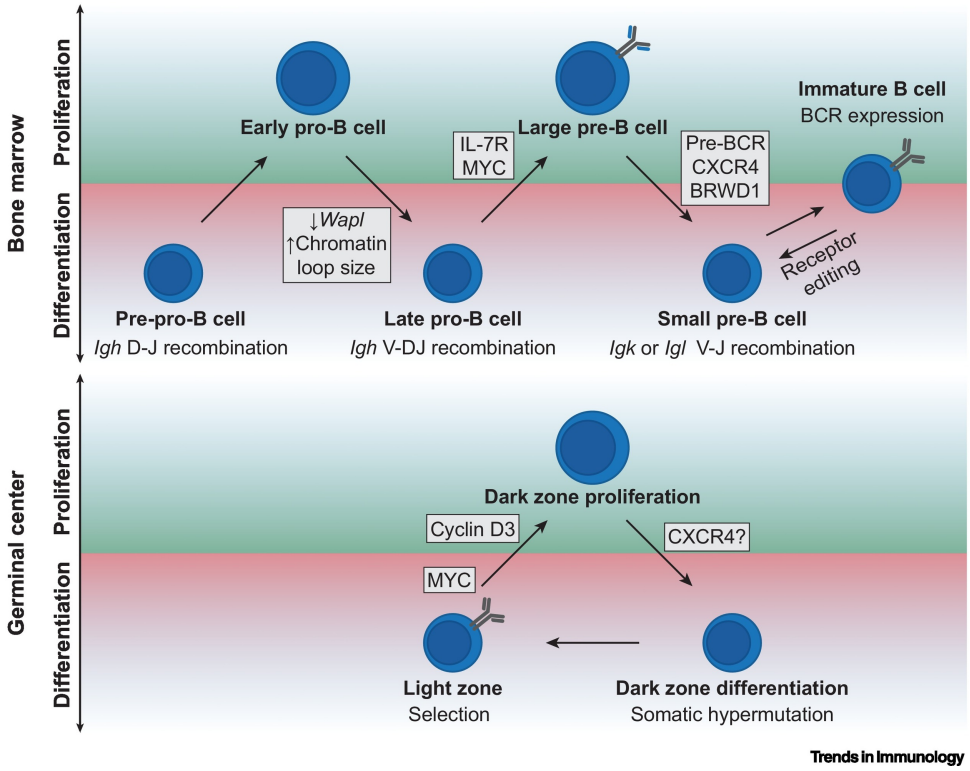

Figure 1.1: Model of mutually exclusive states of B cell proliferation and differentiation in B cell development and in germinal centers in mice. B cell progenitors undergo sequential stages of either proliferation or differentiation, which involve different stages of V(D)J recombination. The transition from proliferating early pro-B cells to late pro-B cells undergoing V to D-J recombination involves a decrease in *Wapl* expression, which causes an increase in chromatin loop size genome-wide (Hill et al., 2020). Proliferating large pre-B cells reside within an IL-7 cytokine niche in the bone marrow, and IL-7 receptor signaling with MYC drives proliferation (Johnson et al., 2005). The transition to small pre-B cells involves pre-B cell receptor (BCR) signaling followed by CXCR4 signaling within a CXCL12 cytokine niche (Mandal et al., 2019). At the small pre-B cell stage, BRWD1 mediates genome-wide changes in chromatin accessibility and opens the *Igk* locus for DNA recombination (Mandal et al., 2018, 2015). Self-reactive immature B cells undergo receptor editing and reverse development to repeat light-chain recombination (Okoreeh et al., 2022). We propose that, within the GC, B cells cycle between three major populations – the light zone (LZ) for selection, the dark zone proliferation (DZp), and the dark zone differentiation (DZd) for somatic hypermutation (Kennedy et al., 2020). Proliferation is first initiated by MYC and is then dependent on cyclin D3 within the DZp (Pae et al., 2020; Finkin et al., 2019; Ramezani-Rad et al., 2020). We hypothesize that CXCR4 signaling mediates the transition between the DZp and DZd (Kennedy et al., 2020). Abbreviations: *Igh*, immunoglobulin heavy-chain; *Igk*, immunoglobulin kappa light-chain; *Igl*, immunoglobulin lambda light-chain.

cells. This three-zone model revealed >10,000 differentially expressed genes by RNA sequencing (RNA-seq) and >51,000 differentially regulated chromatin accessibility peaks by assay for transposase-accessible chromatin and sequencing (ATAC-seq), demonstrating that this strategy captures major molecular differences between three major GC populations (Kennedy et al., 2020). Moreover, transcriptional, proteomic, and flow cytometry analyses revealed that DZp B cells are the main proliferating cell population and are characterized by cyclin B1 expression, whereas DZd B cells are the likely population in which SHM occurs (Kennedy et al., 2020). These two zones are spatially separated because DZp B cells locate next to tingible body macrophages (TBMs) (Kennedy et al., 2020).

Several recent studies performed single-cell (sc)RNA-seq on GC B cells following immunization with model antigens or sheep red blood cells, or following infection with influenza virus or lymphocytic choriomeningitis virus (LCMV) (Duan et al., 2021; Chen et al., 2023; Kennedy et al., 2020; Carvalho et al., 2023; Laidlaw et al., 2020; Mathew et al., 2021; Chen et al., 2021; Pae et al., 2020). Cellular clusters from many of these analyses were largely determined by their cell-cycle stage (S, G2, or M) based on the high expression of genes necessary for DNA replication, chromatin segregation, or cell division (Carvalho et al., 2023; Chen et al., 2021). We hypothesize that some of these clusters may represent subdivisions of the DZp population. Subcellular spatial transcriptomics might reveal whether these cell clusters, defined by scRNA-seq to be in the G2 or M phases of the cell-cycle, are located next to TBMs, as has been shown for the cyclin $B1^+$ DZp B cell population (Kennedy et al., 2020). This would provide additional support for the rationale that proliferation within the GC is spatially separated and proximal to TBMs. Moreover, these scRNA-seq experiments also defined subclusters within the GC, such as positively selected Myc^+ B cells, which may represent a transitional population between the LZ and DZp (Carvalho et al., 2023; Chen et al., 2021). scRNA-seq analyses also characterized pre-memory B cell and pre-plasmablast clusters, which would represent B cells beginning to differentiate into memory B cells and

plasma cells and that subsequently leave the GC (Carvalho et al., 2023). Together, these additional populations identified by scRNA-seq mostly represent transitional populations in the three-zone GC model. Indeed, similar proliferative and transitional cell clusters were also found by scRNA-seq of human tonsillar GCs from pediatric tonsillectomies and in splenic GCs from deceased organ donors, suggesting that the GC subpopulations described in the preceding text are conserved between mice and humans (Holmes et al., 2020; Milpied et al., 2018; King et al., 2021). Finally, clusters identified by scRNA-seq did not neatly separate from one another upon analysis, suggesting that GC B cells are quickly and continually transitioning between transcriptional states that blur together when using scRNA-seq (Holmes et al., 2020; Milpied et al., 2018). By contrast, fractionation into the three distinct GC subsets provides detailed snapshots of major GC cell states.

In addition, these single-cell analyses identified molecular programs that are unique to DZp B cells. Notably, 40% of GC B cells represented proliferating clusters intermediate between canonical LZ and DZ populations, as evidenced by high expression of cell-cycle genes, indicating that proliferation is a major molecular state within the GC (Holmes et al., 2020). Single-cell analyses also revealed that oxidative phosphorylation might be utilized in DZp B cells at the G2/M stage of the cell-cycle to meet the metabolic demands of rapid proliferation (Chen et al., 2021). By contrast, LZ B cells that were recently positively selected for cyclic reentry, and were in the G1 to S phase, primarily use glycolysis for metabolism (Chen et al., 2021). Thus, DZp and LZ B cells have fundamentally different metabolic programs. Furthermore, *Myc* expression, which is determined by the quality of T cell help, primes LZ cells for subsequent proliferation in the DZp region (Calado et al., 2012; Dominguez-Sola et al., 2012; Finkin et al., 2019). Indeed, the degree of *Myc* expression in the LZ is proportional to the subsequent amount of proliferation within the DZp (Finkin et al., 2019). However, the additional proliferative cycles in the DZ depend on cyclin D3, which is expressed once GC B cells have decreased MYC and BCR signaling (Pae et al., 2020; Ramezani-Rad et al., 2020).

Together, these results suggest that the DZp represents a significant and unique GC B cell population within the DZ that requires large shifts in molecular programs as cells transit from the LZ. We posit that insulating proliferative DZp B cells via a unique metabolic and molecular program is essential for GC biology.

We propose that the three-zone model captures three major B cell populations within the GC (Figure 1.2). This model carries an additional benefit of allowing researchers to sort large quantities of specific cells for mechanistic experiments (Kennedy et al., 2020). Indeed, technologies that can currently only be applied to bulk-sorted populations [chromatin immunoprecipitation with sequencing (ChIP-seq), high-throughput sequencing and chromatin conformation capture (Hi-C), and mass spectrometry] and technologies where bulk-sorted populations allow greater sensitivity and depth of sequencing (RNA-seq and ATAC-seq) might be used to better understand the molecular mechanisms and dynamics that insulate proliferation from selection and mutation within the GC.

1.3 Somatic hypermutation within the dark zone differentiation

Many features are consistent with somatic hypermutation (SHM) occurring in the dark zone differentiation (DZd) following proliferation within the dark zone proliferation (DZp); however, it has not been formally tested whether SHM exclusively occurs within the DZd. Relative to LZ and DZp B cells, DZd B cells have increased *Ig* expression, which would be important for SHM. The DNA repair machinery is also necessary for SHM. A phosphoproteome analysis with mass spectrometry (MS) was used to identify active proteins in the three-zone model and found that DZd B cells upregulate the DNA damage response relative to LZ and DZp B cells (Kennedy et al., 2020). Furthermore, MS proteome analysis found increased TP53, PTEN, and RB1 in the DZd, which are tumor suppressors that repress the cell-cycle and become active in response to DNA damage.

Greater evidence for SHM within the DZd will require a better understanding of how

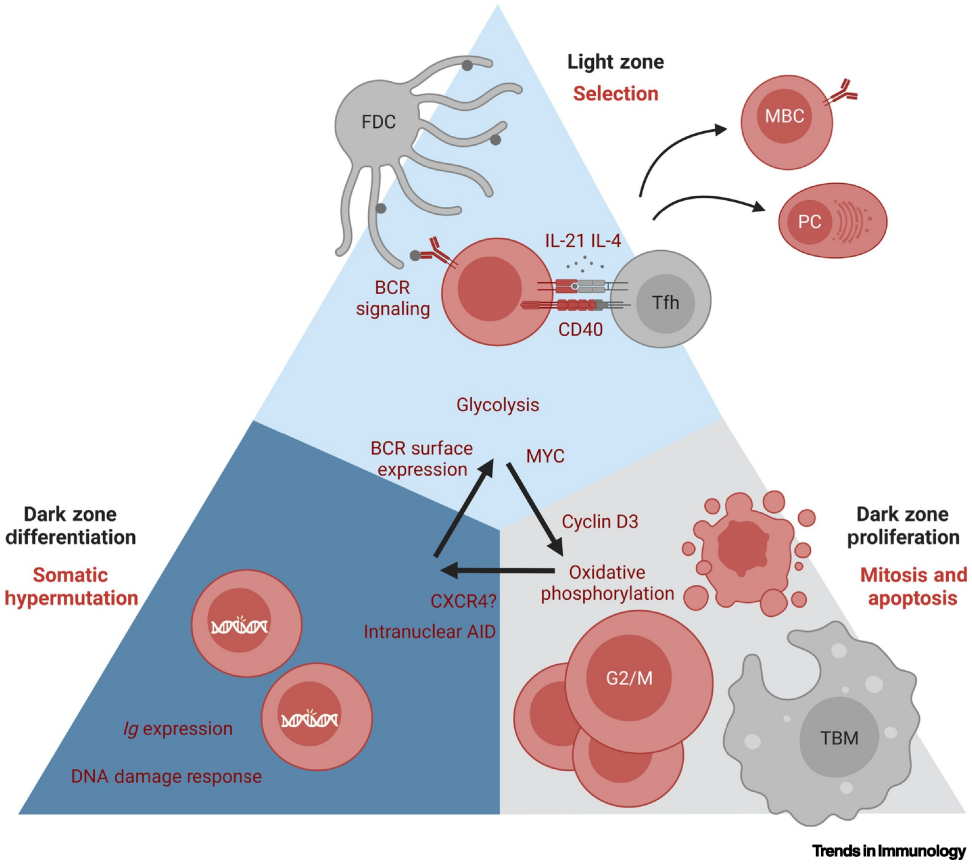

Figure 1.2: Three-zone model of the germinal center. Germinal center (GC) B cells (red) cycle between three different zones with unique functions, locations, transcriptional profiles, and chromatin accessibility states (Kennedy et al., 2020). In the light zone (LZ), $CD83^{+}$ GC B cells pick up antigen on follicular dendritic cells (FDCs) and present this antigen to T follicular helper (Tfh) cells. Tfh cells provide help signals through CD40, IL-21, and IL-4 (Liu et al., 2015; Zotos et al., 2021; Duan et al., 2021). The degree of B cell receptor (BCR) signaling and Tfh help signals determines whether GC B cells cycle through the GC reaction or exit as memory B cells (MBCs) or plasma cells (PCs) (Long et al., 2022; Chen et al., 2023). In the dark zone proliferation (DZp), $CD83^{+}CXCR4^{+}$ GC B cells undergo proliferation or apoptosis, which occur next to tingible body macrophages (TBMs), likely providing a checkpoint to remove apoptotic cells before initiating cell division (Kennedy et al., 2020; Gurwicz et al., 2023; Grootveld et al., 2023). Proliferation is primed by *Myc* expression in the LZ, whereas proliferation is driven by cyclin D3 in the DZp (Calado et al., 2012; Dominguez-Sola et al., 2012; Pae et al., 2020; Finkin et al., 2019; Ramezani-Rad et al., 2020). Metabolically, B cells in the LZ use glycolysis whereas B cells in the DZp use oxidative phosphorylation (Chen et al., 2021). GC B cells within the DZp are larger and can be distinguished by cyclin B1 expression (Kennedy et al., 2020). In the DZ differentiation (DZd), $CXCR4^{+}$ GC B cells undergo somatic hypermutation as measured by increased immunoglobulin gene expression and an elevated DNA damage response (Kennedy et al., 2020). This figure was created using BioRender.com.

activation-induced deaminase (AID) is regulated within the GC. AID, which binds to the *Ig* locus to perform SHM, is localized to the cytoplasm of resting cells (Wang et al., 2017). Following mitosis and breakdown of the nuclear envelope, AID gains access to chromatin (Wang et al., 2017). Subsequent transcription of the *Ig* gene during G1 phase allows AID to mutate DNA before it is exported from the nucleus later in G1 phase (Wang et al., 2017). These mechanisms restrict AID activity and SHM to a brief window following mitosis within the early G1 phase of the cell cycle (Wang et al., 2017; Sharbeen et al., 2012). Thus, SHM in the DZd is consistent with the DZd following mitosis in the DZp. To test whether DZd B cells exclusively perform SHM, we hypothesize that, among GC B cells, only DZd B cells may have DNA-bound AID as well as active *Ig* gene transcription.

1.4 Signaling mechanisms separating proliferation and genotoxic stress

Much is known regarding the signaling mechanisms that separate proliferation from genotoxic stress in B cell lymphopoiesis (McLean and Mandal, 2020). Cytokines and chemokines play decisive, instructional roles. During the pro- and large pre-B cell developmental stages, B cell progenitors reside within IL-7-rich niches where the cells grow and proliferate (Johnson et al., 2005; Mandal et al., 2011, 2009). Upon pre-BCR expression, large pre-B cells undergo a burst of proliferation (McLean and Mandal, 2020). Thus, previous models posited that the pre-BCR in large pre-B cells first synergized with the IL-7 receptor to drive proliferation, and then later instructed cell-cycle exit and *Ig* light-chain recombination (Herzog et al., 2009). This model required that one receptor, the pre-BCR, mediates two incompatible molecular programs at different times. This conundrum was solved by the demonstration that the pre-BCR feeds forward to induce CXCR4, which was demonstrated using *in vitro* cultures of pre-B cells with and without IL-7 and CXCL12 (the ligand for CXCR4), as well as by using the Cre–lox system to delete *Cxcr4* in $Mb1^{\mathrm{cre/wt}}Cxcr4^{\mathrm{fl/fl}}$ mice (Mandal et al.,

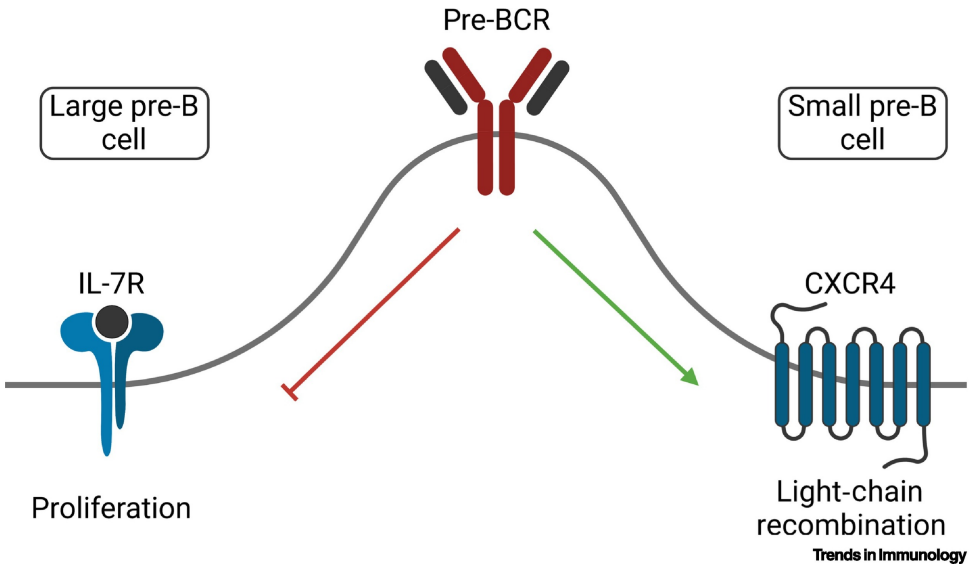

Figure 1.3: The mouse pre-B cell receptor (pre-BCR) mediates the transition between proliferation and light-chain recombination. During B lymphopoiesis, signaling through the IL-7 receptor (IL-7R) drives proliferation and represses immunoglobulin light-chain recombination (Johnson et al., 2005; Mandal et al., 2011). The pre-BCR functions through feedback and feedforward loops to escape IL-7R signaling and initiate signaling through CXCR4, which drives immunoglobulin light-chain recombination and enforces cell-cycle exit in small pre-B cells (Mandal et al., 2019; Okoreeh et al., 2022). This figure was created using BioRender.com.

2019). CXCR4 not only allowed migration out of IL-7-rich niches, and therefore escape from proliferation signals, but it also directly enforced cell-cycle exit and drove both *Igk* and *Igl* recombination (Mandal et al., 2019; Okoreeh et al., 2022). It is now clear that, by initiating essential feedforward and feedback signaling loops, the pre-BCR governs the transition between the stable and exclusive states of proliferation driven by the IL-7 receptor, and light-chain recombination driven by CXCR4 (Figure 1.3) (Mandal et al., 2019; Lee et al., 2021).

Likewise, the niches in which GC cell subsets reside and the environmentally specific cues that they receive are pivotal for GC function. For example, as shown in $Cd21^{\mathrm{cre/wt}}Il4ra^{\mathrm{fl/fl}}$ mice, FDCs in the LZ establish a niche by sequestering IL-4, which acts as a help signal during Tfh-mediated positive selection (Duan et al., 2021). This decreased IL-4 availability in the LZ prevents bystander activation and restricts cyclic reentry to those LZ B cells

selected by Tfh cells (Duan et al., 2021).

It is well established that CXCR4 also plays a key role in GCs because it is required for B cell migration from LZ to DZ (Bannard et al., 2013). However, it is unknown whether CXCR4 provides direct instructional signals in the GC as it does in bone marrow (Mandal et al., 2019). Given its function in the bone marrow, we suggest that CXCR4 might have a similar function during the transition between the DZp and DZd cell states. Although having a potentially instructive role, it is unlikely to mediate movement between the DZp and DZd regions because its ligand, CXCL12, is expressed by reticular cells throughout the DZ, and there is probably no CXCL12 gradient between the DZp and DZd (Pikor et al., 2020). Thus, we posit that an additional unknown factor mediates migration between the DZp and DZd, whereas CXCR4 signaling is necessary for transitioning between the different molecular programs.

Mitosis within the GC is also niche-specific and occurs next to TBMs (Kennedy et al., 2020). Intravital live imaging of the lymph nodes of CX3CR1^{GFP} transgenic mice demonstrated that GCs contain an average of 25 TBMs and that TBMs are stationary within the GC (Gurwicz et al., 2023). Moreover, immunofluorescence microscopy revealed that cyclin B1^{+} DZp cells proliferate in clusters next to TBMs residing primarily within the DZ (Kennedy et al., 2020). Apoptosis within the GC also occurs next to TBMs. Indeed, apoptosis is a major event within the GC, and around one half of GC B cells die every 6 h for the duration of the GC reaction (Mayer et al., 2017; Stewart et al., 2018). In the experiment described in the preceding text, early B cell apoptosis occurred away from TBMs, as measured by caspase-3 activity via immunofluorescence microscopy (Gurwicz et al., 2023). However, later stages of apoptosis measured by terminal deoxynucleotidyl transferase dUTP nick end labeling (TUNEL) occurred entirely next to or within TBMs (Kennedy et al., 2020; Gurwicz et al., 2023; Grootveld et al., 2023). These findings suggest that the spatial coordination of apoptosis and mitosis occurs next to TBMs. The data also point toward the existence

of a major checkpoint whereby apoptotic cells are removed before attempting cell division, presumably preventing mitotic catastrophe and necrosis (Kennedy et al., 2020). By contrast, G1/S phases occurred throughout the GC based on bromodeoxyuridine (BrdU)–ethynyl-2'-deoxyuridine (EdU) dual pulse labeling experiments, indicating that only the G2/M phase is specifically located next to TBMs (Kennedy et al., 2020). Furthermore, the migration of apoptotic cells toward TBMs might suggest that they either receive instructive signals or are primed to migrate toward TBMs and begin apoptosis.

As described, the locations of proliferation and apoptosis appear to be restricted to TBMs. This is relevant because it is probably important for preventing autoimmunity. For instance, patients with systemic lupus erythematosus have fewer TBMs and increased apoptotic cells within GCs relative to non-lupus controls, as measured by TUNEL staining (Baumann et al., 2002). Accordingly, mice lacking the intracellular signaling domain of the phagocytic receptor MERTK failed to clear apoptotic cells and developed lupus-like autoimmunity (Cohen et al., 2002; Scott et al., 2001). We hypothesize that the location of proliferating B cells next to TBMs is also necessary for the clearance of cells that experience oncogenic mutations during proliferation.

1.5 Epigenetic chromatin regulation

The transition between proliferative large pre-B cells and recombining small pre-B cells is accompanied by dramatic changes in the epigenetic landscape and transcriptional program (Mandal et al., 2018). Moreover, comparably large shifts in epigenetic and transcriptional programs occur during GC subset transitions, as demonstrated by RNA-seq and ATAC-seq using the three-zone model (Kennedy et al., 2020). In both cases, chromatin accessibility is regulated at many transcription factor (TF) binding sites, suggesting that a single TF or even a program of TFs is unlikely to mediate this dramatic reordering of the genomic landscape. Instead, it is becoming increasingly clear that this wholesale rewiring of lymphocyte programs

is epigenetically mediated.

The large to small pre-B cell transition is mediated by the epigenetic reader and scaffolding molecule BRWD1 (Mandal et al., 2018, 2015). BRWD1 coordinately represses early developmental enhancers, including those that induce proliferation, and opens enhancers required for light-chain recombination (Mandal et al., 2018). Indeed, this single molecule differentially regulates >7000 genes (Mandal et al., 2018). That BRWD1 functions over a megabase scale to regulate promoter and enhancer accessibility suggests that BRWD1 might regulate cohesin activity and chromatin loop extrusion, a mechanism that could help to explain this long-distance regulation. BRWD1 is also highly and differentially expressed in GC B cell subsets, suggesting that it may be important for regulating chromatin accessibility within the three-zone model (Kennedy et al., 2020). Therefore, we postulate that BRWD1 plays a similar role in GC subset transitions.

Chromatin remodeling complexes that are necessary for B lymphopoiesis are also important in the GC. For instance, the Cre–lox system in mice has been used to robustly describe how several histone-modifying enzymes, including EZH2, KMT2D, LSD1, and CREBBP, are important for maintaining the GC response, and many of these enzymes are frequently mutated in human GC B cell-derived lymphomas (Béguelin et al., 2013; Caganova et al., 2013; Zhang et al., 2015; Béguelin et al., 2017; Ortega-Molina et al., 2015; Jiang et al., 2017; Zhang et al., 2017a; Hatzi et al., 2019). Indeed, loss of the H1C and H1E histones, using $H1c^{-/-}H1e^{-/-}$ mice, caused genome-wide decompaction of chromatin in GC B cells (Yusufova et al., 2021). Relative to wild-type (WT) mice, $H1c^{-/-}H1e^{-/-}$ mice displayed lymphoproliferative disease that invaded peripheral tissues, and $H1c^{-/-}H1e^{-/-}$ mice crossed with *VavP–Bcl2* transgenic mice had more aggressive lymphomagenesis and shorter survival times compared to mice with only the *VavP–Bcl2* transgene (Yusufova et al., 2021). These examples imply that chromatin regulation in GC B cells may be a primary mechanism to prevent oncogenesis.

Broadly, multiple TFs play parallel roles in both the bone marrow and GC. For example, BCL6 allows small pre-B cells and GC B cells to survive following DNA damage produced by light-chain recombination and SHM, respectively, as shown by *in vitro* analyses of mouse B cell progenitors and ChIP-seq of BCL6 in human tonsil GC B cells (Duy et al., 2010; Ci et al., 2009; Basso et al., 2010). Furthermore, proliferation in both large pre-B cells and DZp GC B cells depends on cyclin D3, as shown in *Ccnd3*$^{-/-}$ mice (Pae et al., 2020; Cooper et al., 2006). These observations suggest that there are conserved mechanisms to address the common molecular restraints whereby proliferation and genomic stress must be segregated into distinct cell states in both B cell development and within the GC.

1.6 BRWD1 coordinates cell-cycle exit and *Igk* recombination.

The epigenetic reader BROMO domain and WD repeat containing protein 1 (BRWD1) is necessary for the large to small pre-B cell transition. BRWD1 expression is highest in the murine B cell lineage, and expression is first turned on in small pre-B cells (Mandal et al., 2015). BRWD1 then binds to a specific epigenetic landscape defined by histone 3 serine 10 phosphorylation (H3S10p) and acetylation of histone 3 lysines 9 and 14 (H3K9acK14ac) (Mandal et al., 2015; Filippakopoulos et al., 2012; Dunn and Davie, 2005).

Although BRWD1 has BROMO and WD40 domains, it contains no known catalytic activity. Indeed, it has been shown to immunoprecipitate with the BAF complex (Fulton et al., 2022). However, the functions of BRWD1 are more complex, and it is likely part of a large, multimeric complex that orchestrates many functions that determine enhancer landscapes in small pre-B cells.

At the local scale, BRWD1 repositions nucleosomes relative to GAGA DNA motifs (Fig 1.4), suggesting a function similar to the GAGA factor (GAF) described in *Drosophila* which displaces nucleosomes bound to GAGA DNA motifs to form open chromatin regions (Mandal et al., 2015; Chetverina et al., 2021). During VJ recombination in the J region of

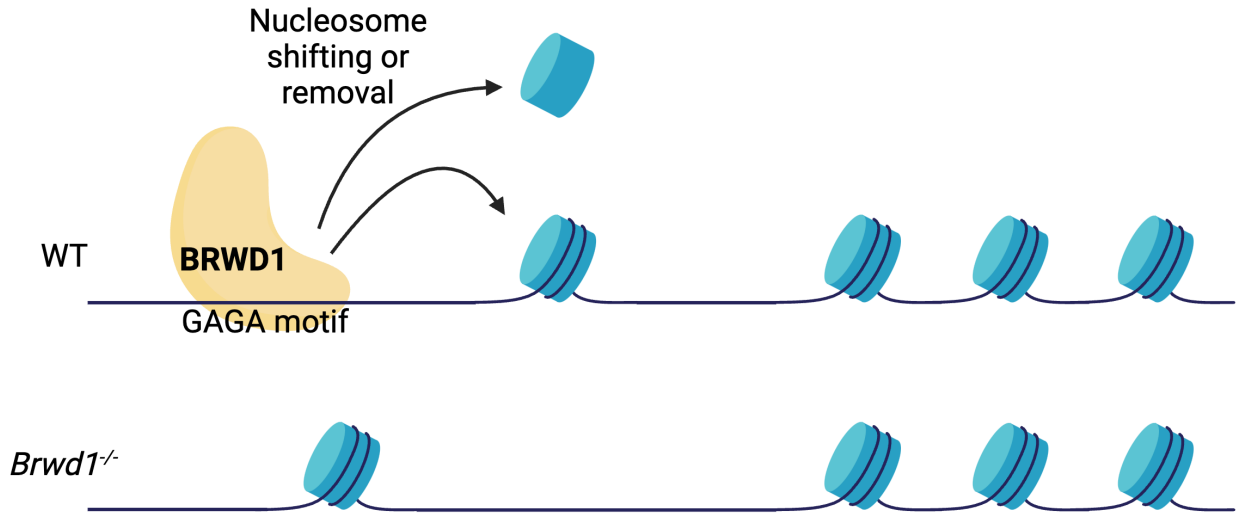

Figure 1.4: Model of BRWD1-mediated nucleosome repositioning. BRWD1 binds to chromatin at GA repeats and is associated with nucleosome depletion and increased chromatin accessibility at these sites (Mandal et al., 2015). BRWD1 may deplete nucleosomes by either shifting or removing nucleosomes. These BRWD1-mediated changes in nucleosome positioning are likely important for transcription factor binding. This figure was created using BioRender.com.

Igk, this nucleosome repositioning both exposes recombination signal sequences (RSSs) for recombination-activating 1 (RAG1) binding and positions a nucleosome 5′ to each RSS for RAG2 recruitment (Mandal et al., 2015).

BRWD1 also regulates accessibility at enhancers far removed from apparent BRWD1 binding (Mandal et al., 2018). In small pre-B cells, BRWD1 regulates chromatin accessibility and transcription up to 5 Mb away, and closes early developmental enhancers and opens late developmental enhancers for transcription factor (TF) binding in small pre-B cells (Mandal et al., 2018). BRWD1 binds throughout the *Myc* locus and silences enhancers to repress proliferation (Mandal et al., 2018). Recently, Mandal et al. (2024) demonstrated that BRWD1 converts static cohesin to dynamic cohesin to mediate these long range changes in chromatin accessibility (Fig 1.5). Thus, BRWD1 drives *Igk* recombination and represses proliferation, which are the pivotal molecular events during the transition between large and small pre-B cells (Clark et al., 2014). Finally, the importance of BRWD1 in B cell de-

velopment is clinically important because BRWD1 mutations are common in patients with idiopathic hypogammaglobulinemia (Mandal et al., 2018).

1.7 Cohesin and the regulation of chromatin topology

Ultimately, gene regulation requires the association of activated enhancer elements with promoters, whereas *Ig* gene recombination requires apposition of V gene segments onto distant recombination centers at J gene segments. The most likely mechanism for both is chromatin loop extrusion mediated by the multimeric, ring-shaped cohesin complex (Davidson et al., 2019; Vian et al., 2018; Kagey et al., 2010). It is well documented that the cofactor NIPBL drives chromatin loop extrusion, and the cofactor WAPL releases cohesin from chromatin to allow cohesin recycling (Bauer et al., 2021; Liu et al., 2021; Haarhuis et al., 2017).

Regulation of cohesin and cohesin cofactors is a major mechanism underlying the transitions between cell states in B cell lymphopoiesis. During early B cell development, pro-B cells complete *Ig* heavy-chain V to D-J recombination, and the contraction of this 2.4 Mb region is mediated by cohesin and loop extrusion (Zhang et al., 2022). For example, depletion of the cohesin component, RAD21, using a mini auxin-inducible degron (mAID) in a v-Abl-transformed pro-B cell line, was found to abrogate all V to D-J recombination (Ba et al., 2020). These experiments and others demonstrate that cohesin can mediate long-range locus contraction and recombination at the *Ig* heavy-chain locus (Ba et al., 2020; Zhang et al., 2019b; Dai et al., 2021). Pro-B cells perform this long-range contraction of the *Ig* heavy-chain gene by decreasing *Wapl* expression by fourfold relative to B cell-biased lymphoid progenitors (Dai et al., 2021; Hill et al., 2020). Of note, *Wapl* expression was inhibited by binding of PAX5 and the recruitment of polycomb repressive complex 2 (PRC2) to the *Wapl* promoter, demonstrating how TFs can regulate the factors that determine chromatin topology (Hill et al., 2020). This decrease in *Wapl* expression diminished cohesin unloading, extended the length of loop extrusion across the *Ig* heavy-chain locus, and increased the size

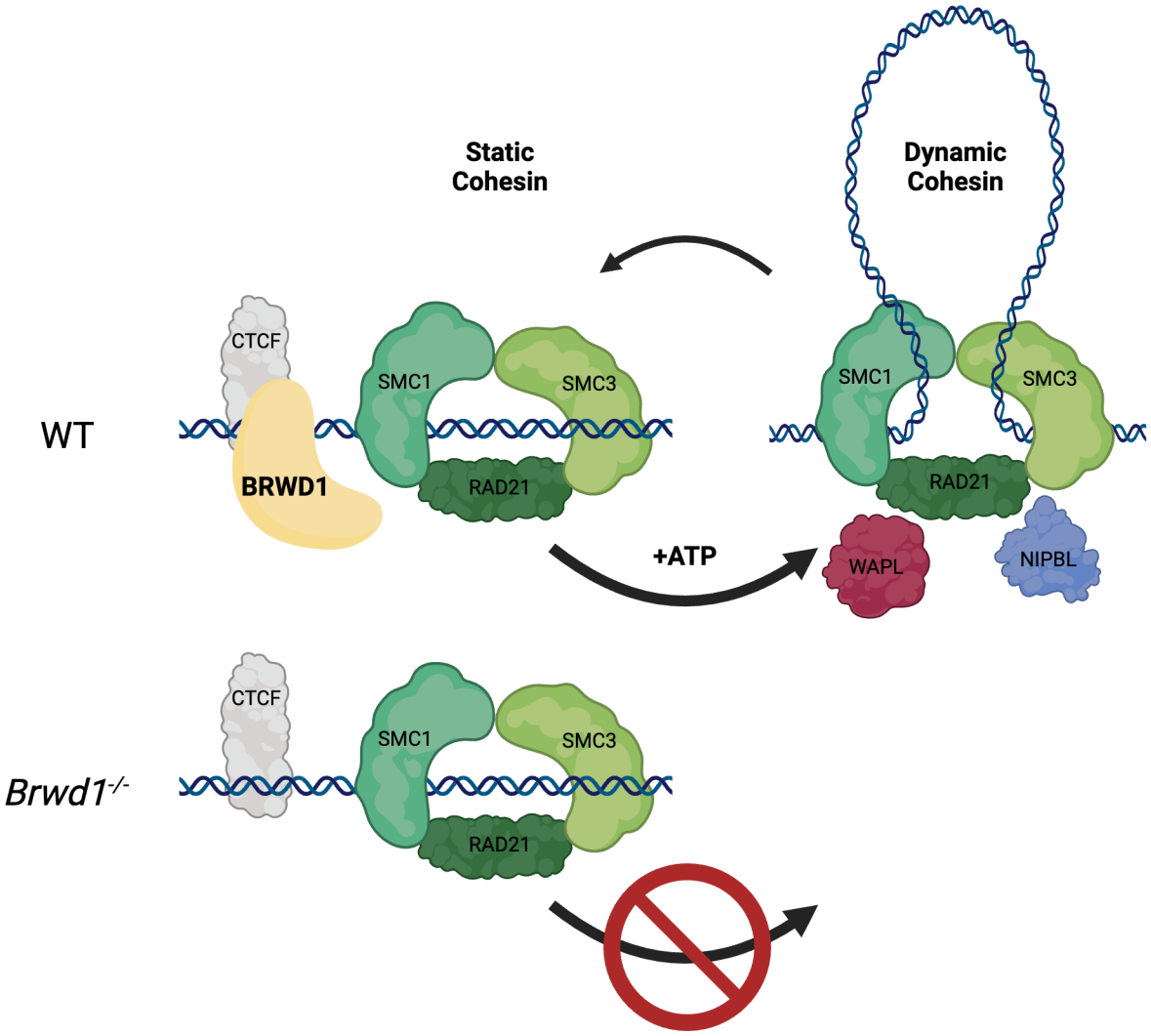

Figure 1.5: Model of BRWD1-mediated static to dynamic cohesin conversion. BRWD1 complexes at CTCF sites to convert chromatin-bound static cohesin to dynamic cohesin complexes competent for loop extrusion. The static cohesin complex includes SMC1, SMC3, and RAD21. Dynamic cohesin complexes include co-incident WAPL and NIPBL; however, the exact conformation of how the cohesin complex, NIPBL, and WAPL interact with one another is unknown. Conversion of static cohesin to dynamic cohesin requires ATP. This BRWD1-dependent mechanism mediates long-range chromatin looping and is important for enhancers to interact with promoters. This figure was created using BioRender.com and was previously published with modifications in Mandal et al. (2024).

of chromatin loops genome-wide, as measured by Hi-C of *ex vivo* WT pro-B cells compared to $Vav^{\mathrm{cre/wt}}Pax5^{\mathrm{fl/fl}}$ pro-B cells (Hill et al., 2020). Together, these experiments demonstrate that the regulation of cohesin and its cofactors represents a major mechanism controlling pro-B cell differentiation.

Transitions into and out of the GC require dynamic shifts in genomic architecture. During the transition from naïve B cells to GC B cells, 28% of chromatin compartments change, and 85 000 new chromatin interactions are established (Vilarrasa-Blasi et al., 2021; Bunting et al., 2016). Many of these chromatin interactions reverse when GC B cells further differentiate into memory B cells (Vilarrasa-Blasi et al., 2021). Furthermore, a recent study used $C\gamma 1^{\mathrm{cre/wt}}Smc3^{\mathrm{fl/wt}}$ mice to study haploinsufficiency for the cohesin subunit SMC3 in GC B cells (Rivas et al., 2021). GC B cells from these mice had decreased chromatin interactions within 50 kb relative to $C\gamma 1^{\mathrm{cre/wt}}$ mice, and much of the impaired looping occurred between enhancers and promoters (Rivas et al., 2021). Many of the affected genes were tumor-suppressor genes, resulting in increased proliferation and accelerated lymphomagenesis when crossed with mice constitutively expressing *Bcl6* (Rivas et al., 2021). This study further suggested that regulation of cohesin is a primary mechanism by which GC B cells adjust their epigenetic states.

GC B cells must cycle quickly between the epigenetically distinct GC zones, as revealed by ATAC-seq using the three-zone model (Kennedy et al., 2020). Because loop extrusion can rapidly alter chromatin 3D structure, we hypothesize that regulation of the cohesin complex and its cofactors might help to explain how epigenetic states quickly change within the GC. Furthermore, site-specific regulation of the loop extrusion machinery might allow different chromatin sites to be uniquely accessible within each GC zone. For example, it is likely important that the *Ig* locus is most accessible in the DZd during SHM, and that the *Myc* locus is most accessible in the LZ when cells are primed for positive selection to prevent lymphomagenesis (Finkin et al., 2019; Wang et al., 2017). Together, the aforementioned

discoveries support the concept that cohesin-mediated loop extrusion may be a primary mechanism that insulates the molecular programs between disparate cell states.

1.8 Concluding remarks and outstanding questions

Recent discoveries in B cell progenitors and GC B cells have provided new models for how cytokine signaling, epigenetic chromatin regulation, and loop extrusion regulate the segregation of proliferation from somatic mutation in B cells. In the bone marrow, a three-receptor model, and their orchestration of these complex molecular programs, provides a framework for understanding late B cell development. Similarly, a three-zone GC model segregates selection, proliferation, and SHM. However, we have incomplete knowledge of the signaling cues that order this GC architecture. In particular, we do not know how proliferation in the DZp transitions to SHM in the DZd. However, the three-zone paradigm can enable further investigations into these questions and, more broadly, reveal how complex molecular programs are integrated across the GC cycle. A precise molecular understanding of the GC will ultimately require a robust *in vitro* model. Furthermore, an *in vitro* GC system would greatly accelerate the development of novel therapeutics to enhance GC function or treat GC-derived lymphomas. However, expectations for what cardinal features this model must replicate will require further studies of GC biology in mice and humans.

Many outstanding questions remain:

Does CXCR4 signaling instruct cell-cycle exit and immunoglobulin accessibility when B cells transition between the DZp and the DZd? Recent discoveries have shown that mouse B cell progenitors use CXCR4 signaling to exit the cell-cycle and begin light-chain recombination. GC B cells must undergo a similar transition between proliferation and mutation, but the signaling mechanisms that guide this transition remain unknown.

What signals instruct proliferating and preapoptotic GC B cells to locate next to TBMs? The three-zone model shows that proliferating and apoptotic GC B cells are next to TBMs

in mice. The consequences of B cells completing mitosis or apoptosis away from TBMs are unknown.

Does AID activity and SHM occur exclusively in GC B cells within the DZd region? Features of SHM such as elevated immunoglobulin expression and an increased DNA damage response are observed in B cells in the DZd; however, it remains to be determined how AID is regulated within the GC three-zone model.

Are 3D chromatin conformations and the cohesin complex dynamically regulated between GC zones? GC B cells quickly cycle between zones with large differences in chromatin accessibility, and regulation of loop extrusion may contribute to this phenomenon. In addition, a recent study in mice showed that cohesin is important for chromatin looping between enhancers and promoters, and for preventing lymphomagenesis in GC B cells.

CHAPTER 2

MATERIALS AND METHODS

2.1 Mice

Brwd1-floxed mice were generated by Ingenious Targeting Laboratory. A targeting vector was designed containing a Lox71 site 5′ of *Brwd1* exon 6, a neomycin-resistance cassette flanked by flippase recognition target (FRT) sites between *Brwd1* exons 7 and 8, an inverse tdTomato (tdT) reporter with a bovine growth hormone polyadenylation sequence (BGHpA), and a Lox66 site 3′ of *Brwd1* exon 8. The Lox72 and Lox66 sites were in opposite orientation to one another. The targeting vector was introduced by electroporation to C57BL/6 embryonic stem cells containing flippase. Resulting cells were microinjected into Balb/c blastocysts. Resulting chimeras with a high percentage black coat color were mated to C57BL/6 WT mice to generate germline neomycin-resistance cassette-deleted mice. PCR and sequencing were used to confirm the deletion of the neomycin-resistance cassette, the presence of the tdTomato cassette, and the presence of the Lox66 site. PCR was used to confirm the absence of the flippase transgene and the presence of the Lox71 site.

Routine genotyping of the *Brwd1*-floxed mice was done with the LOX1 and SDL2 primers, which cover the 5′ Lox71 site (Table 2.1). PCR conditions were 94 °C for 2 min, then 35 cycles of 94 °C for 30 s, 60 °C for 30 s, and 72 °C for 1 min, followed by 72 °C for 2 min. The WT amplicon is 389 bp and the floxed amplicon is 431 bp.

Wild type C57BL/6J mice (stock #000664), $Mb1^{Cre}$ mice (stock #020505), $Aicda^{Cre}$ mice (stock #007770), and Ai14 Rosa-CAG-LSL-tdTomato-WPRE mice (stock #007914) were purchased from Jackson Laboratory. $Cd23^{Cre}$ mice were obtained from the laboratory of Jayanta Chaudhuri (Memorial Sloan Kettering). Mice were housed in the University of Chicago animal facilities, and studies were performed in accordance with the guidelines of the Institutional Animal Care and Use Committee (protocol no. 71577). Female and male

Table 2.1: List of primers

Primer Name	Sequence
Brwd1-floxed	
LOX1	TGAGCTGAAGGCAAGCCAACAG
SDL2	TGAGGGGAACTTAAAACATCTCAG
Mb1-cre	
29589	ACTGAGGCAGGAGGATTGG
30016	CTCTTTACCTTCCAAGCACTGA
30017	CATTTTCGAGGGAGCTTCA
Cd23-cre	
21218	CAGGTTTTGGTGCACAGTCA
25781	TGAAAAAGTCCACTAATTAAAACCA
25782	CTAACAACCCTTTCTCTCAAGGT
26639	TGAAACCAGATCACTTCCAGA
Aicda-cre	
oIMR7505	CACTCGTTGCATCGACCGGTAATG
oIMR7537	GGACCCAACCCAGGAGGCAGATGT
oIMR7538	CCTCTAAGGCTTCGCTGTTATTACCAC
IgG1 GLTs	
Igamma1	GGCCCTTCCAGATCTTTGAG
Cgamma1	GGATCCAGAGTTCCAGGTCACT
Actin4-F	TACCTCATGAAGATCCTGA
Actin5-R	TTCATGGATGCCACAGGAT
SHM Primers	
Cy1-cDNA	CATGGAGTTAGTTTGGGCAG
mCy1-cDNA	TGACAGCAGCGCTGTAGCAC
Cy1-PCR	ATCCAGGGGCCAGTGGATAGAC
V186.2-leader	AGCTGTATCATGCTCTTCTTGGCA
V186.2-nested	CATGCTCTTCTTGGCAGCAACAG

mice were used at 6-12 weeks of age.

2.2 Immunizations

Mice were immunized intraperitoneally with 10^9 sheep red blood cells (SRBCs) (Lampire Biological Laboratories) in 1X phosphate-buffered saline (PBS) and boosted with 10^9 SRBCs 5 days later. Alternatively, mice were immunized intraperitoneally with 200 μl of 4-hydroxy-3-nitrophenyl-acetyl (NP)-keyhole limpet hemocyanin (KLH) (1 mg/ml, valency of 27 or 33) in a 1:1 ratio with Complete Freund's Adjuvant (CFA) (Heise and Klein, 2017). Mice were boosted with NP-KLH in a 1:5 ratio with Incomplete Freund's Adjuvant (IFA) at day 5. Mice were also immunized intraperitoneally with 10^9 SRBCs conjugated with NP by incubating NP-OSu in 0.15 M $NaHCO_3$ with SRBCs. For this experiment, mice were boosted with NP-SRBCs at days 5 and 56 post-immunization.

2.3 Flow cytometry

On day 5 or 14 post-immunization, spleens were harvested, and cells were resuspended in PBS with 3% (v/v) fetal bovine serum (FBS). Erythrocytes were lysed with ACK lysis buffer (Lonza). Splenocytes were passed through a cell strainer to obtain single cell suspensions. Fc block was done with anti-mouse-CD16/CD32 (2.4G2). Cells were stained with viability dye eFluor506 (eBioscience).

For flow cytometry of B cell progenitors, cells were stained with anti-CD19-PE/Cy7 (6D5), anti-B220-APC/Cy7 (RA3-6B2), anti-IgM-APC (II/41), and anti-CD43-FITC (S7).

Fol B cells were stained with anti-B220-APC/Cy7 (RA3-6B2), anti-CD19-PerCP/Cy5.5 (1D3), anti-CD93-BV421 (AA4.1), anti-CD23-PE/Cy7 (B3B4), and anti-CD21-APC (7G6).

GC B cells were stained with anti-B220-AF488 (RA3-6B2), GL7-PerCP/Cy5.5, anti-CD95-BV421 (Jo2), anti-CD83-PE/Cy7 (Michel-19), and anti-CXCR4-APC (2B11). Cells

were also stained with various combinations of anti-CD138-APC (281-2), anti-IgD-PE/Cy7 (11-26c), anti-BCL6-PE/Cy7 (K112-91), Annexin V-FITC (BD Biosciences), FxCycle Violet (Invitrogen), and the FAM FLICA poly caspase kit (Bio-Rad). Cells were fixed with the Foxp3/Transcription factor staining buffer kit (eBioscience).

Tfh cells were stained with anti-CXCR5-BV421 (L138D7), anti-PD-1-PerCP/Cy5.5 (RMPI-30), anti-CD4-APC (RM4-5), and anti-CD3-FITC (145-2C11).

For flow cytometry of MBC subsets, cells were stained with anti-CD38-BUV496 (90/CD38), anti-IgM-BUV615 (II/41), anti-PD-L2-BUV737 (TY25), anti-CCR6-BV421 (29-2L17), anti-IgD-BV480 (11-26c.2a), anti-CD80-BV650 (16-10A1), anti-IgG1-BV711 (A85-1), anti-CD95-BV786 (Jo2), anti-B220-AF488 (RA3-6B2), GL7-PerCP/Cy5.5, anti-CD83-PE/Cy7 (Michel-19), anti-CXCR4-APC (2B11), anti-CD138-APC-R700 (281-2), anti-CD73-APC-Fire750 (TY/11.8), and viability dye eFluor506 (eBioscience) with Brilliant Stain Buffer Plus.

Flow cytometry was done with a LSRFortessa (BD Biosciences) running FACSDiva version 8.0.2, and spectral flow cytometry was done with a Cytek Aurora. Flow cytometry data was analyzed with FlowJo version 10.8.1 (BD Biosciences).

2.4 Cell sorting

Fol B cells were sorted by staining with anti-B220-BV421 (RA3-6B2), anti-CD93-FITC (AA4.1), anti-CD21-APC (7G6), and anti-CD23-PE/Cy7 (B3B4). Enrichment of GC B cells for fluorescence-activated cell sorting (FACS) was done using magnetic-activated cell sorting (MACS), as previously described (Cato et al., 2011). GC B cell enrichment was done with anti-CD43-biotin (S7), anti-CD11c-biotin (N418), and anti-IgD-biotin (11-26c.2a), streptavidin microbeads (Miltenyi Biotec), and LS columns (Miltenyi Biotec). FACS was performed on a FACSAria Fusion (BD Biosciences) running FACSDiva version 8.0.2.

2.5 Microscopy

On day 14 post-immunization, spleens were harvested, transferred to OCT (Fisher HealthCare) and frozen on dry ice in 2-methylbutane. Frozen spleens were sectioned at 6 μm. For immunofluorescence microscopy, sections were fixed with 4% paraformaldehyde, permeabilized with 1X NP40 Permeating Solution in PBS (Boston Products), and Fc receptors were blocked with anti-mouse-CD16/CD32 (2.4G2, 1:200) in 10% normal donkey serum (Jackson ImmunResearch).

For $Mb1^{Cre/wt}$ $Brwd1^{fl/fl}$ mice, tissue was stained with Hoechst 33342 (1:1000, Invitrogen), anti-B220-AF647 (RA3-6B2), and anti-CD3-FITC (145-2C11) (all 1:20) in 5% normal donkey serum. Images were captured at 40X magnification. For $Cd23^{Cre/wt}$ $Brwd1^{fl/fl}$ mice mice, spleens were collected day 14 post-immunization. Tissue was stained with GL7-AF647 (1:20) in 5% normal donkey serum. Images were acquired at 10X magnification.

For $Aicda^{Cre/wt}$ $Brwd1^{fl/fl}$ mice, tissue was stained with GL7-AF647 (1:20), anti-CD4-AF594 (GK1.5, 1:20), anti-CD35-BV421 (8C12, 1:20), anti-IgD-BV711 (11-26c.2a, 1:20), anti-tdTomato (polyclonal, Rockland, 1:50), followed by donkey anti-rabbit-IgG-AF488 (polyclonal, Invitrogen, 1:1000) in 5% normal donkey serum. The GL7 channel and differential interference contrast (DIC) were collected at 10X magnification, and all channels were collected for individual GCs at 20X magnification.

For apoptosis microscopy, tissue was stained with anti-CD35-BV421 (8C12), anti-CD68-AF594 (FA11), and GL7-AF647 (all 1:20) in 5% normal donkey serum. Tissue was also stained with TUNEL-FITC (Abcam) according to the manufacturer's instructions and with Hoechst 33342 (1:1000, Invitrogen) in 5% normal donkey serum.

Immunofluorescence microscopy was done with a Leica Stellaris 8 laser scanning confocal microscope (Leica Microsystems).

Tissue was also stained with hematoxylin and eosin (H&E) and imaged at 40X magnification on an Olympus VS200 Slideview Research Slide Scanner (Evident).

2.6 Image analysis

Images were visualized and analyzed with Fiji version 2.9.0 (Schindelin et al., 2012). For quantification of GC size, GL7 images were Gaussian filtered (sigma = 10), and an intensity threshold and size exclusion threshold were used to remove background signal.

For mean pixel intensity (MPI) image analysis, images collected at 20X magnification were normalized to the 99^{th} percentile for each channel. For a given channel, each image in the dataset was standardized through histogram matching to ensure similar contrast throughout the dataset. GCs were segmented by applying a Gaussian filter (sigma = 5) to the GL7 channel, then adjusting contrast and thresholding. The binary mask created by this segmentation algorithm was separated by instance using the regionprops function in the sci-kit image python library (Walt et al., 2014). After identifying discrete objects (GCs) from the binary segmentation mask, small objects were rejected using a size filter, and GCs at the image boundaries were rejected to ensure each GC was only measured once. GC area was computed from the resulting segmentation masks. The LZ was segmented by applying a similar Gaussian filtering and thresholding algorithm to the CD35 channel. Resulting LZ segmentations were masked using the GC mask defined above to ensure that the segmented LZ was fully encompassed within the GC segmentation. MPI (pixel value sum/segmented area) was calculated for each marker within the regions defined by the GC and LZ masks.

H&E images were visualized with QuPath (Bankhead et al., 2017). H&E debris scores were quantified by a pathologist by grouping samples into three categories with a score of 3 having the greatest degree of debris away from TBMs. Debris was quantified by first manually segmenting GCs with Fiji. Then object segmentation was done with Cellpose 2.0 (Pachitariu and Stringer, 2022) with the following settings: model = cyto, diameter = 18, flow_threshold = 0.75. Debris was quantified as the number of objects $<0.5\ \mu m^2$ normalized to the area of the GC.

2.7 *In vitro* class switch recombination

Splenic cells were harvested as above. B cells were enriched by incubating cells with anti-CD43-biotin (S7) and magnetic enrichment with LS columns (Miltenyi Biotec). For class switching to IgG1, cells were cultured in RPMI 1640 with L-Glutamine media (Gibco) with 10% FBS, 0.1% β-mercapto-ethanol, and 1% penicillin-strep at 37 °C, 5% CO_2. For class switching to IgG1, 25 μg/ml LPS (Sigma-Aldrich) and 10 ng/ml IL-4 (R&D Systems) were added to the media.

After 72 hr, cells were collected, and RNA was isolated using a RNeasy kit (Qiagen). IgG1 germline transcripts were measured by qPCR using primers to the Iγ1 and Cγ1 region and Power SYBR Green Master Mix (Applied Biosystems). Data was normalized using the $\Delta\Delta$Ct method

$$FoldChange = 2^{-((KO_{TEST} - KO_{HOUSEKEEPING}) - (WT_{TEST} - WT_{HOUSEKEEPING})}$$

using *Actin* as the housekeeping gene. After 96 hr, class switching was measured by flow cytometry. Cells were stained with anti-CD19-APC/Cy7 (1D3), anti-IgD-PE/Cy7 (11-26c.2a), anti-IgM-APC (II/41), anti-IgG1-FITC (RMG1-1), and eFluor506 viability dye (eBioscience).

2.8 Somatic hypermutation

RNA was extracted from sorted GC B or plasma cells using the RNeasy Mini Kit (Qiagen). cDNA was generated using the SuperScript III First-Strand Synthesis System for RT-PCR kit (Invitrogen) and the mCy1-cDNA primer for GC B cells or the Cy1-cDNA primer for plasma cells. A semi-nested PCR was performed using the V186.2-leader and V186.2-nested primers with the Cy1-PCR primer as has been described (Heise and Klein, 2017). PCR products were purified with the MinElute PCR Purification Kit (Qiagen). Cloning was

performed with the TOPO TA Cloning & Bacterial Transformation kit (Invitrogen). DNA from colonies was isolated with the PureLink Quick Plasmid Miniprep Kit (Invitrogen). DNA was sequenced with the M13 Forward primer.

The vector sequence was trimmed with 4Peaks (Nucleobytes). Alignment and mutations were analyzed with IMGT/V-QUEST (Brochet et al., 2008). Duplicate sequences from the same mouse, sequences that did not align most closely to V186.2, and sequences with an uneven distribution of mutations were not used. Mutations in CDR3 introduced by junctional diversity were not counted to measure SHM.

2.9 Enzyme-linked immunospot (ELISPOT) assay

At day 13 post-immunization, a Nunclon Delta Surface plate (Thermo Scientific) was coated with NP_{52}-BSA (5 mg/ml) (Heise and Klein, 2017). At day 14, cells were serially diluted in RPMI-1640 media containing 10% FBS, 1% Pen-Strep, 1% L-Glutamine, 1% HEPES, and 1% sodium pyruvate. Cells were incubated at 37 °C in 5% CO_2 overnight. At day 15, plates were stained sequentially with anti-mouse IgG-biotin (1:1000), streptavidin-AP (1:500), and NBT/BCIP (Thermo Fisher Scientific). Plates were imaged with a CTL ImmunoSpot Analyzer.

2.10 Anti-nuclear antibody test

Mouse sera was diluted 1:100 in PBS. Kallestad HEp-2 cell line slides (BioRad) were incubated with the sera. Slides were stained with donkey anti-mouse-IgG-AF647 (1:000) and Hoechst 33342 (1:1000). Immunofluorescence microscopy was done with a Dragonfly 200 confocal microscope (Andor).

2.11 LCMV infection and plaque assay

Mice were infected with 2 x 10^6 plaque forming units (pfu) of LCMV clone 13 via the tail vein. Mice were euthanized at day 42 post-infection. A kidney, liver, and half of the spleen were frozen in OCT on dry ice in 2-methylbutane.

A plaque assay was performed by growing Vero e6 cells (ATCC CRL-1586) to 90% confluency. Spleens and kidneys were homogenized in DMEM (supplemented with 1% FBS and 1% Penicillin/Streptomycin). Tenfold serial dilutions of the homogenate were incubated with the Vero cells for 1 hr at 37 °C. A 1:1 mixture of 1% agarose and 2X 199 media (supplemented with 20% FBS, 2% Penicillin/Streptomycin, 2% L-glutamine, and phenol red) was added to the cells. At day 5, neutral red was added 1:50 to a 1:1 mixture of 1% agarose and 2X 199 media, and this solution was added to each well. At day 6, plaques were counted, and pfu per mg of tissue were calculated.

2.12 RNA-seq

Total RNA was isolated using a RNeasy kit (Qiagen). Libraries were prepared by the University of Chicago Genomics Facility before sequencing on the NovaSeq-X-Plus (Illumina). Raw reads were aligned to reference genome mm9 in a splice-aware manner using STAR (Dobin et al., 2013). Gene expression was quantified using FeatureCounts (Liao et al., 2014) against UCSC genes, with Ensembl IG genes from mm10 converted to mm9 coordinates with UCSC liftOver.

2.13 ATAC-seq

Cells were washed with PBS, then lysed with ATAC lysis buffer (10 mM Tris-HCl, pH 7.4, 10 mM NaCl, 3 mM $MgCl_2$, 0.1% IGEPAL CA-630). Resulting nuclei were then incubated with tagmentation enzyme (Illumina). Libraries from purified samples were made with the

Nextera Indexing kit (Illumina).

Raw reads were aligned to reference genome mm9 using BWA MEM (Li, 2013). Apparent PCR duplicates were removed using Picard MarkDuplicates (https://github.com/broadinstitute/ picard/releases/ tag/2.11.0)

For ATAC-seq, read alignments were first adjusted to account for TAC transposon binding: +4 bp for +strand alignments, −5 bp for −strand alignments. The open chromatin enrichment track was generated by first creating a bedGraph from the raw reads using bedtools genomcov (Quinlan and Hall, 2010), then converted to bigWig using UCSC tool bedGraphToBigWig. Tracks were normalized by the sum of alignment lengths over 1 billion. Open chromatin peaks were called using Macs2 with no model set and no background provided (Zhang et al., 2008). Peaks with a score greater than 5 were retained. To quantitatively measure changes in epigenetic enrichment, we first identified empirical regulatory elements based on the peak calls obtained from each sample in the analysis. Peaks were merged into a uniform set of regulatory elements using bedtools merge (Quinlan and Hall, 2010). Enrichment levels for each regulatory element were then quantified with featureCounts (Liao et al., 2014).

2.14 Differential expression of RNA-seq and ATAC–seq

Differential expression statistics (fold-change and p value) were computed using edgeR on raw expression counts obtained from quantification (either genes or peaks) (Robinson et al., 2010). Pairwise comparisons were computed using exactTest, and multigroup comparisons using the generalized linear modeling capability in edgeR. In all cases, p values were adjusted for multiple testing using the FDR correction of Benjamini and Hochberg.

2.15 Next generation sequencing analysis

RNA-seq, ATAC-seq, and ChIP-seq data was visualized with the Integrated Genome Browser (Freese et al., 2016). Heatmaps were generated with ComplexHeatmap and Circlize in R, and plots were made with ggplot2 (Gu et al., 2016, 2014). Metascape data portal was used for pathway analyses and for RNA-seq circle plots (Zhou et al., 2019). Hypergeometric optimization of motif enrichment (HOMER) was used to perform known transcription factor binding motif analyses using the FindMotifsGenome function to generate enrichment and p values (Heinz et al., 2010). Gene set enrichment analysis (GSEA) was performed as described using the Molecular Signatures Database hallmark genes sets (Subramanian et al., 2005; Liberzon et al., 2015). Hi-C data was visualized using Juicebox (Robinson et al., 2018). Hi-C arc plots were generated with HiCcompare by normalizing Hi-C matrices using the hic_loess function and calculating differences using the hic_compare function (Stansfield et al., 2018). Then the plotBedpe function from Sushi.R was used to plot differences with $p < 0.05$ (Phanstiel et al., 2014).

2.16 Statistical analysis

Statistical analyses were performed with GraphPad Prism. Bar graphs are displayed as the mean ± standard deviation. Significance as defined by p value or false discovery rate (q value) are defined in the figure legends. All measurements were taken from distinct samples as described in the figure legends.

2.17 Data availability

The data that support the findings of this study are available from the corresponding authors upon reasonable request. RNA-seq and ATAC-seq data were deposited in the Gene Expression Omnibus (GEO) database with accession code GSE264164. WT GC B cell RNA-seq and

ATAC-seq data from GEO accession code GSE133743 was analyzed in this study (Kennedy et al., 2020). Small pre-B cell Hi-C and ChIP-seq from GEO accession code GSE221519 was also analyzed (Mandal et al., 2024).

CHAPTER 3

BRWD1 IN FOLLICULAR B CELLS

3.1 Introduction

The activation and differentiation of B cells is central to initiation of the humoral adaptive immune response (Fig 3.1). Naïve IgM^+IgD^+ B cells locate within the follicles of secondary lymphoid organs, while T cells reside in neighboring T cell zones (Cyster and Allen, 2019). In T cell-dependent responses, B cells activate upon encountering antigen and migrate to the border of the follicle and T cell zone as well as the interfollicular region (Okada et al., 2005; Kerfoot et al., 2011). Here 1 to 2 days following antigen exposure, B and T cells form long-lasting interactions (Okada et al., 2005; Kerfoot et al., 2011). Activated B cells can differentiate down multiple pathways to become either plasmablasts, memory B cells, or germinal center (GC) B cells according to the input of multiple signals from the B cell receptor (BCR), costimulatory molecules, T cell help, and cytokines (Cyster and Allen, 2019). Early differentiation along the GC B cell pathway occurs as B cells express low levels of BCL6, an essential transcription factor (TF) for the GC B cell molecular program (Kitano et al., 2011; Zhang et al., 2017b; Dent et al., 1997; Fukuda et al., 1997). Indeed, B cells with greater BCL6 expression later preferentially enter the GC (Robinson et al., 2020). These $BCL6^+$ B cells re-enter the follicle to form GCs around day 4 following immunization (Silva and Klein, 2015; Huang et al., 2014).

Within the GC, B cells canonically cycle between the light zone (LZ), where selection takes place, and the dark zone (DZ) (Victora and Nussenzweig, 2022). The DZ can be further subdivided into the DZ proliferation (DZp) and the DZ differentiation (DZd) where somatic hypermutation occurs (Kennedy et al., 2020; Wright et al., 2023; Kennedy and Clark, 2021). This pathway from naïve to GC B cell requires large shifts in molecular programs, which includes switches between TF programs and changes in chromatin accessibility (Silva and

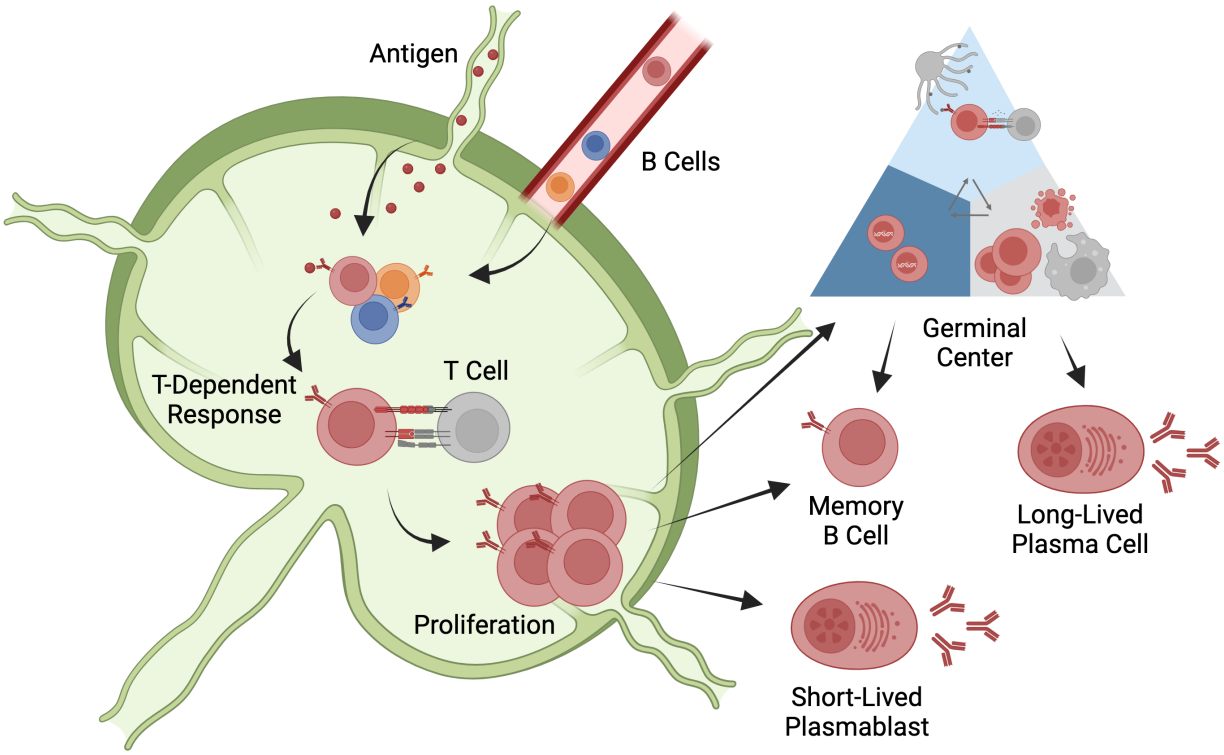

Figure 3.1: Follicular B cell differentiation in response to antigen. Circulating naïve B cells enter and survey lymph nodes. Following infection or vaccination, antigens drain to the lymph node and activate cognate naïve follicular B cells. In a T cell-dependent response, activated B cells present antigen to $CD4^+$ T cells and proliferate. Activated B cells may then differentiate into short-lived plasmablasts, memory B cells, or germinal center B cells. Germinal center B cells may also further differentiate into memory B cells, short-lived plasmablasts, or long-lived plasma cells. This figure was created using BioRender.com and was inspired by Cyster and Allen (2019).

Klein, 2015; Papin et al., 2022). Notably, differentiation of GC B cells from naïve B cells involves decompaction of chromatin genome-wide (Vilarrasa-Blasi et al., 2021; Bunting et al., 2016; Doane et al., 2021).

B cell progenitors also experience large shifts in molecular programs as they develop in the bone marrow (Clark et al., 2014; McLean and Mandal, 2020). As proliferating large pre-B cells transition to small pre-B cells that undergo *Igk* recombination, >10,000 genes change expression (Mandal et al., 2018). The epigenetic reader bromodomain and WD repeat-containing protein 1 (BRWD1) regulates 7,000 of these differentially expressed genes (Mandal et al., 2018). BRWD1 binds to chromatin according to specific histone modifications – histone 3 (H3) lysine 9 acetylation (K9Ac), serine 10 phosphorylation (S10p), and K14Ac and regulates chromatin via multiple mechanisms (Mandal et al., 2015). At the local scale, BRWD1 repositions nucleosomes relative to GAGA DNA motifs to open and close chromatin, which in small pre-B cells is important for *Igk* recombination (Mandal et al., 2015). BRWD1 also mediates long range chromatin looping over a megabase scale (Mandal et al., 2024). Chromatin loop extrusion, the process by which distal chromatin regions are brought proximal to one another through formation of a loop, is mediated by the ring-shaped cohesin complex (Davidson et al., 2019; Vian et al., 2018; Kagey et al., 2010). The cohesin cofactor NIPBL drives loop extrusion while the cofactor WAPL releases cohesin from chromatin (Bauer et al., 2021; Liu et al., 2021; Haarhuis et al., 2017). The boundaries of chromatin loops are often anchored by CTCF, which binds DNA and blocks further loop extrusion by cohesin (Nora et al., 2020). BRWD1 mediates chromatin loop extrusion by converting static cohesin to dynamic cohesin that includes WAPL and NIPBL and is capable of loop extrusion (Mandal et al., 2024). In these ways, BRWD1 coordinates the transcriptional, epigenetic, and chromatin 3D transitions necessary for B cell progenitors to stop proliferation and begin recombination. BRWD1 is also highly expressed in follicular (Fol) B cells, yet its contributions to the differentiation of Fol B cells in response to antigen have not been

explored.

Upon activation and before entering the germinal center, B cells may undergo class switch recombination (CSR) to replace the IgM-encoding constant region with a different downstream constant region of an alternate antibody class (Roco et al., 2019). The class switch locus is flanked 5′ by the iEμ enhancer and 3′ by the *Igh* regulatory region (*Igh*RR) super enhancer, both of which are necessary for CSR (Perlot et al., 2005; Li et al., 2010; Vincent-Fabert et al., 2010; Pinaud et al., 2001; Saintamand et al., 2016). Multiple chromatin loop extrusion events are necessary for CSR (Zhang et al., 2022). First, cohesin-mediated loop extrusion forms a large chromatin loop between iEμ and the *Igh*RR in resting naïve B cells (Zhang et al., 2019a; Wuerffel et al., 2007). Second, upon activation, secondary loop extrusion pulls the alternate constant regions into the larger loop anchor (Zhang et al., 2019a; Wuerffel et al., 2007). Subsequent apposition of constant region promoters with the *Igh*RR induces transcription of germline transcripts (GLTs) (Wuerffel et al., 2007). This secondary loop is formed by cohesin-mediated loop extrusion and causes the switch region of IgM (Sμ) to align with the switch region of the targeted constant region (Zhang et al., 2019a). Once this 3D chromatin architecture is established, activation-induced deaminase (AID) causes double strand breaks in the switch regions to initiate CSR (Noia and Neuberger, 2007). Thus, the 3D structure of the class switch locus is dynamically regulated upon B cell activation and is necessary for class switch recombination (Zhang et al., 2022).

Here we designed a *Brwd1*-floxed mouse to conditionally delete *Brwd1* in Fol B cells and to investigate the role of BRWD1 in the differentiation of naïve Fol B cells. We demonstrate that BRWD1 is important for GC initiation and CSR.

3.2 Results

3.2.1 BRWD1 may regulate similar transcriptional programs in peripheral B cells as in B cell development

We previously observed that the small pre-B cell stage of B cell development (Fraction D) marks a transcriptional reflection point in B cell development with over 10,000 genes turned on or off across this developmental stage (Mandal et al., 2018). BRWD1 regulated over 7,000 of these genes (Mandal et al., 2018). To study whether any transcriptional transitions across small pre-B cell differentiation are mirrored in peripheral B cells, we used RNA-seq data from the Immunological Genome Project to plot transcription across the entire B cell lineage (Fig 3.2a). This analysis revealed that several genes turned on in small pre-B cells are also turned on in GC B cell centroblasts and centrocytes as well as the inverse. To study whether any of these genes are directly regulated by BRWD1, we compared RNA-seq of small pre-B cells from either wild type (WT) or *Brwd1*$^{-/-}$ mice with a germline mutation in *Brwd1* (Fig 3.2b). This analysis revealed that a portion of genes with similar expression between small pre-B cells and GC B cells are directly regulated by BRWD1 in small pre-B cells and included genes important for B cell biology such as *Myc*. Thus, the transcriptional program between small pre-B cells and GC B cells is not entirely recycled, but BRWD1 may regulate important genes in both populations.

3.2.2 Design of a Brwd1-floxed mouse

Brwd1 is first expressed by small pre-B cells in the bone marrow where it mediates widespread epigenetic changes (Mandal et al., 2018, 2015). Using RNA-seq from different B cell populations in WT mice, we found that *Brwd1* expression was over twice as high in Fol B cells than in small pre-B cells (Fig 3.3a). Furthermore, *Brwd1* expression changed across GC B cell subsets, with the greatest expression in the DZd (Kennedy et al., 2020). This dynamic regu-

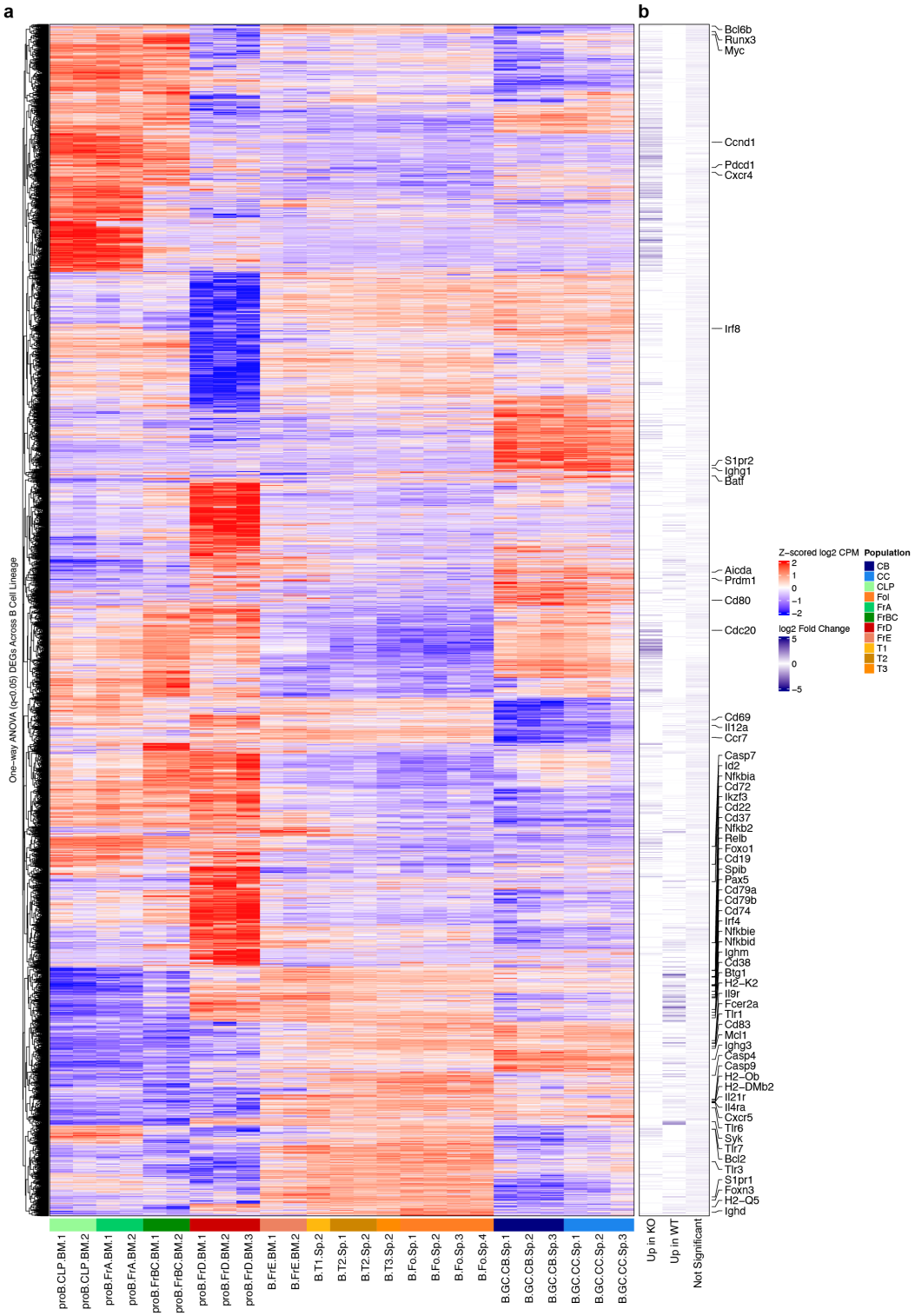

Figure 3.2: BRWD1-regulated genes differentially expressed across the B cell lineage. *Caption continued on the next page.*

Figure 3.2: **(a)** Heatmap of 11,790 differentially expressed genes (one-way ANOVA, $q < 0.05$) across the B cell lineage using RNA-seq data of listed B cell populations from the Immunological Genome Project. Z-scored $\log_2$ counts per million (CPM) are plotted. **(b)** Heatmap of BRWD1-regulated genes by comparing WT and *Brwd1*$^{-/-}$ small pre-B cells ($\log_2$ fold change >1, $q < 0.05$). Log_2 fold change is plotted. Notable genes important for peripheral B cell biology and that are regulated by BRWD1 are labeled. (CB = centroblasts, CC = centrocytes, CLP = common lymphoid progenitors, Fol = follicular B cells, Fr = Fraction, T = Transitional)

lation of *Brwd1* in Fol and GC B cells suggested that BRWD1 may mediate both transitions between and maintenance of peripheral B cells.

To study the role of BRWD1 in peripheral C57BL/6 B cells, we derived a *Brwd1*-floxed mouse with Lox71 and Lox66 sites in opposite orientations surrounding *Brwd1* exons 6, 7, and 8 (Fig 3.3b). The targeting construct included an inverse tdTomato (tdT) reporter so that following Cre recombination, exons 6, 7, and 8 are inverted and tdT is expressed (Fig 3.3c). To delete *Brwd1* in Fol B cells, we crossed these mice with mice expressing Cre under the *Fcer2a* promoter (*Cd23*^{Cre}) (Kwon et al., 2008). Using RNA-seq, we confirmed that tdT^{+} Fol B cells in *Cd23*$^{Cre/wt}$ *Brwd1*$^{fl/fl}$ (KO) mice do not transcribe exons 6, 7, and 8 of *Brwd1* (Fig 3.3d). Homozygous *Cd23*$^{Cre/wt}$ *Brwd1*$^{fl/fl}$ mice had greater tdT median fluorescence intensity (MFI) than heterozygous *Cd23*$^{Cre/wt}$ *Brwd1*$^{fl/wt}$ mice, demonstrating that both alleles were deleted in homozygous mice (Fig 3.3e).

3.2.3 BRWD1 is necessary for B cell development in the bone marrow

Mice carrying a germline mutation of *Brwd1* have a partial block in B cell development following the small pre-B cell stage when BRWD1 is necessary for *Igk* recombination (Mandal et al., 2015). To test whether conditional deletion of *Brwd1* only in B cell progenitors produces a similar phenotype, we crossed the *Brwd1*-floxed mouse with mice that express Cre recombinase under the control of the *Cd79a* promoter (*Mb1*^{Cre}) to delete *Brwd1* in early B cell progenitors. Among B cell progenitors from *Mb1*$^{Cre/wt}$ *Brwd1*$^{fl/fl}$ mice, 43% of

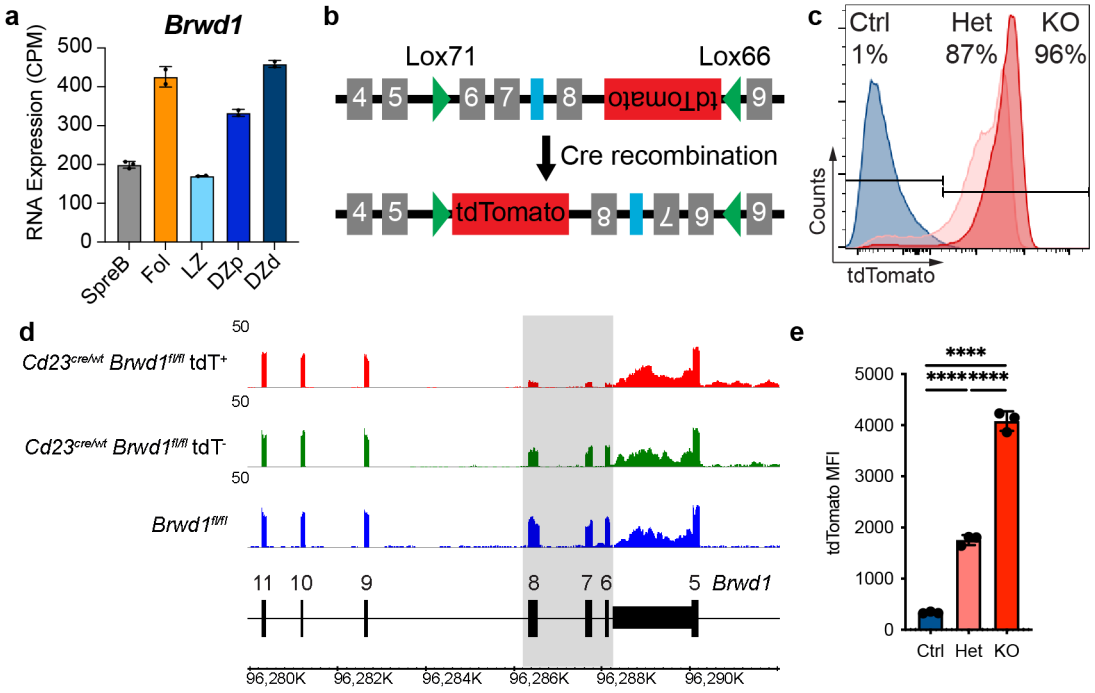

Figure 3.3: Design and characterization of a *Brwd1*-floxed mouse. **(a)** RNA-seq of *Brwd1* expression for small pre-B, Fol B, and GC B cells in the LZ, DZp, and DZd (n = 3 for small pre-B cells, n = 2 for all other cell types). **(b)** Model of LoxP sites (green) surrounding exons 6, 7, and 8 of *Brwd1* with a tdTomato (tdT) reporter in the inverse orientation. A single flippase recognition target (FRT) site (blue) remained following removal of a selection cassette. **(c)** tdTomato expression by flow cytometry of splenic $B220^{+}CD19^{+}CD93^{-}CD23^{+}CD21^{+}$ Fol B cells in $Cd23^{Cre/wt}$ $Brwd1^{fl/fl}$ (KO), $Cd23^{Cre/wt}$ $Brwd1^{fl/wt}$ (Het), and $Brwd1^{fl/fl}$ (Ctrl) mice. Frequency of tdT^{+} Fol B cells is shown. **(d)** RNA-seq of *Brwd1* transcripts mapped to the *Brwd1* locus in sorted $Cd23^{Cre/wt}$ $Brwd1^{fl/fl}$ tdT^{+}, $Cd23^{Cre/wt}$ $Brwd1^{fl/fl}$ tdT^{-}, and $Brwd1^{fl/fl}$ Fol B cells. The region flipped in orientation following Cre recombination is highlighted grey. **(e)** Median fluorescence intensity (MFI) of tdT^{+} Fol B cells from $Cd23^{Cre/wt}$ $Brwd1^{fl/fl}$ (KO), $Cd23^{Cre/wt}$ $Brwd1^{fl/wt}$ (Het), and $Brwd1^{fl/fl}$ (Ctrl) mice (n = 3 mice per group). (****p<0.0001, two-sided unpaired t-test, bar plots show mean ± standard deviation)

pro-B cells and over 95% of immature B cells deleted *Brwd1* as measured by tdT expression (Fig 3.4a). In the bone marrow, $Mb1^{Cre/wt}$ $Brwd1^{fl/fl}$ mice had fewer B cell progenitors beginning at the large pre-B cell stage compared to $Mb1^{Cre/wt}$ and $Brwd1^{fl/fl}$ control mice (Fig 3.4b). The frequency of pre-pro-B cells was increased in $Mb1^{Cre/wt}$ $Brwd1^{fl/fl}$ mice, suggesting a compensatory effect in the earliest stages of B cell development (Fig 3.4c).

In the spleen, there was no change in the number or frequencies of peripheral B cell populations, suggesting that BRWD1 is not necessary for these populations (Fig 3.4d-e). Indeed, immunofluorescence microscopy of splenic sections demonstrated that $Mb1^{Cre/wt}$ $Brwd1^{fl/fl}$ mice had a normal distribution of T and B cell zones (Fig 3.4f). Together these results demonstrate that conditional deletion of *Brwd1* in B cell progenitors results in a similar phenotype as the germline *Brwd1* mutation by inhibiting B cell development in the bone marrow. However, a portion of *Brwd1*-deficient B cells are still able to develop by unknown compensatory mechanisms and successfully fill the splenic niche.

We previously observed that $Brwd1^{-/-}$ mice have an abnormal splenic architecture with no T cell zones adjacent to B cell follicles (Fig 3.4g). In comparison with the normal splenic architecture of $Mb1^{Cre/wt}$ $Brwd1^{fl/fl}$ mice, this demonstrates that *Brwd1* is likely important in the organization of splenic T cells.

3.2.4 BRWD1 is not necessary for maintenance of follicular B cells

To study whether BRWD1 is important for the maintenance of peripheral B cells, we characterized $Cd23^{Cre/wt}$ $Brwd1^{fl/fl}$ (KO) mice at the steady state. Flow cytometry demonstrated that control ($Brwd1^{fl/fl}$), heterozygous, and KO mice had comparable numbers of $CD20^{+}CD19^{+}CD93^{-}$ mature B cells in the spleen (Fig 3.5a-b). Additionally, these mice had the same number and frequency of Fol and marginal zone (MZ) B cells (Fig 3.5c-f). Approximately 96% of Fol B cells and 82 % of MZ B cells expressed tdT, confirming efficient Cre recombination in KO mice (Fig 3.5g-h). Together these results demonstrate that steady

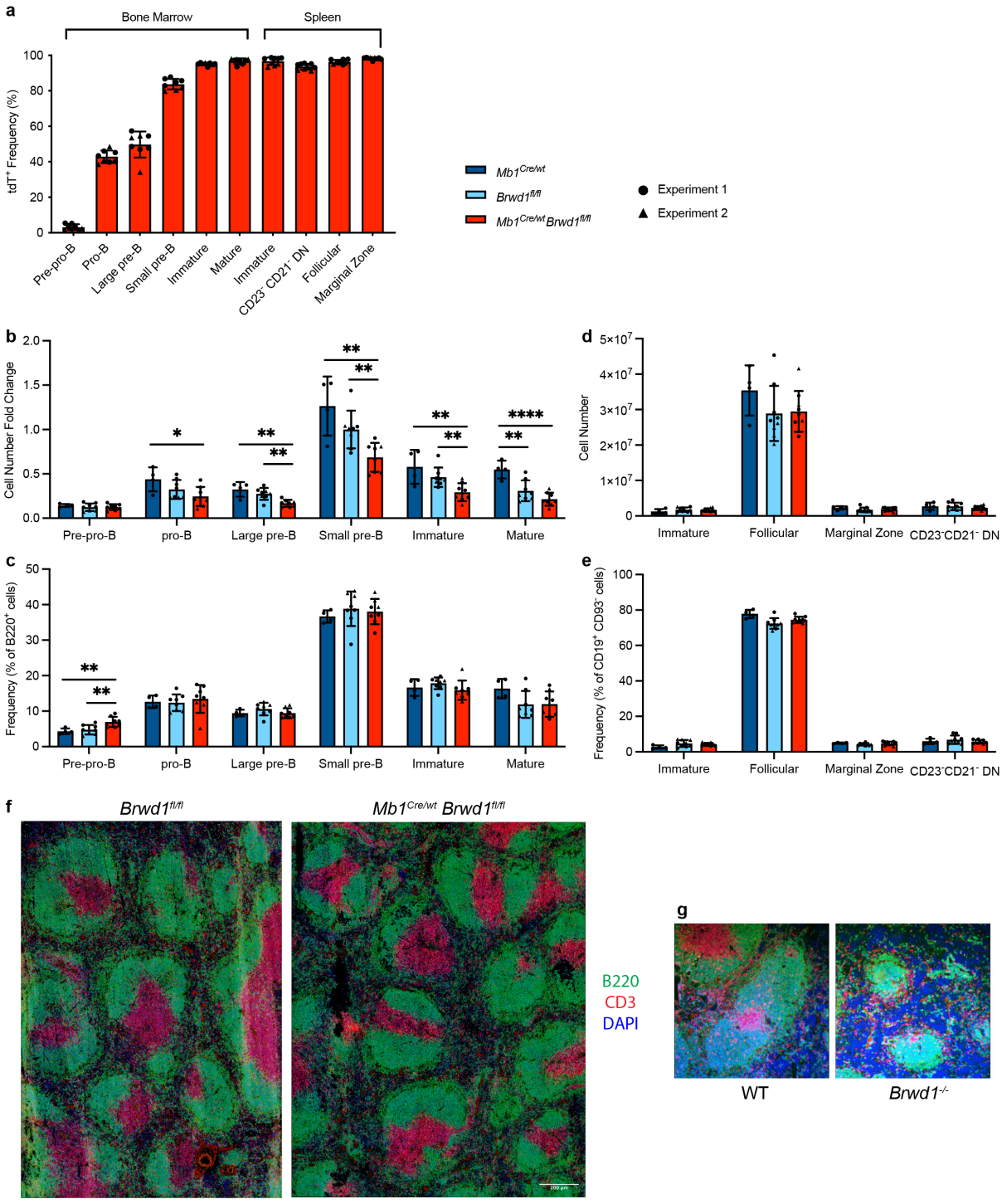

Figure 3.4: BRWD1 is necessary for B cell development in the bone marrow. **(a)** Frequency of tdT^{+} cells at each stage of B cell development in the bone marrow and spleens of $Mb1^{Cre/wt}$ $Brwd1^{fl/fl}$ mice (bone marrow n = 8 mice, spleen n = 9 mice). *Caption continued on the next page.*

Figure 3.4: **(b)** Number of bone marrow B cell progenitors in *Mb1*$^{Cre/wt}$ (Cre control), *Brwd1*$^{fl/fl}$ (Flox control), and *Mb1*$^{Cre/wt}$ *Brwd1*$^{fl/fl}$ (KO) mice. Data is shown as the fold change relative to *Brwd1*$^{fl/fl}$ small pre-B cell numbers to account for variation in total bone marrow extracted between experiments. (Pre-pro-B = B220^{+}CD19^{-}, Pro-B = B220^{+}CD19^{+}CD43^{+}, Large pre-B = B220^{+}CD19^{+}CD43^{-}FSC^{high}, Small pre-B = B220^{+}CD19^{+}CD43^{-}FSC^{low}, Immature = B220^{+}CD19^{+}CD43^{-}IgM^{+}, Mature = B220^{high}CD19^{+}CD43^{-}IgM^{+}) (Cre control n = 4 mice, Flox control n = 8 mice, KO n = 8 mice) **(c)** Frequency of bone marrow B cell progenitors. **(d)** Number of splenic B cells. DN = double negative. (Cre control n = 4 mice, Flox control n = 9 mice, KO n = 9 mice) **(e)** Frequency of splenic B cells calculated as the proportion of CD19^{+}CD93^{-} cells. **(f)** Representative images of immunofluorescence microscopy of spleens from *Brwd1*$^{fl/fl}$ and *Mb1*$^{Cre/wt}$ *Brwd1*$^{fl/fl}$ mice. Scale bar = 200 μm. (n = 4 mice per group) **(g)** Representative images of immunofluorescence microscopy of spleens from WT and *Brwd1*$^{-/-}$ mice. (*p<0.05, **p<0.01, ****p<0.0001, two-sided unpaired t-test, bar plots show mean ± standard deviation)

state splenic B cells do not require BRWD1.

3.2.5 BRWD1 is important for germinal center initiation

Upon antigenic stimulation, Fol B cells differentiate into GC B cells. To determine whether BRWD1 is important for the differentiation of Fol B cells, we intraperitoneally immunized *Cd23*$^{Cre/wt}$ *Brwd1*$^{fl/fl}$ (KO) mice with sheep red blood cells at days 0 and 5 and analyzed spleens 14 days post-immunization at the peak of the GC response (Fig 3.6a-b) (Weisel et al., 2016). The number of B220^{+} B cells was equivalent between KO and control mice (Fig 3.6c). However, the number and frequency of GL7^{+}CD95^{+} GC B cells were decreased over twofold in the KO mice (Fig 3.6d-e). This decrease was observed in GC B cells within the LZ, DZp, and DZd (Fig 3.6g). Over 85% of GC B cells expressed tdT in the KO mice, demonstrating that the smaller GC population primarily contained *Brwd1*$^{-/-}$ GC B cells (Fig 3.6f). Antigen presentation by GC B cells to Tfh cells induces Tfh cell proliferation (Merkenschlager et al., 2021). Indeed, the KO mice had no significant change in the number of Tfh cells but did have a decreased Tfh cell frequency (Fig 3.6h-i). Furthermore, the

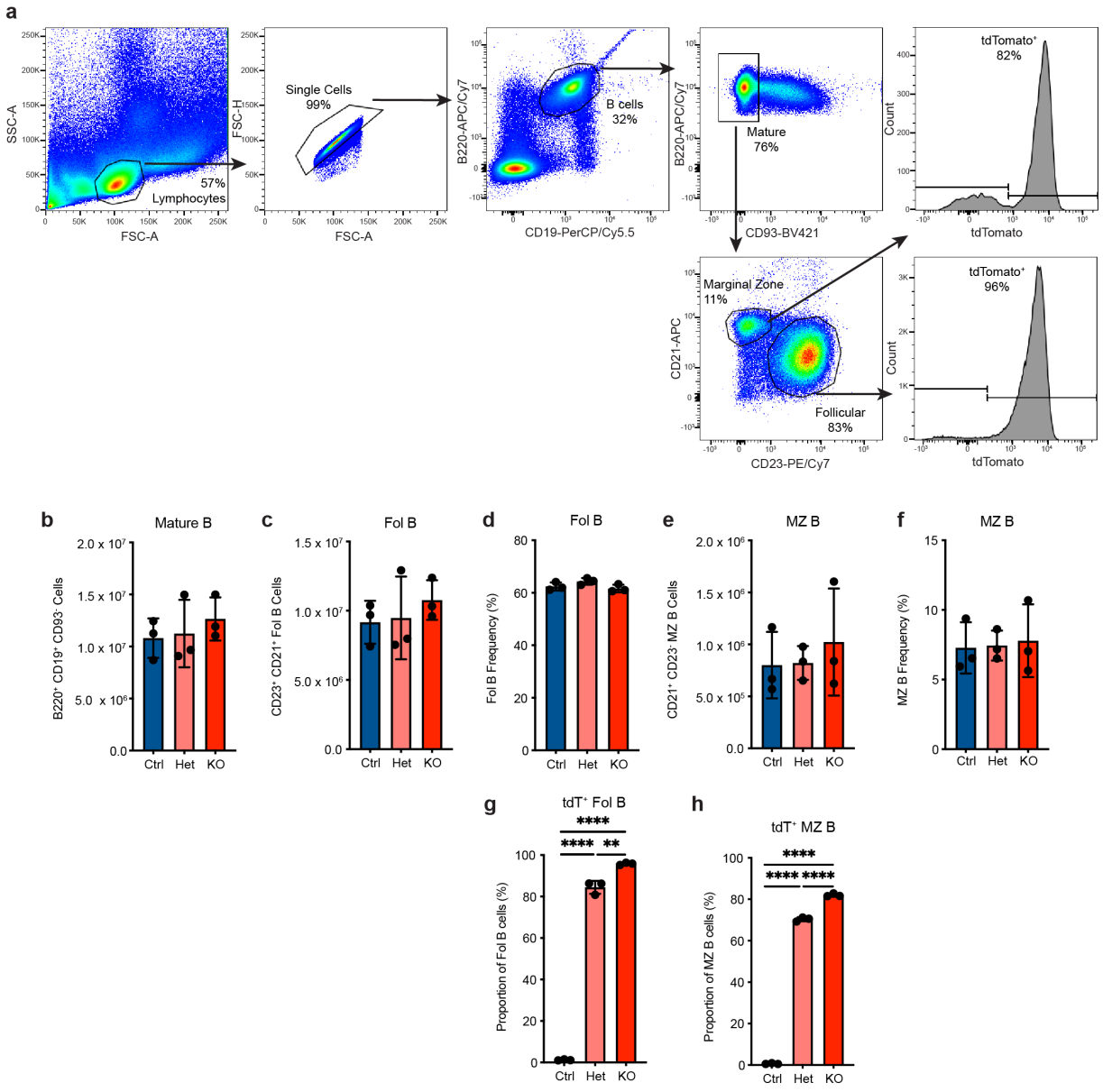

Figure 3.5: BRWD1 is not necessary for maintenance of follicular or marginal zone B cells. **(a)** Splenic Fol B cells were gated as $B220^+CD19^+CD93^-CD23^+CD21^+$ cells by flow cytometry. Representative data from a $Cd23^{Cre/wt}$ $Brwd1^{fl/fl}$ mouse is shown. **(b)** Number of $B220^+CD19^+CD93^-$ mature B cells from $Brwd1^{fl/fl}$ (Ctrl), $Cd23^{Cre/wt}$ $Brwd1^{fl/wt}$ (Het), and $Cd23^{Cre/wt}$ $Brwd1^{fl/fl}$ (KO) mice (n = 3 mice per group). **(c)** Number of $CD23^+CD21^+$ Fol B cells. **(d)** Frequency of Fol B cells as a proportion of all $B220^+CD19^+$ cells. **(e)** Number of $CD21^+CD23^-$ MZ B cells. **(f)** Frequency of MZ B cells as a proportion of all $B220^+CD19^+$ cells. **(g)** Frequency of tdT^+ Fol B cells. **(h)** Frequency of tdT^+ MZ B cells. ($^{**}p < 0.01$, $^{****}p < 0.0001$, two-sided unpaired t-test, bar plots show mean ± standard deviation)

frequency of GC B cells and Tfh cells positively correlated with one another, showing that the decreased Tfh cell frequency was consistent with the smaller GC B cell response (Fig 3.6j).

We confirmed a defect in the GC response by immunofluorescence microscopy. Spleens from KO mice had fewer GCs per splenic area than controls (Fig 3.7a-b). Additionally, GCs from KO mice were smaller compared to controls as measured by GL7 fluorescence (Fig 3.7c). Together, these results demonstrate that BRWD1 is important for a proper GC response.

This diminished GC B cell response in KO mice could reflect either a defect in the initial differentiation of Fol B cells into GC B cells or in the expansion and maintenance of GC B cells in the 14 days following immunization. Because GCs form about day 4 post-immunization, we measured the GC response at day 5 post-immunization (Fig 3.6k) (Kerfoot et al., 2011; Zhang et al., 2017b). At this time point, we observed a 2.5-fold decrease in both the number and frequency of GC B cells, suggesting that BRWD1 is important for GC initiation (Fig 3.6l-m). Approximately 80% of GC B cells expressed tdT, suggesting that *Brwd1*$^{-/-}$ GC B cells can populate the GC once the response is initiated (Fig 3.6n).

We considered and ruled out several possibilities for this defect in GC initiation. First, the decreased GC response at day 5 post-immunization was not caused by *Brwd1*$^{-/-}$ B cells differentiating into plasmablasts, because there was no significant difference in the number or frequency of CD138^{+} plasmablasts compared to controls (Fig 3.8a-c). Next, GC B cells in KO mice had no change in the prevalence of apoptosis or cell death as measured by Annexin V or fluorescent inhibitors of caspase (FLICA) (Fig 3.8d-g). The proliferating subpopulation among GC B cells is marked by the highest CD83 and CXCR4 expression (Kennedy et al., 2020). There was no difference in the proportion of proliferating cells among the CD83$^{\text{high}}$CXCR4$^{\text{high}}$ population as measured by DAPI$^{\text{high}}$ cells in the S, G2, or M phases of the cell cycle (Fig 3.8h). Furthermore, there was no change in the DZp to LZ ratio or the

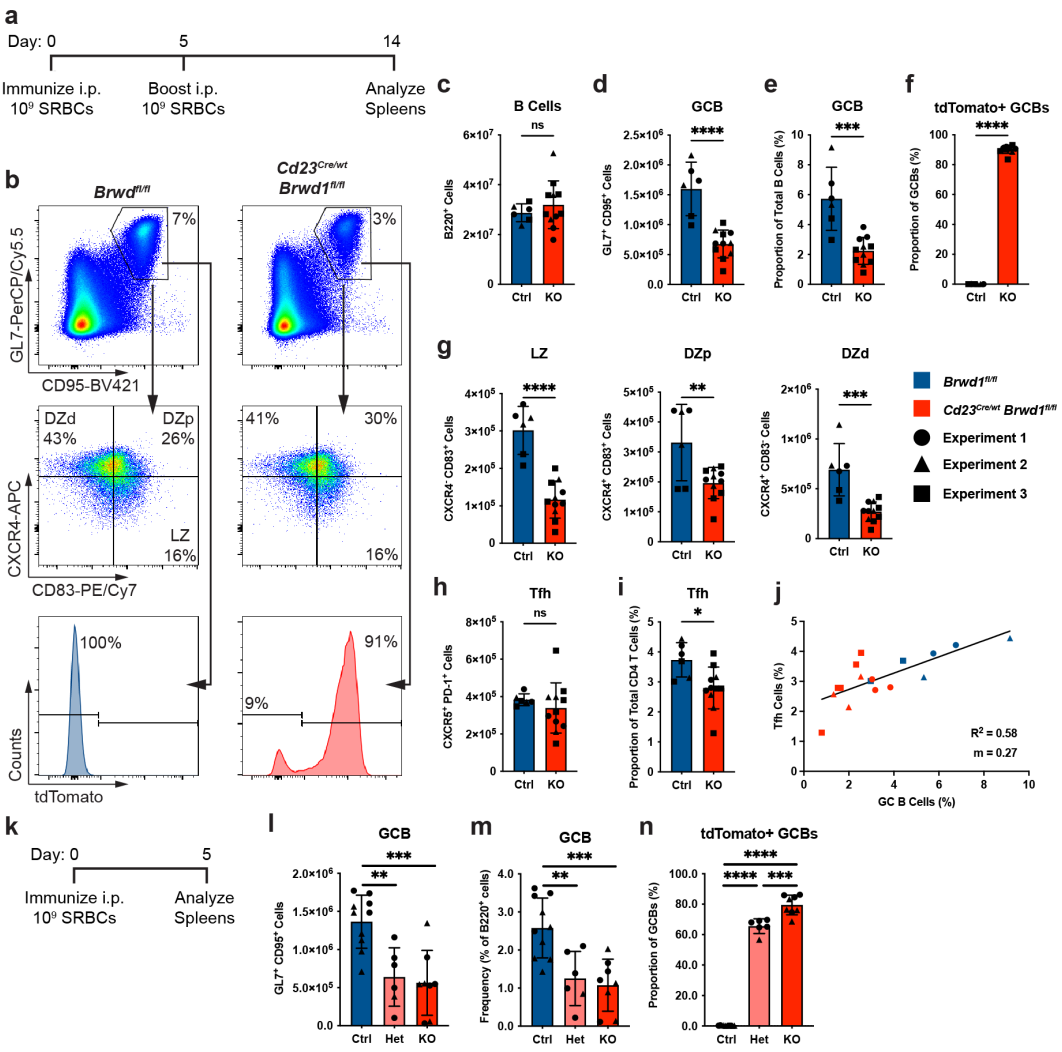

Figure 3.6: Deletion of *Brwd1* in follicular B cells represses germinal center initiation. **(a)** $Cd23^{Cre/wt}$ $Brwd1^{fl/fl}$ (KO) and $Brwd1^{fl/fl}$ (Ctrl) mice were immunized intraperitoneally (i.p.) with 10^9 sheep red blood cells (SRBCs) at days 0 and 5. Spleens were collected at day 14 post-immunization (Ctrl n = 6 mice, KO n = 11 mice). **(b)** Representative flow plots first gated on live $B220^+$ cells. **(c)** Total number of $B220^+$ B cells. **(d-e)** Absolute number (d) and frequency (e) of $GL7^+CD95^+$ GC B cells. **(f)** Proportion of GC B cells expressing tdTomato. **(g)** Number of LZ, DZp, and DZd GC B cells. **(h-i)** Total number (h) and frequency (i) of $CXCR5^+PD\text{-}1^+$ Tfh cells. **(j)** Linear regression of frequency of GC B cells vs. frequency of Tfh cells. m = slope. **(k)** $Cd23^{Cre/wt}$ $Brwd1^{fl/fl}$, $Cd23^{Cre/wt}$ $Brwd1^{fl/wt}$ (Het), and $Brwd1^{fl/fl}$ mice were immunized i.p. with 10^9 SRBCs, and spleens were harvested at day 5 (Ctrl n = 10 mice, Het n = 6 mice, KO n = 8 mice). **(l-m)** Total number (l) and frequency (m) of $GL7^+CD95^+$ GC B cells. **(n)** Proportion of GC B cells expressing tdT. (*p<0.05, **p<0.01, ***p<0.001, ****p<0.0001, j: simple linear regression, all others: two-sided unpaired t-test, bar plots show mean ± standard deviation)

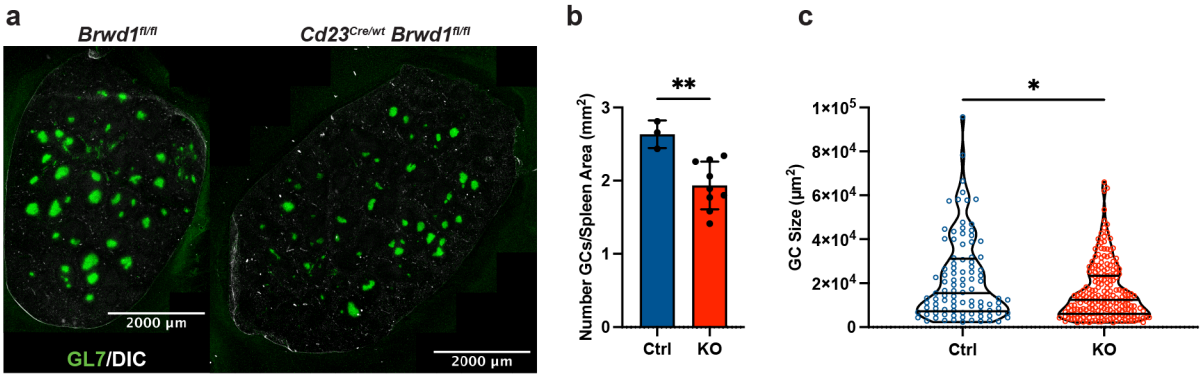

Figure 3.7: Deletion of *Brwd1* in follicular B cells causes fewer and smaller germinal centers. (a) Representative images of spleen sections from $Cd23^{Cre/wt}$ $Brwd1^{fl/fl}$ (KO) and $Brwd1^{fl/fl}$ (Ctrl) mice imaged at 10x magnification and stained with GL7. (DIC = differential interference contrast, scale bar = 2,000 μm, KO n = 3 mice, Ctrl n = 9 mice) **(b)** Number of GCs per spleen area. (**p<0.01, two-sided unpaired t-test, bar plot shows mean ± standard deviation) **(c)** Size of GCs as measured by area of GL7 staining. (Violin plots show median and quartiles, *p<0.05, Mann-Whitney)

DZd to LZ ratio (Fig 3.8i-j).

We next examined the expression of BCL6 because of its role in GC differentiation. GC B cells from KO mice expressed lower levels of BCL6 as measured by flow cytometry (Fig 3.8k). This was due to a bimodal BCL6 distribution where some GC B cells had intermediate BCL6 expression between that of control GC B cells and naïve $B220^{+}CD95^{-}GL7^{-}$ B cells (Fig 3.8l). The GC precursor population expresses intermediate BCL6 and peaks around day 4 post-immunization (Zhang et al., 2017b). Thus, these results further support that BRWD1 is necessary for the initial differentiation of Fol B cells into GC B cells.

3.2.6 BRWD1 facilitates class switch recombination

Class switch recombination (CSR) occurs following B cell antigen exposure and before entry into the GC (Roco et al., 2019). CSR requires large shifts in chromatin topology, so we investigated whether BRWD1 is important for CSR (Zhang et al., 2022). Indeed, at day 14 post-immunization, fewer tdT^{+} GC B cells were IgM^{-} when compared with tdT^{-} cells from the same mouse, suggesting that $Brwd1^{-/-}$ B cells undergo less CSR (Fig 3.9a). Next, we

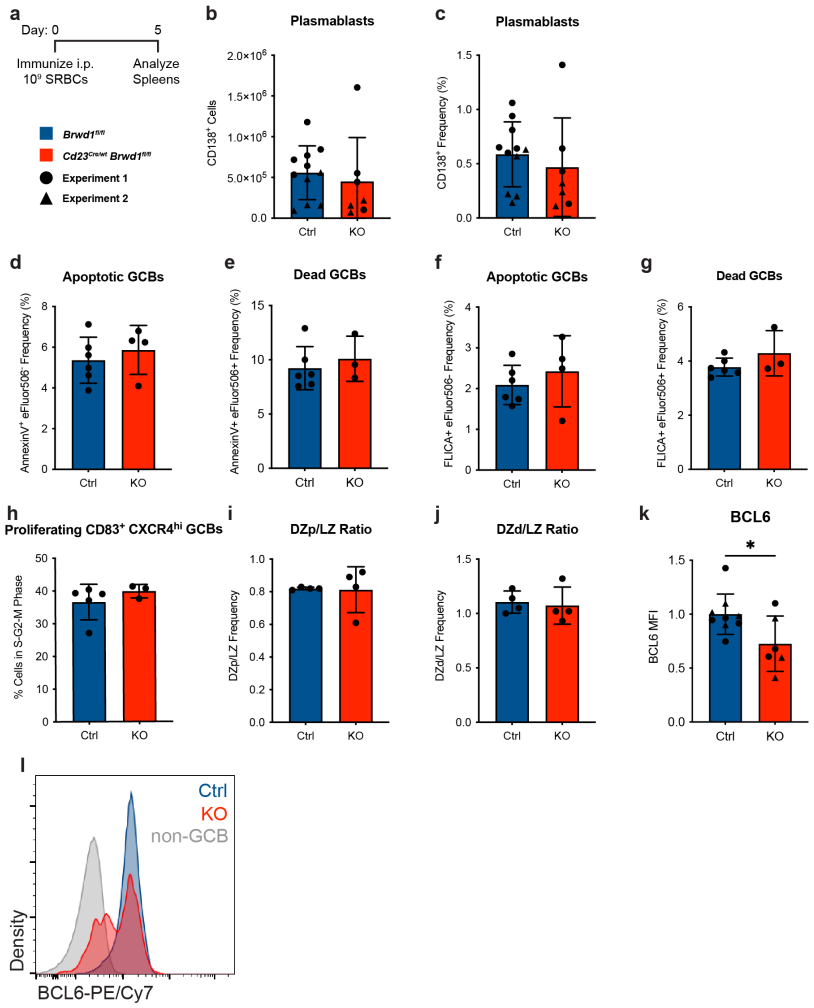

Figure 3.8: Deletion of *Brwd1* in follicular B cells results in decreased BCL6 expression in germinal center B cells. (a) $Cd23^{Cre/wt}$ $Brwd1^{fl/fl}$ (KO) and $Brwd1^{fl/fl}$ (Ctrl) mice were immunized intraperitoneally (i.p.) with 10^9 sheep red blood cells (SRBCs), and spleens were collected at day 5 post-immunization. **(b-c)** Total number (b) and frequency (c) of $CD138^+$ plasmablasts (Ctrl n = 11 mice, KO n = 7 mice). **(d)** Frequency of apoptotic $AnnexinV^+eFluor506^-$ GC B cells. Data is gated on $B220^+CD95^+GL7^+$ cells (Ctrl n = 6 mice, KO n = 4 mice). **(e)** Frequency of dead $AnnexinV^+eFluor506^+$ GC B cells. **(f)** Frequency of apoptotic $FLICA^+eFluor506^-$ GC B cells. **(g)** Frequency of dead $FLICA^+eFluor506^+$ GC B cells. **(h)** Frequency of $DAPI^{high}CD83^{high}CXCR4^{high}$ DZp GC B cells (Ctrl n = 5 mice, KO n = 3 mice). **(i-j)** Ratios of DZp frequency to LZ frequency (i) and of DZd frequency to LZ frequency (j) (Ctrl n = 4 mice, KO n = 4 mice). **(k)** Median fluorescence intensity (MFI) of BCL6 in GC B cells. Control data was normalized to 1 to account for voltage differences between flow cytometry experiments (Ctrl n = 9 mice, KO n = 6). **(l)** Representative histogram of BCL6 intensity in Ctrl and KO GC B cells and in non-GC $B220^+CD95^-GL7^-$ B cells. (*$p<0.05$, two-sided unpaired t-test, bar plots show mean ± standard deviation)

cultured Fol B cells *in vitro* with IL-4 and TGFβ to induce class switching to IgG1. tdT^{+} cells from KO mice had decreased switching to IgG1 compared to controls (Fig 3.9b). tdT^{-} from KO mice had no change in IgG1 class switching *in vitro*, demonstrating that *Brwd1* plays a cell-intrinsic role in CSR (Fig 3.9b).

CSR requires precise chromatin loop extrusion across the class switch locus (Zhang et al., 2022, 2019a). During B cell development, a loop across the entire locus is established that brings together the 5′ iEμ enhancer and the 3′ *Igh* regulatory region (Fig 3.9d), and this loop is maintained in naïve Fol B cells (Zhang et al., 2019a). Upon antigenic stimulation, secondary loops form to bring the switch regions of alternative isotypes into proximity with the Sμ switch region. Because BRWD1 regulates cohesin to modulate chromatin looping, we measured BRWD1 and components of the cohesin complex at the class switch locus (Mandal et al., 2024). Chromatin immunoprecipitation followed by sequencing (ChIP-seq) revealed that in small pre-B cells, BRWD1 binds at multiple sites within the *Igh* locus, with an especially strong peak at iEμ (Fig 3.9e). In WT cells, we observed a dynamic cohesin complex containing NIPBL and WAPL at the 3′ end of the locus (Fig 3.9e, highlighted green). In *Brwd1*$^{-/-}$ small pre-B cells, the 3′ dynamic cohesin complex was lost and instead static cohesin was found at the 3′ CTCF sites (highlighted yellow). Invariant cohesin complexes at CTCF sites (highlighted red) were also observed throughout the locus. This loss of the dynamic cohesin complex was associated with decreased Hi-C contacts and decreased looping across the locus (Fig 3.9e-f). Thus, BRWD1 binds at and is necessary for chromatin looping across the class switch locus during B cell development.

In *Brwd1*$^{-/-}$ small pre-B cells, the loss of looping resulted in decreased *Ighm* expression compared to WT small pre-B cells (Fig 3.9g). However, naïve Fol B cells in *Cd23*$^{Cre/wt}$ *Brwd1*$^{fl/fl}$ mice had no difference in *Ighm* expression (Fig 3.9h). Thus, deletion of *Brwd1* in naïve Fol B cells likely does not disrupt looping of the class switch locus in these cells. Instead, the effects of *Brwd1* deletion are realized upon B cell activation.

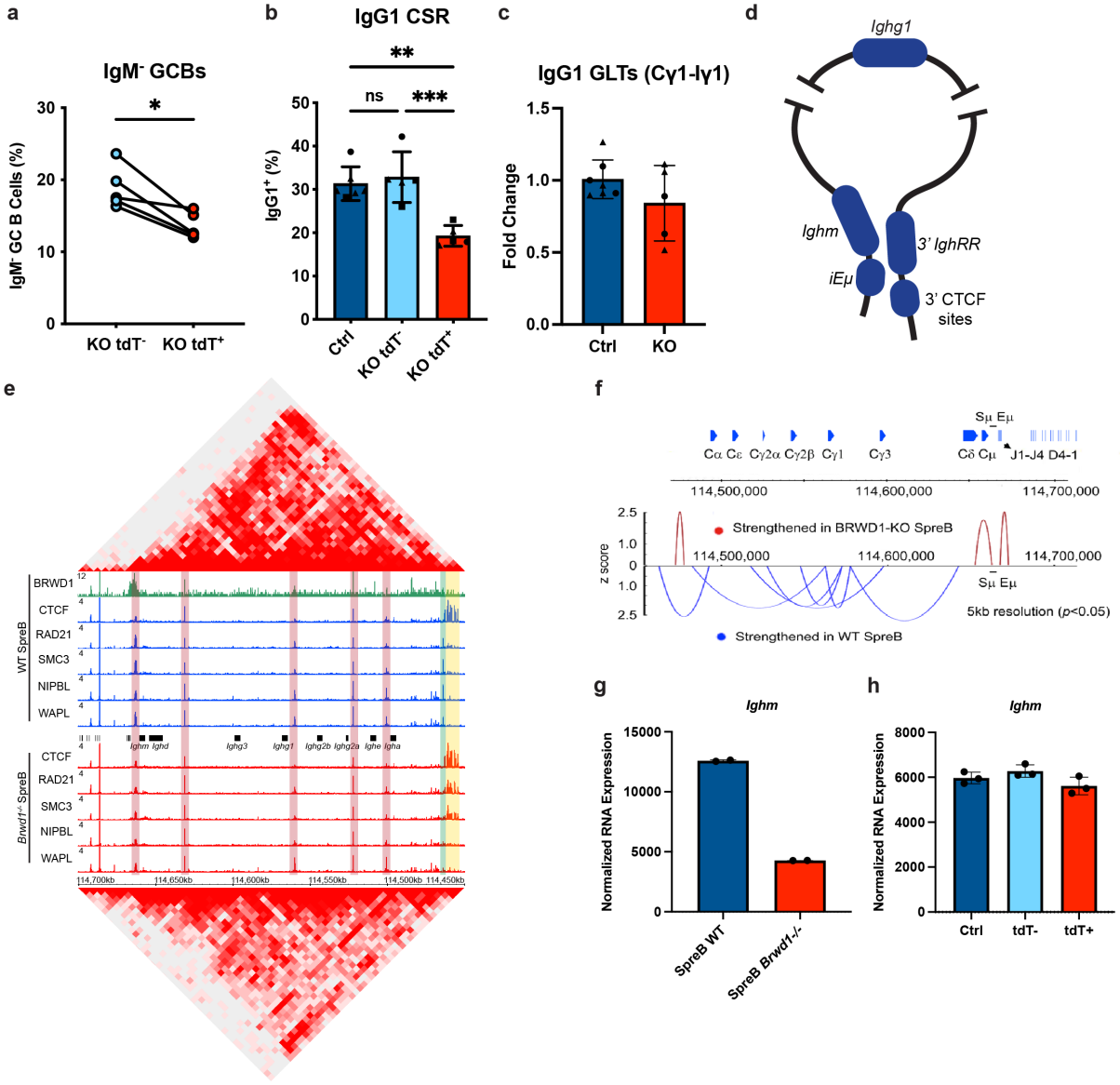

Figure 3.9: BRWD1 enhances class switch recombination. **(a)** Frequency of IgM$^-$ cells after gating on tdT$^-$ or tdT$^+$ GC B cells. *Cd23*$^{Cre/wt}$ *Brwd1*$^{fl/fl}$ (KO) mice were immunized intraperitoneally with sheep red blood cells at days 0 and 5. Spleens were analyzed day 14 post-immunization. **(b)** *In vitro* class switching to IgG1. Splenic B cells were cultured for 96 hours with LPS and IL-4, and class switching was measured by flow cytometry (Ctrl n = 6 mice, KO n = 5 mice). **(c)** Fold change of IgG1 germline transcripts (GLTs) measured by qPCR of the Cγ1-Iγ1 region. KO includes both tdT$^-$ and tdT$^+$ cells. **(d)** Model of chromatin looping between the 5′ iEμ enhancer and the 3′ *Igh* regulatory region (*Igh*RR) at the class switch locus. *Caption continued on the next page.*

Figure 3.9: **(e)** Hi-C heatmap, ChIP-seq tracks for BRWD1, CTCF, RAD21, SMC3, NIPBL, and WAPL in WT (top) and *Brwd1*$^{-/-}$ (bottom) small pre-B cells (SpreB). Analysis of data sets previously published (Mandal et al., 2024). The dynamic cohesin complex is highlighted green, the static cohesin complex is highlighted yellow, and invariant cohesin complexes at CTCF sites are highlighted red. Data is representative of n = 2 data sets. **(f)** Arc plots indicating strengthened Hi-C interactions ($p < 0.05$) in WT or *Brwd1*$^{-/-}$ small pre-B cells across the class switch locus at 5 kb resolution. **(g-h)** RNA-seq expression of *Ighm* expression in WT and *Brwd1*$^{-/-}$ small pre-B cells (g) and Fol B cells (h). ($*p<0.05$, $**p<0.01$, $***p<0.001$, two-sided unpaired t-test, bar plots show mean ± standard deviation)

We next tested whether BRWD1 is important for the formation of secondary class switch loops upon antigenic stimulation. Following *in vitro* CSR to IgG1, we measured IgG1 germline transcripts (GLTs), which are transcribed when the IgG1 promoter forms a loop to contact the iEμ enhancer. We observed no significant difference in GLTs in the KO cells (Fig 3.9c). However, tdT$^+$ and tdT$^-$ cells were not separated for this experiment. These results suggest that although BRWD1 is necessary for the first loop formation at the class switch locus during development, the decrease in CSR is not due to a decrease in secondary loop formation in Fol B cells, although more experiments are necessary.

In total, BRWD1 binds at and is necessary for chromatin looping across the class switch locus during B cell development. These data suggest that the BRWD1-dependent chromatin topology established in small pre-B cells is necessary for efficient CSR upon Fol B cell activation.

3.2.7 BRWD1 establishes epigenetic states for germinal center initiation

We next studied whether *Brwd1* deletion affects the transcriptional or epigenetic states of resting Fol B cells. We first sorted tdT$^+$ and tdT$^-$ cells from KO mice and performed RNA-seq. tdT$^+$ and tdT$^-$ Fol B cells clustered with Fol B cells from control mice by principal component analysis (PCA) when compared with WT GC B cells (Fig 3.10a). Fol B cells were also highly similar by a Pearson correlation (Fig 3.10b). Only 17 genes ($\log_2$FC > 1,

$q < 0.05$) were differentially expressed between tdT$^+$ Fol B cells and control Fol B cells from *Brwd1*$^{fl/fl}$ mice (Fig 3.10c). tdT$^+$ and tdT$^-$ Fol B cells also had few differentially expressed genes (Fig 3.10d). These results demonstrate that deletion of *Brwd1* in Fol B cells has minimal transcriptional effects. Notably, *Brwd1* expression was decreased in tdT$^-$ Fol B cells relative to controls (Fig 3.10e). This suggests that tdT$^-$ Fol B cells are not an adequate control relative to tdT$^+$ Fol B cells for molecular comparisons.

To determine whether loss of BRWD1 affects the chromatin accessibility of Fol B cells, we performed ATAC-seq. By PCA, tdT$^+$ Fol B cells from KO mice clustered separately from both WT Fol B cells and GC B cells (Fig 3.10f). Chromatin accessibility was more different across Fol B cell populations than the differences observed in transcription (Fig 3.10g, note scale).

When we compared differential chromatin accessibility peaks ($\log_2$FC > 1, $q < 0.05$) between tdT$^+$ and WT Fol B cells, we observed 1,956 peaks increased in WT and 2,141 peaks increased in *Brwd1*$^{-/-}$ Fol B cells (Fig 3.10h). Interestingly, the accessibility of many of these peaks in WT Fol B cells matched the accessibility in GC B cells, suggesting that the accessibility of these sites is maintained by BRWD1 as Fol B cells differentiate into GC B cells. TF motif accessibility was altered between WT and *Brwd1*$^{-/-}$ Fol B cells for TFs important in B cell differentiation (Fig 3.10i). For example, binding sites for OCT2, which prepares and facilitates Fol to GC B cell differentiation programs, were more accessible in WT Fol B cells (Doane et al., 2021; Song et al., 2021; Hodson et al., 2016). Conversely, accessibility at ETS family binding sites, which can restrain B cell activation and differentiation programs, were increased in *Brwd1*$^{-/-}$ Fol B cells (Sunshine et al., 2019; Luo et al., 2014; Willis et al., 2017; Bonetti et al., 2013). Accessibility at IRF4 and 8 binding sites, which regulate activated B cell differentiation programs were also increased in *Brwd1*$^{-/-}$ Fol B cells (Xu et al., 2015; Ochiai et al., 2013). These results suggest that in Fol B cells BRWD1 primes genomic accessibility for transition to the GC state following antigen stimulation. Together

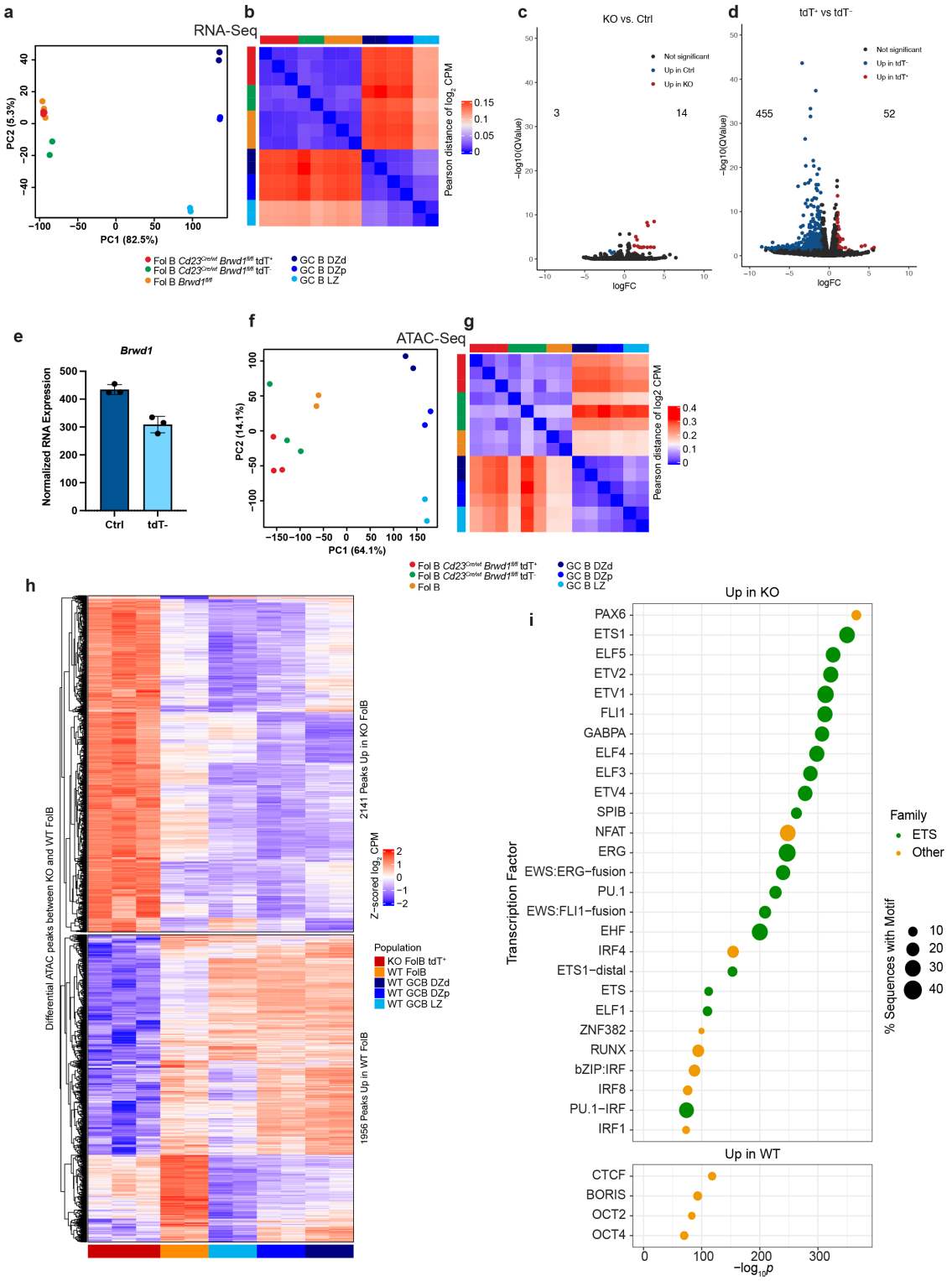

Figure 3.10: BRWD1 determines genomic accessibility in resting follicular B cells. *Caption continued on the next page.*

Figure 3.10: **(a)** PCA plot of RNA-seq from *Cd23*$^{Cre/wt}$ *Brwd1*$^{fl/fl}$ tdT$^+$ Fol B cells (KO tdT$^+$), *Cd23*$^{Cre/wt}$ *Brwd1*$^{fl/fl}$ tdT$^-$ Fol B cells (KO tdT$^-$), *Brwd1*$^{fl/fl}$ Fol B cells (Ctrl), and WT GC B cell subsets (KO tdT$^+$ Fol B n = 3 mice, KO tdT$^-$ Fol B n = 3 mice, Ctrl Fol B n = 3 mice). WT GC B cell RNA-seq (n = 2 for each cell population) was previously published (Kennedy et al., 2020). **(b)** Pearson correlation heatmap of RNA-seq from listed populations. **(c)** Volcano plot of differentially expressed genes ($q < 0.05$, $\log_2$ fold change > 1) between tdT$^+$ *Cd23*$^{Cre/wt}$ *Brwd1*$^{fl/fl}$ (KO) and *Brwd1*$^{fl/fl}$ (Ctrl) Fol B cells. **(d)** Volcano plot of differentially expressed genes ($q < 0.05$, $\log_2$ fold change > 1) between tdT$^+$ and tdT$^-$ Fol B cells from *Cd23*$^{Cre/wt}$ *Brwd1*$^{fl/fl}$ mice. **(e)** *Brwd1* expression in Ctrl and KO tdT$^-$ Fol B cells. **(f)** PCA plot of ATAC-seq from *Cd23*$^{Cre/wt}$ *Brwd1*$^{fl/fl}$ tdT$^+$ Fol B cells (KO tdT$^+$), *Cd23*$^{Cre/wt}$ *Brwd1*$^{fl/fl}$ tdT$^-$ Fol B cells (KO tdT$^-$), WT Fol B cells (Ctrl), and WT GC B cell subsets (KO Fol B n = 3 mice, Ctrl Fol B n = 2 mice). WT GC B cell ATAC-seq (n = 2 for each cell population) was previously published (Kennedy et al., 2020). **(g)** Pearson correlation heatmap of ATAC-seq from listed populations. Note scale differences between g and b. **(h)** Heatmap of differential accessibility peaks ($q < 0.05$, $\log_2$ fold change > 1) between tdT$^+$ *Cd23*$^{Cre/wt}$ *Brwd1*$^{fl/fl}$ and WT Fol B cells. Accessibility by ATAC-seq is shown for listed populations. **(i)** TF motifs enriched in accessible regions up in KO (top) or WT (bottom) Fol B cells generated using HOMER. TF motifs in the ETS family, which have similar binding sequences, are shown in green, while all other TF motifs are in orange. TF motifs with $p < 10^{-30}$ are shown.

these results suggest that BRWD1 regulates accessibility at some sites in Fol B cells that are important for Fol B cell differentiation into GC B cells.

3.3 Discussion

3.3.1 Brwd1-floxed mouse model

Here we describe a *Brwd1*-floxed mouse model used to delete *Brwd1* in different B cell populations. By inserting a tdTomato fluorescent reporter that is only expressed following Cre recombination, we were able to track and confirm *Brwd1* deletion. RNA-seq revealed that deletion of *Brwd1* exons 6, 7, and 8 was specific to tdT$^+$ cells. Interestingly, we still detected normal levels of transcripts containing *Brwd1* exons downstream of exon 8. We have not tested whether any of these transcripts are translated. We also confirmed that homozygous *Brwd1*-floxed mice delete both *Brwd1* alleles. Because none of the various

mouse models we used deleted *Brwd1* in all targeted cells, the tdTomato reporter allowed us to sort *Brwd1*$^{-/-}$ cells for bulk sequencing experiments.

3.3.2 BRWD1 in B cell progenitors

Deletion of *Brwd1* in B cell progenitors using *Mb1*^{Cre} mice resulted in decreased B cell progenitors beginning with the large pre-B cell stage of development. In contrast, *Brwd1*$^{-/-}$ mice, which have a germline mutation in *Brwd1*, have fewer B cell progenitors beginning with the immature B cell stage of development (Mandal et al., 2015). It is unclear why *Mb1*$^{Cre/wt}$ *Brwd1*$^{fl/fl}$ mice have decreased cell numbers earlier in B cell development than *Brwd1*$^{-/-}$ mice. Prior experiments in *Brwd1*$^{-/-}$ mice had a non-significant decrease in small pre-B cells and used fewer mice per group, suggesting that more replicates would reveal decreased small pre-B cells in this mouse model. Furthermore, *Brwd1*$^{-/-}$ mice were originally derived on the C3HeB/FeJ background and were crossed with C57BL/6J mice for four generations. Thus, differences in the cellular phenotype may be strain specific. Differences may also be due to the age of mice used for different experiments as bone marrow cell numbers decrease with age. Our experiments with *Mb1*$^{Cre/wt}$ *Brwd1*$^{fl/fl}$ mice used *Brwd1*$^{fl/fl}$ littermates to control for effects from age. Furthermore, *Brwd1* expression increases as cells transition between the large pre-B and small pre-B stages of development. However, *Brwd1* is still expressed in pro-B cells, so it is not surprising that *Brwd1* deletion decreases cell number in large pre-B cells. Lastly, we did not characterize whether small pre-B cells from *Mb1*$^{Cre/wt}$ *Brwd1*$^{fl/fl}$ mice have decreased *Igk* recombination as has been characterized in *Brwd1*$^{-/-}$ mice. Considering the cellular phenotype, we would predict a similar molecular phenotype between *Mb1*$^{Cre/wt}$ *Brwd1*$^{fl/fl}$ and *Brwd1*$^{-/-}$ mice.

Mb1$^{Cre/wt}$ *Brwd1*$^{fl/fl}$ and *Brwd1*$^{-/-}$ mice also had different phenotypes in splenic B cell populations. *Mb1*$^{Cre/wt}$ *Brwd1*$^{fl/fl}$ mice had no difference in mature Fol B cell numbers, demonstrating that the developmental defect in the bone marrow is compensated for by the

time B cells fill peripheral niches. The spatial organization of B cell follicles and T cell zones was also normal. Meanwhile, *Brwd1*$^{-/-}$ mice had decreased splenic mature Fol B cells and no T cell zones neighboring B cell follicles (Mandal et al., 2015). These results suggest that *Brwd1* is important for other cell types such as T cells. Indeed, *Brwd1* is expressed in the T cell lineage.

3.3.3 BRWD1 in germinal center initiation

We also crossed *Brwd1*-floxed mice with *Cd23*^{Cre} mice to delete *Brwd1* in Fol B cells. In agreement with results from *Mb1*$^{Cre/wt}$ *Brwd1*$^{fl/fl}$ mice, BRWD1 was not important for maintenance of peripheral Fol B cell populations in *Cd23*$^{Cre/wt}$ *Brwd1*$^{fl/fl}$ mice despite *Brwd1* being highly expressed. It is possible that additional compensatory mechanisms exist, such as the similar proteins PHIP and BRWD3, that allow resting Fol B cells to survive without BRWD1. Additionally, it is unlikely that Fol B cells require the same degree of epigenetic regulation when resting as compared to small pre-B cells undergoing light chain rearrangement or activated B cells differentiating and performing CSR.

While *Cd23*$^{Cre/wt}$ *Brwd1*$^{fl/fl}$ mice successfully deleted *Brwd1* in Fol B cells, we do not know whether BRWD1 protein remains bound to DNA in Fol B cells in this mouse model. It is possible that a low turnover rate of BRWD1 protein or its stability on chromatin allow BRWD1 to remain in resting Fol B cells despite genetic deletion at this cell stage. There is no good antibody to detect BRWD1 by Western blot, and ChIP-seq of BRWD1 is lower quality than ChIP-seq of other chromatin factors. *Brwd1* expression greatly increases in Fol B cells relative to small pre-B cells. Thus, we predict that BRWD1 binds the same sites in Fol B cells as in small pre-B cells as well as additional Fol B cell-specific sites. If BRWD1 remains present in the Fol B cells of *Cd23*$^{Cre/wt}$ *Brwd1*$^{fl/fl}$ mice, then we would predict that BRWD1 only remains at the binding sites established in small pre-B cells.

Rather than being important for maintenance of Fol B cells, we observed that BRWD1

is instead important following B cell activation as B cells differentiate into GC B cells (Fig 3.11). We observed a decreased GC response by both flow cytometry and immunofluorescence microscopy day 14 post-immunization. Furthermore, a two-fold decrease in GC B cells 5 days after immunization showed a defect in GC initiation in these mice. At this time point, we observed decreased BCL6 in GC B cells due to more cells with intermediate BCL6 expression. Because GC B cell precursors express intermediate BCL6, these results suggest a partial block in GC B cell differentiation in these mice (Zhang et al., 2017b). These results are consistent with prior work on BRWD1 in B cell development where BRWD1 is important during transitions between cell states and prepares cells for the next stage of differentiation (Mandal et al., 2018, 2015). Furthermore, the differentiation of Fol B cells into GC B cells requires large shifts in chromatin accessibility and chromatin compartments (Vilarrasa-Blasi et al., 2021; Doane et al., 2021). The proliferative burst following activation may dilute any remaining BRWD1 protein following conditional deletion or any compensatory homologs such as PHIP or BRWD3.

GC B cells also experience large shifts in chromatin accessibility as they transition between different subpopulations (Kennedy et al., 2020). By deleting *Brwd1* prior to GC initiation, we were unable to observe how and whether BRWD1 is important within the GC reaction. Furthermore, we did not observe a complete block in GC initiation, with some GCs still forming. This suggests that loss of *Brwd1* has additional effects once cells have completed differentiation into GC B cells, which is further examined in the next chapter.

Deletion of BRWD1 in Fol B cells suggests that it facilitates molecular transitions rather than maintains cell states. Indeed, BRWD1 did not substantially contribute to the transcriptional state of Fol B cells. However, greater differences were observed when comparing chromatin accessibility by ATAC-seq. Remarkably, this differential chromatin accessibility between *Brwd1*$^{-/-}$ and WT Fol B cells predicted later chromatin accessibility across GC B cell subsets. Furthermore, changes in chromatin accessibility opened different TF binding

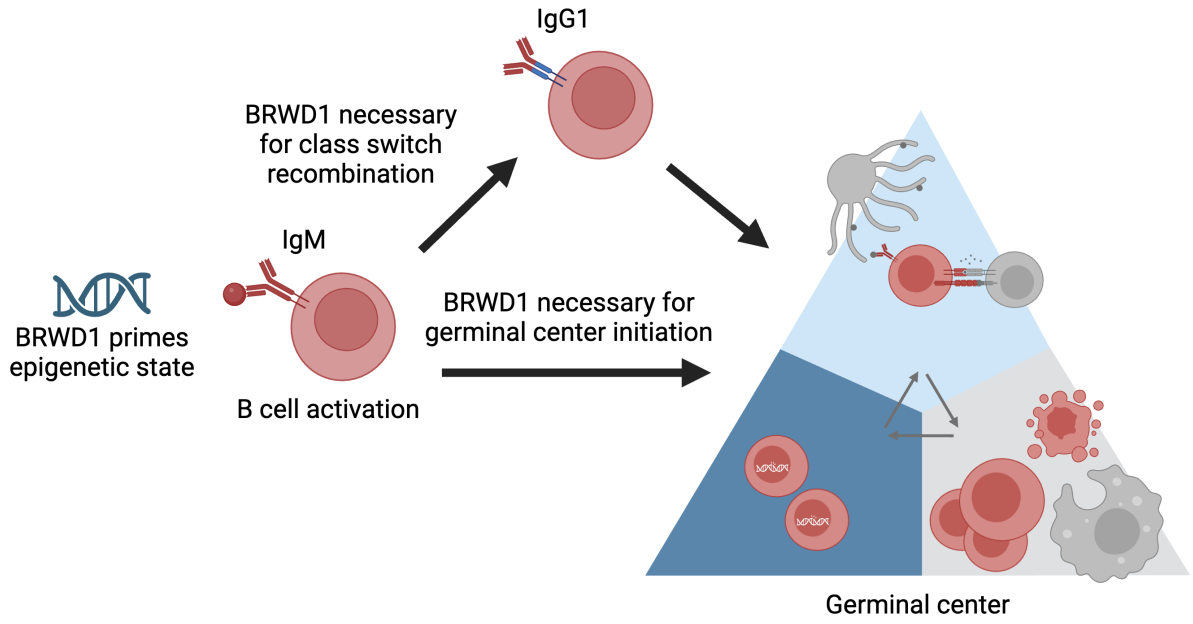

Figure 3.11: Model of BRWD1 in follicular B cells. We propose that BRWD1 primes the epigenetic landscape of follicular B cells prior to activation; however, BRWD1 is not required for the maintenance of follicular B cells at the steady state. Following antigen-induced activation, BRWD1 is necessary for follicular B cells to differentiate into germinal center B cells. BRWD1 is also necessary for activated B cells to perform class switch recombination. This figure was created using BioRender.com.

motifs in Fol B cells that are important in later B cell differentiation. For example, chromatin accessibility sites up in WT Fol B cells were enriched for the OCT2 binding motif. OCT2 binding in naïve Fol B cells is necessary for later changes in chromatin accessibility observed as activated B cells differentiate into GC B cells (Doane et al., 2021). Meanwhile, chromatin accessibility sites up in *Brwd1*$^{-/-}$ Fol B cells were enriched for ETS family binding sites, which restrain B cell activation and differentiation programs (Sunshine et al., 2019; Luo et al., 2014; Willis et al., 2017; Bonetti et al., 2013). These results are consistent with prior work in B cell development where BRWD1 mediates transitions between cell states by priming cells for the next stage of differentiation (Mandal et al., 2015, 2018). Indeed, our data support a general model that throughout the B cell lineage the opening and closing of TF motifs precede cellular differentiation (Okoreeh et al., 2022).

3.3.4 BRWD1 in class switch recombination

We previously characterized how BRWD1 converts static cohesin, consisting of the core cohesin subunits RAD21 and SMC3, to a dynamic cohesin complex that includes the core cohesin ring co-incident with the cofactors NIPBL and WAPL (Mandal et al., 2024). The functions of NIPBL and WAPL are opposite one another. NIPBL mediates chromatin loop extrusion while WAPL restricts loop extrusion to allow cohesin recycling (Bauer et al., 2021; Haarhuis et al., 2017; Liu et al., 2021). Furthermore, the protein structure of the core cohesin ring does not allow binding of both NIPBL and WAPL (Gligoris and Löwe, 2016). Thus, the exact conformation of how cohesin, NIPBL, and WAPL interact with one another is unknown. However, bulk ChIP-seq shows that all of these proteins bind the same chromatin sites, and that the presence of these peaks correlates with long-range chromatin contacts as measured by Hi-C (Mandal et al., 2024).

In addition to preparing the epigenetic landscape for GC differentiation, BRWD1 enabled CSR by remodeling the 3D organization of the class switch locus. CSR requires chromatin

looping across the class switch locus, and this loop is established during B cell development (Wuerffel et al., 2007). Using *Brwd1*$^{-/-}$ mice, we showed by ChIP-seq that *Brwd1* is necessary for a dynamic cohesin complex within the loop and that loss of this complex was associated with decreased Hi-C chromatin contacts. These results demonstrate that cohesin conversion is a major mechanism behind looping of the class switch locus (Mandal et al., 2024).

However, cohesin conversion at the class switch locus differed from other loci. First, the dynamic cohesin complex was close (<5 kb) to the 3′ CTCF sites that static cohesin builds up at in *Brwd1*$^{-/-}$ mice. In contrast, many other loci have multiple dynamic cohesin complexes that are located further from CTCF sites and loop boundaries. Second, BRWD1 bound at the 5′ end of the locus, opposite the 3′ static and dynamic cohesin complexes. If BRWD1 converts static to dynamic cohesin, then we would expect all of these complexes to be proximal to one another. One possibility is that BRWD1 converts distant cohesin on the same chromosome if static cohesin is within genomic distances accessible by diffusion. Alternatively, it is possible that the initial loop forms through a different unknown mechanism. Then once the loop is established, BRWD1 and the cohesin complex are proximal and BRWD1 can maintain the loop through cohesin conversion.

It is unclear how loss of BRWD1 in *Cd23*$^{Cre/wt}$ *Brwd1*$^{fl/fl}$ mice decreases class switching. Normal expression of *Ighm* in resting Fol B cells suggested that this loop is maintained prior to activation, consistent with the results described above in resting Fol B cells. However, it is possible that upon activation BRWD1 is no longer able to maintain the loop. A second possibility is that following activation the loop is maintained and BRWD1 is instead important for secondary loop formation whereby alternative heavy chain constant regions are pulled into the recombination center. Finally, it is also unknown whether BRWD1 is necessary for class switching to other immunoglobulin isotypes.

CHAPTER 4

BRWD1 IN GERMINAL CENTER B CELLS

4.1 Introduction

GCs form in secondary lymphoid tissues in response to immunogens and are where GC B cells undergo affinity maturation. We previously demonstrated that a three-zone model of the GC accurately describes the three major functions within the GC and reveals molecular mechanisms regulating GC B cells (Kennedy et al., 2020; Wright et al., 2023). First in the light zone (LZ), GC B cells pick up antigen found on follicular dendritic cells (FDCs) and subsequently present this antigen to T follicular helper cells (Tfh) cells. Second in the Dark Zone proliferation (DZp), B cells undergo mitosis or apoptosis adjacent to tingible body macrophages (TBMs). Third in the Dark Zone differentiation (DZd), B cells perform somatic hypermutation (SHM). GC B cells can exit the GC by differentiating into memory B cells (MBCs) or plasma cells (PCs). We previously demonstrated that GC B cells from each of the three zones have large differences in transcription and chromatin accessibility (Kennedy et al., 2020). Thus, a three-zone model spatially separates the three primary functions within the germinal center while revealing large differences in the molecular programs of each zone. However, it was unclear how and whether these molecular differences were important for GC biology.

In the previous chapter, we used $Cd23^{Cre/wt}$ $Brwd1^{fl/fl}$ mice to demonstrate that BRWD1 is important for initiation of the GC response by deleting *Brwd1* in Fol B cells. The differentiation of naïve B cells into GC B cells includes multiple stages over approximately four days, and this differentiation is different from the cycling between zones of mature GC B cells. Thus, to study the role of BRWD1 in fully differentiated GC B cells, we used $Aicda^{Cre/wt}$ $Brwd1^{fl/fl}$ mice to delete *Brwd1* in GC B cells. Here we demonstrate that loss of *Brwd1* results in a striking loss of molecular differences between GC zones in the

three-zone model. This causes a loss of specific functions within the GC, namely control of proliferation, affinity maturation, and tolerance. These results demonstrate that the large molecular differences revealed by the three-zone model are maintained by BRWD1 and are necessary for GC function. Furthermore, these results and previous studies (Mandal et al., 2018, 2024) indicate that at multiple stages, BRWD1 orchestrates B cell transitions between proliferation and states in which DNA is recombined or mutated to generate diversity and shape immune responses to infection.

4.2 Results

4.2.1 BRWD1 restrains germinal center B cell proliferation

While BRWD1 was important for GC initiation, it is also expressed in GC subsets and therefore may have additional roles once B cells have fully differentiated into GC B cells. To study this, we crossed the *Brwd1*-floxed mice with *Aicda*^{Cre} mice to delete *Brwd1* in GC B cells approximately 4 days post-immunization once GCs had begun to form (Kerfoot et al., 2011; Silva and Klein, 2015; Crouch et al., 2007). We immunized *Aicda*$^{Cre/wt}$ *Brwd1*$^{fl/fl}$ mice and control *Brwd1*$^{fl/fl}$ mice and analyzed spleens after 14 days (Fig 4.1a-b). We observed no significant difference in the total number of B220^{+} B cells in *Aicda*$^{Cre/wt}$ *Brwd1*$^{fl/fl}$ mice compared with controls (Fig 4.1c). However, there was a significant increase in the total number and frequency of GC B cells in the *Aicda*$^{Cre/wt}$ *Brwd1*$^{fl/fl}$ mice (Fig 4.1d-e). In the *Aicda*$^{Cre/wt}$ *Brwd1*$^{fl/fl}$ mice, 80% of GC B cells had deleted *Brwd1* as shown by tdT expression (Fig 4.1f), and this frequency was consistent across GC B cell subsets (Fig 4.2a). tdT MFI varied across the three GC subsets, with the greatest tdT expression in the LZ (Fig 4.2b-c). The increase in GC B cell number was observed across each of the three GC subsets (Fig 4.1g), with minimal changes in the relative proportion of cells within each GC subset as measured by the DZd/LZ and DZp/LZ ratios (Fig 4.1h-i). Similar results were observed

in heterozygous *Aicda*$^{Cre/wt}$ *Brwd1*$^{fl/wt}$ mice (Fig 4.3a-e). As a control, *Aicda*$^{Cre/wt}$ mice had the same GC B cell frequency as *Brwd1*$^{fl/fl}$ mice, demonstrating that the GC defect observed in *Aicda*$^{Cre/wt}$ *Brwd1*$^{fl/fl}$ mice was not due to *Aicda* haploinsufficiency (Fig 4.3h). In total, both *Brwd1* deletion and *Brwd1* haploinsufficiency are sufficient to alter GC B cell numbers.

We next examined the Tfh cell compartment. The number and frequency of CD3^{+}CD4^{+} CXCR5^{+}PD-1^{+} Tfh cells were significantly increased in *Aicda*$^{Cre/wt}$ *Brwd1*$^{fl/fl}$ mice (Fig 4.1j-k). The frequency of GC B cells strongly correlated with the frequency of Tfh cells within each spleen (Fig 4.1l). These results are consistent with the increase in GC B cells, because increased antigen presentation to Tfh cells results in greater Tfh cell proliferative expansion (Merkenschlager et al., 2021). This suggests that antigen presentation in *Brwd1*$^{-/-}$ GC B cells is intact.

To determine whether *Brwd1*$^{-/-}$ GC B cells were undergoing greater proliferation, we stained cells with DAPI to measure the proportion of cells in the S, G2, or M phases of the cell cycle. When gated on total GC B cells, *Aicda*$^{Cre/wt}$ *Brwd1*$^{fl/fl}$ mice had a greater proportion of proliferating GC B cells (Fig 4.1m). In prior work, we demonstrated that the CXCR4$^{\text{high}}$CD83$^{\text{high}}$ DZp population within the GC is where GC B cells undergo mitosis, and that expression of both surface markers positively correlates with DNA content (Kennedy et al., 2020). Gating on this CXCR4$^{\text{high}}$CD83$^{\text{high}}$ DZp population showed an increase in proliferating cells in *Aicda*$^{Cre/wt}$ *Brwd1*$^{fl/fl}$ mice compared to controls (Fig 4.1n-o). CXCR4^{+}CD83^{-} DZd GC B cells also had greater proliferation, suggesting a blending of proliferative programs throughout the GC, although most proliferation was still confined to the DZp (Fig 4.2d-e). Finally, differences in GC B cell numbers were not due to differences in cell viability (Fig 4.2f). These results demonstrate that BRWD1 represses proliferation in GC B cells, consistent with BRWD1's role as a *Myc* repressor in small pre-B cells (Mandal et al., 2018).

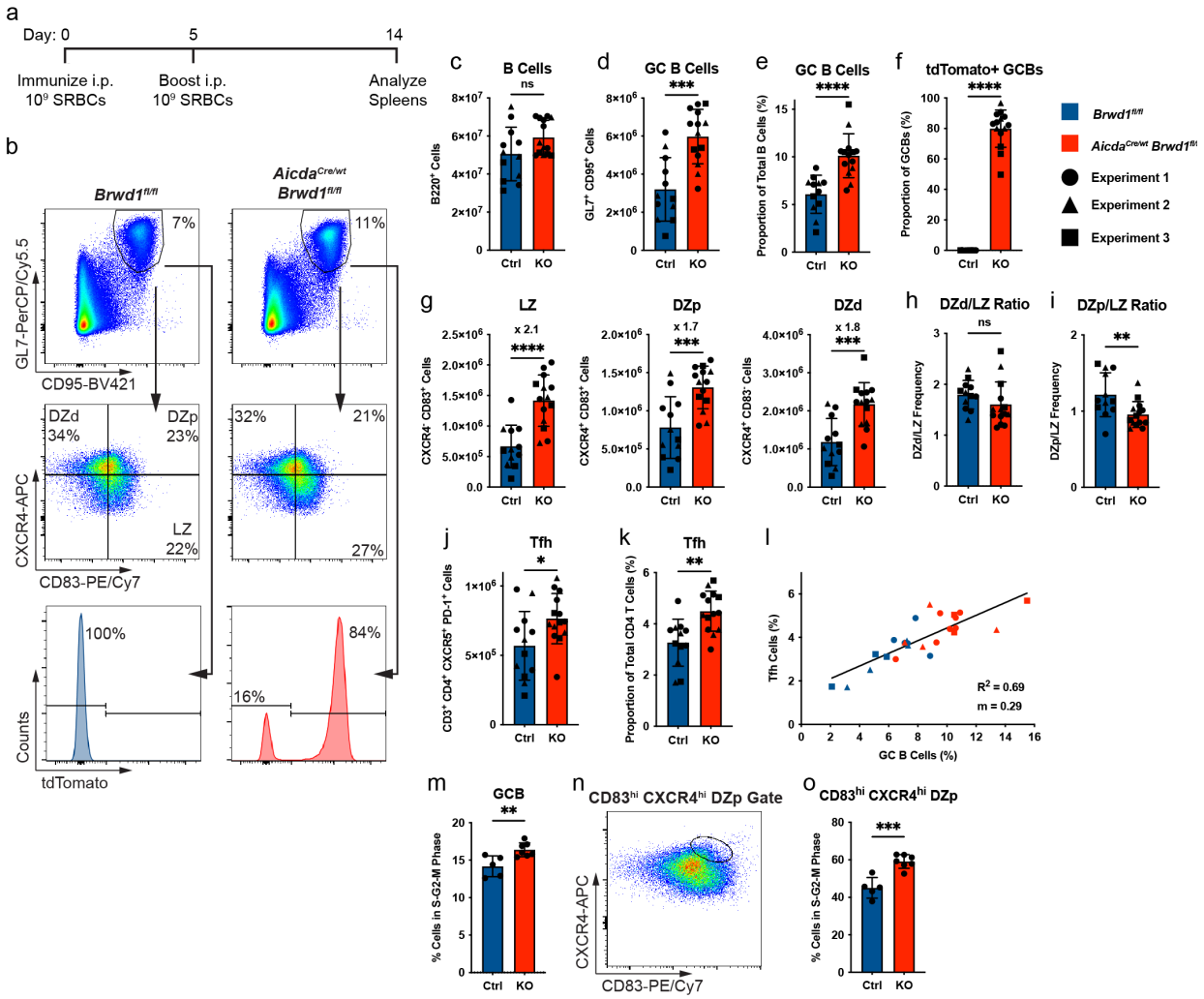

Figure 4.1: BRWD1 restrains proliferation in germinal center B cells. **(a)** *Aicda*$^{Cre/wt}$ *Brwd1*$^{fl/fl}$ (KO) and *Brwd1*$^{fl/fl}$ (Ctrl) mice were immunized intraperitoneally (i.p.) with 10^9 sheep red blood cells (SRBCs) at days 0 and 5. Spleens were collected at day 14 post-immunization (Ctrl n = 12 mice, KO n = 14 mice). **(b)** Representative flow plots first gated on B220$^+$ cells. **(c)** Total B cell number. **(d-e)** Total number (d) and frequency (e) of GL7$^+$CD95$^+$ GC B cells. **(f)** Proportion of GC B cells expressing tdT. **(g)** Number of LZ, DZp, and DZd GC B cells. **(h)** Ratio of DZd and LZ frequency. **(i)** Ratio of DZp and LZ frequency. **(j-k)** T follicular helper (Tfh) cell number (j) and frequency (k). **(l)** Correlation of GC B cell and Tfh cell frequency. m = slope **(m)** Frequency of proliferating GC B cells in the S, G2, or M phases of the cell cycle as measured by DAPI^{high} frequency (Ctrl n = 5 mice, KO n = 7 mice). **(n)** Flow cytometry gate on CXCR4^{high}CD83^{high} DZp GC B cells. **(o)** Frequency of proliferating CXCR4^{high}CD83^{high} GC B cells. (*p<0.05, **p<0.01, ***p<0.001, ****p<0.0001, two-sided unpaired t-test, bar plots show mean ± standard deviation)

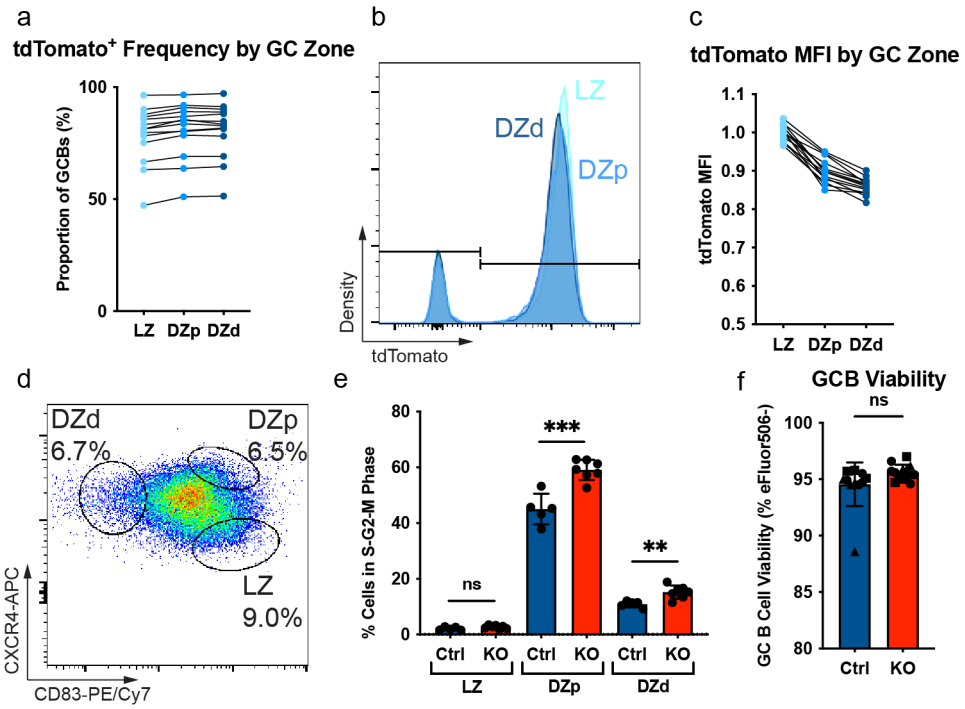

Figure 4.2: BRWD1 restrains DZp and DZd cell proliferation in the germinal center. **(a)** Frequency of tdT^{+} GC B cells across each GC subset of immunized *Aicda*$^{Cre/wt}$ *Brwd1*$^{fl/fl}$ mice. Dots are connected for each mouse (n = 14 mice). **(b)** Representative flow plot of tdT fluorescence. **(c)** tdT median fluorescence intensity (MFI) across each GC subset. MFI was normalized due to differences in flow cytometry voltage settings between 3 independent experiments. **(d)** Flow cytometry gating strategy of LZ, DZp, and DZd GC B cells. Previously gated on B220^{+}GL7^{+}CD95^{+} cells. **(e)** Frequency of proliferating GC B cells in the S, G2, or M phases of the cell cycle as measured by DAPI^{high} frequency (Ctrl n = 5 mice, KO n = 7 mice). **(f)** GC B cell viability measured by the frequency of the viability dye eFluor506^{-} cells (Ctrl n = 12 mice, KO n = 14 mice). (**p<0.01, ***p<0.001, two-sided unpaired t-test, bar plots show mean ± standard deviation)

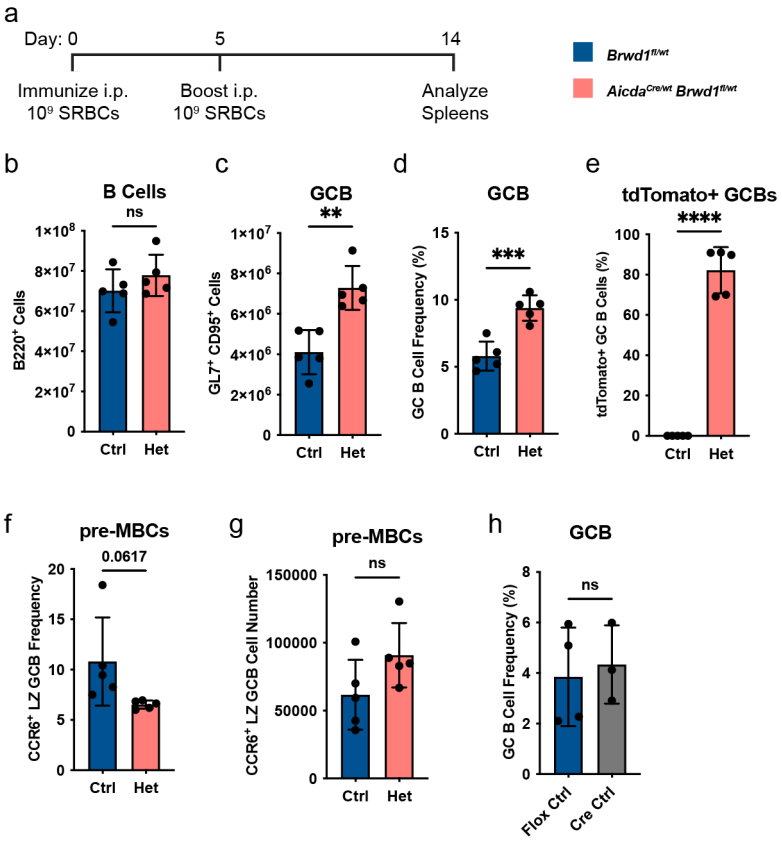

Figure 4.3: Heterozygous *Aicda*$^{Cre/wt}$ *Brwd1*$^{fl/wt}$ mice have a similar phenotype to the complete knockout. **(a)** *Aicda*$^{Cre/wt}$ *Brwd1*$^{fl/wt}$ and *Brwd1*$^{fl/wt}$ mice were immunized with sheep red blood cells (SRBCs) and boosted at day 5. Splenic cells were analyzed at day 14 post-immunization (Ctrl n = 5 mice, Het n = 5 mice). **(b)** Total B cell number. **(c)** Total GC B cell number. **(d)** GC B cell frequency. **(e)** Proportion of GC B cells expressing tdT. **(f-g)** Frequency (f) and number (g) of CCR6^{+}CD83$^{\text{high}}$ pre-MBCs in *Aicda*$^{Cre/wt}$ *Brwd1*$^{fl/wt}$ (Het) and *Brwd1*$^{fl/wt}$ (Ctrl) mice (Ctrl n = 5 mice, Het n = 5 mice). **(h)** GC B cell frequency comparing *Brwd1*$^{fl/fl}$ (Flox Ctrl) and *Aicda*$^{Cre/wt}$ (Cre Ctrl) mice (Flox Ctrl n = 4 mice, Cre Ctrl n = 3 mice). (**p<0.01, ***p<0.001, ****p<0.0001, two-sided unpaired t-test, bar plots show mean ± standard deviation)

4.2.2 BRWD1 restrains germinal center size

We further characterized GC responses by immunofluorescence microscopy of spleen sections from *Aicda*$^{Cre/wt}$ *Brwd1*$^{fl/fl}$ mice. GCs from *Aicda*$^{Cre/wt}$ *Brwd1*$^{fl/fl}$ mice had a normal architecture with distinct light and dark zones (Fig 4.4a). However, GCs from *Aicda*$^{Cre/wt}$ *Brwd1*$^{fl/fl}$ mice were significantly larger (Fig 4.4b). This analysis also revealed that a portion of GCs in *Aicda*$^{Cre/wt}$ *Brwd1*$^{fl/fl}$ mice were twice as large in cross-sectional area as GCs from control mice, with a greater spread in the distribution. There was no significant difference in the number of GCs per spleen area (Fig 4.4c), nor was the ratio of the LZ size to the total GC size different (Fig 4.4d). In agreement with the Tfh flow cytometry data, there was an increase in the CD4 mean pixel intensity within the LZ (Fig 4.4e). As a control, the mean pixel intensity for tdT was greater in the knockout (Fig 4.4f). In summary, *Brwd1* deficiency in GC B cells caused an increase in GC size without affecting GC architecture.

4.2.3 BRWD1 is not required for post-germinal center memory B cells or plasma cells

GC B cells can exit the GC reaction by further differentiating into MBCs or PCs. To determine whether BRWD1 is important for these transitions, we studied the prevalence of MBCs and PCs in the spleens of *Aicda*$^{Cre/wt}$ *Brwd1*$^{fl/fl}$ mice 14 days post-immunization (Fig 4.5a). We observed no significant difference in the number or frequency of B220^{+}CD38^{+}GL7^{-}IgD^{-} MBCs nor of B220$^{\text{int}}$CD138^{+} PCs (Fig 4.5b-e).

MBC progenitors, pre-MBCs, differentiate from LZ B cells in the GC and express some MBC markers such as CCR6 (Suan et al., 2017; Laidlaw et al., 2017; Inoue et al., 2020). We observed a decreased frequency of pre-MBCs in the LZ of *Aicda*$^{Cre/wt}$ *Brwd1*$^{fl/fl}$ mice (Fig 4.5f). However, due to the increase in the total number GC B cells in these mice, the total number of pre-MBCs was comparable to control mice (Fig 4.5g). A similar trend in pre-MBCs was observed in heterozygous *Aicda*$^{Cre/wt}$ *Brwd1*$^{fl/wt}$ mice (Fig 4.3f-g).

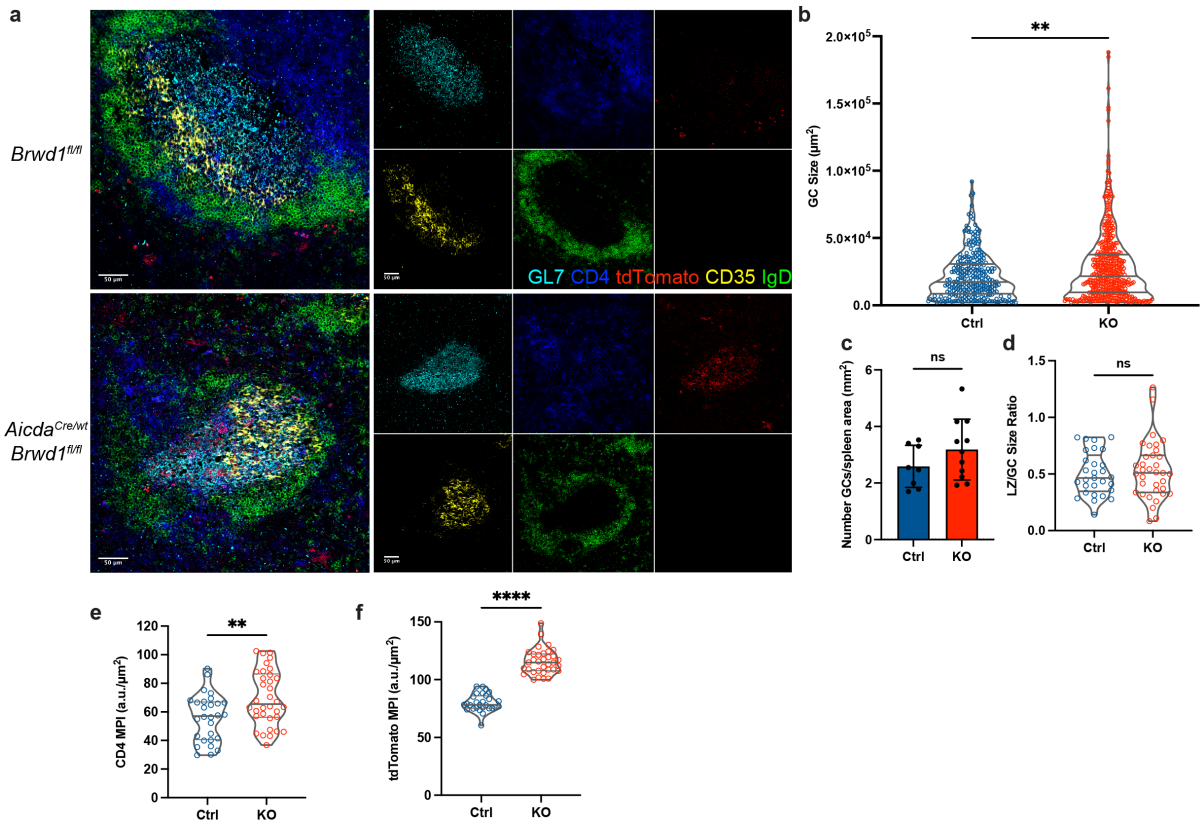

Figure 4.4: BRWD1 restrains germinal center size. **(a)** Representative immunofluorescence imaging of spleens at 20x magnification using GL7, anti-CD4, anti-tdT, anti-CD35, and anti-IgD (Ctrl n = 4 mice, 29 GCs; KO n = 4 mice, 35 GCs). **(b)** GC size measured by GL7 fluorescence (Ctrl n = 8 mice, KO n = 11 mice). **(c)** Number of GCs normalized by spleen area (mm^2). **(d)** Ratio of LZ size to total GC size. **(e)** CD4 mean pixel intensity (MPI, arbitrary units/μm^2) within the LZ per GC imaged. **(f)** tdT MPI per GC imaged. (**$p<0.01$, ****$p<0.0001$, b, d-f: two-sided Mann-Whitney, c: two-sided unpaired t-test, bar plots show mean ± standard deviation, violin plots show median and quartiles)

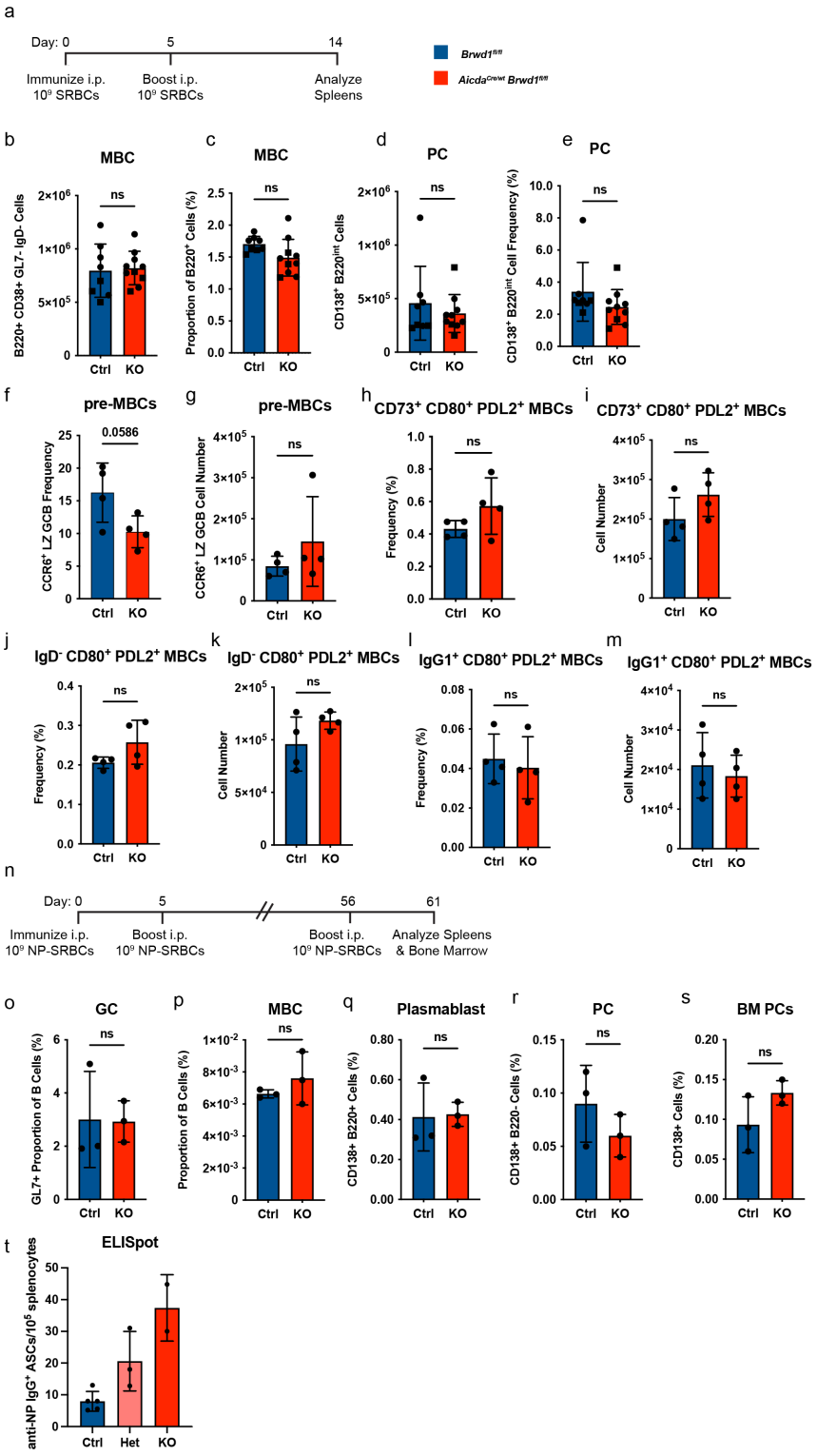

Figure 4.5: BRWD1 is not required for germinal center-derived memory B cells and plasma cells. *Caption continued on the next page.*

Figure 4.5: **(a)** *Aicda*$^{Cre/wt}$ *Brwd1*$^{fl/fl}$ (KO) and *Brwd1*$^{fl/fl}$ (Ctrl) mice were immunized with SRBCs i.p. and boosted at day 5. Splenic cells were analyzed at day 14 post-immunization (Ctrl n = 8 mice, KO n = 10 mice). **(b)** Number of B220^{+}CD38^{+}GL7^{-}IgD^{-} MBCs. **(c)** Frequency of MBCs as a proportion of all B220^{+} cells. **(d-e)** Number (d) and frequency (e) of CD138^{+}B220$^{\text{int}}$ PCs. **(f-g)** Frequency (f) and number (g) of CCR6^{+}CD83$^{\text{high}}$ pre-MBCs (Ctrl n = 4 mice, KO n = 4 mice). **(h-m)** Frequency or number of different CD80^{+}PD-L2^{+} MBC populations either gating first on CD73^{+} cells (h-i), IgD^{-} cells (j-k), or IgG1^{+} cells (l-m). Frequencies are calculated as a proportion of B220^{+}CD38^{+}GL7^{-} cells (Ctrl n = 4 mice, KO n = 4 mice). **(n)** *Aicda*$^{Cre/wt}$ *Brwd1*$^{fl/fl}$ (KO) and *Brwd1*$^{fl/fl}$ (Ctrl) mice were immunized with NP-SRBCs i.p. at days 0, 5, and 56. Spleens and bone marrow were analyzed at day 61 post-immunization (Ctrl n = 3 mice, KO n = 3 mice). **(o)** GC B cell frequency. **(p)** B220^{+}CD38^{+}GL7^{-}IgD^{-} MBC frequency. **(q)** CD138^{+}B220^{+} plasmablast frequency. **(r)** Splenic CD138^{+}B220^{-} PC frequency. **(s)** Bone marrow (BM) CD138^{+}B220^{-} PC frequency. **(t)** ELISpot to measure splenic NP-specific IgG-producing antibody secreting cells (ASCs). *Aicda*$^{Cre/wt}$ ROSA26-LSL-tdTomato$^{\text{fl/fl}}$ (Ctrl), *Aicda*$^{Cre/wt}$ *Brwd1*$^{fl/wt}$ (Het), and *Aicda*$^{Cre/wt}$ *Brwd1*$^{fl/fl}$ (KO) mice were immunized with NP-KLH. (two-sided unpaired t-test, bar plots show mean ± standard deviation)

The MBC population is heterogeneous, and MBCs can differentiate from both activated B cells and GC B cells (Viant et al., 2021). Next, we measured GC-dependent MBC populations. Although there is no definitive marker for mature MBCs that differentiated from the GC, multiple markers including CD73, CD80, PD-L2, IgG1, and the absence of IgD are enriched in GC-derived MBCs (Callahan et al., 2024; Zuccarino-Catania et al., 2014; Weisel et al., 2016; Kaji et al., 2012; Taylor et al., 2012; Conter et al., 2014). Flow cytometry for various combinations of these markers showed no difference in the GC-derived MBC subsets in *Aicda*$^{Cre/wt}$ *Brwd1*$^{fl/fl}$ mice (Fig 15h-m).

To determine whether *Aicda*$^{Cre/wt}$ *Brwd1*$^{fl/fl}$ mice produce long-lived PCs in the BM and mount a memory recall response, we immunized mice with SRBCs conjugated to 4-hydroxy-3-nitrophenylacetyl (NP) followed by a boost immunization at day 5. On day 56, we immunized again with NP-SRBCs, and on day 61 we measured B cell populations in the spleen and bone marrow (Fig 4.5n). There were not significant differences in the number or frequency of CD38^{+}GL7^{-}IgD^{-} MBCs, GL7^{+} GC B cells, CD138^{+}B220^{+} plasmablasts, or CD138^{+}B220^{-} PCs (Fig 4.5o-r). Similarly, we observed no significant difference in bone

marrow CD138$^+$ PCs (Fig 4.5s). In total, these results indicate that BRWD1 is not important for differentiation of GC-dependent MBCs, PCs, or plasmablasts.

To measure antigen-specific, antibody-secreting cells (ASCs), we immunized mice with NP-KLH and performed an enzyme-linked immunosorbent spot (ELISpot) assay. We compared heterozygous *Aicda*$^{Cre/wt}$ *Brwd1*$^{fl/wt}$ and knockout *Aicda*$^{Cre/wt}$ *Brwd1*$^{fl/fl}$ mice with control *Aicda*$^{Cre/wt}$ *Brwd1*$^{fl/fl}$ mice. Knockout and heterozygous mice had increased anti-NP IgG1$^+$ ASCs relative to controls (Fig 4.5t). Although the ELISpot assay cannot distinguish between plasmablasts and GC-derived plasma cells, the GC-specific deletion of *Brwd1* in this model suggests that loss of *Brwd1* results in increased antigen-specific plasma cells.

4.2.4 BRWD1 is necessary for optimal affinity maturation

We next explored whether BRWD1 is important for the principal functions of the GC, SHM and affinity maturation. We immunized mice with NP bound to keyhole limpet hemocyanin (KLH), which elicits a B cell response in which most antibodies specific to NP are of the IgG1 isotype and include the V_H186.2 variable heavy chain gene segment (Fig 4.6a) (Heise and Klein, 2017). We used *Aicda*$^{Cre/wt}$ ROSA-LSL-tdTomato$^{fl/fl}$ mice to control for *Aicda* heterozygosity. At day 14 post-immunization, we sorted tdT$^+$ GC B cells by FACS and cloned the V_H186.2 segment for sequencing (Heise and Klein, 2017). To prevent contamination by plasma cells which have high levels of *Ig* transcripts, we used a primer specific to the Cγ1-membrane-encoding exon (Heise and Klein, 2017).

Sequencing of V_H186.2 revealed that tdT$^+$ GC B cells from *Aicda*$^{Cre/wt}$ *Brwd1*$^{fl/fl}$ KO mice and *Aicda*$^{Cre/wt}$ *Brwd1*$^{fl/wt}$ Het mice undergo the same rate of SHM as GC B cells from *Aicda*$^{Cre/wt}$ ROSA-LSL-tdTomato$^{fl/fl}$ control mice (Fig 4.6b). The rate of silent SHM, which is not affected by selection, was also similar between KO, Het, and control GC B cells (Fig 4.6c). In contrast to control GC B cells, KO and Het GC B cells had a significantly broader distribution of SHM with some clones containing a high number of mutations and

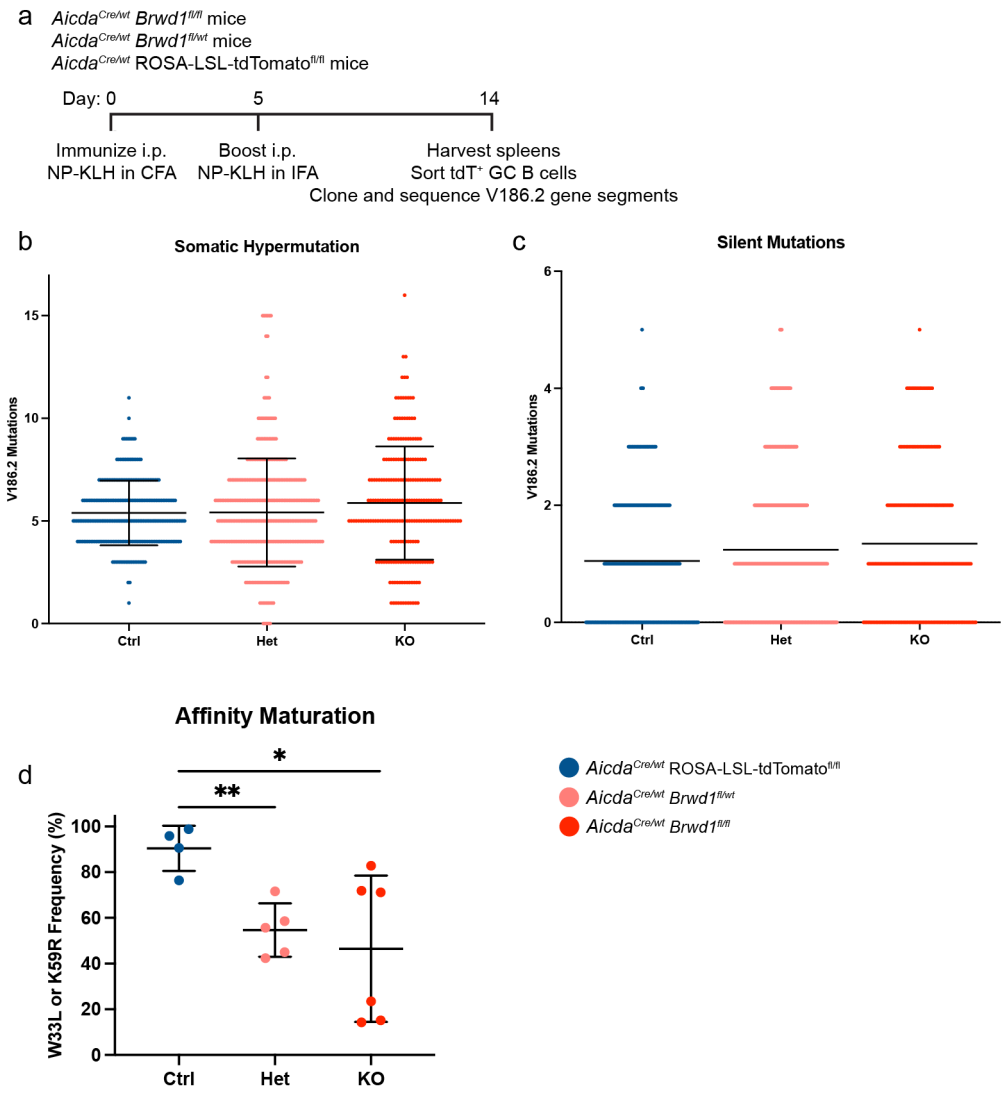

Figure 4.6: BRWD1 enhances affinity maturation. (a) *Aicda*$^{Cre/wt}$ *Brwd1*$^{fl/fl}$ (KO), *Aicda*$^{Cre/wt}$ *Brwd1*$^{fl/wt}$ (Het), and *Aicda*$^{Cre/wt}$ ROSA26-LSL-tdTomato$^{fl/fl}$ (Ctrl) mice were immunized i.p. with NP-KLH in complete Freund's adjuvant (CFA) and boosted with NP-KLH in incomplete Freund's adjuvant (IFA) at day 5. At day 14 post-immunization, spleens were collected, tdT^{+} GC B cells were sorted, and V_H186.2 gene segments were cloned and sequenced (Ctrl n = 4 mice, Het = 5 mice, KO n = 6 mice). **(b)** Frequency of mutations within V_H186.2 in GC B cells. **(c)** Frequency of silent mutations within V_H186.2 in GC B cells. **(d)** Frequency of W33L or K59R amino acid substitutions that increase the affinity of V_H186.2 to NP. (*p<0.05, **p<0.01, two-sided unpaired t-test, lines show mean ± standard deviation)

some clones with none or one mutation (F test, $p < 0.0001$). In clones with a high amount of SHM, mutations were distributed throughout $V_H186.2$ (Fig 4.7a). Furthermore, the increased SHM distribution relative to controls was consistent across individual mice (Fig 4.7b). The rate of mutations within framework regions and complementarity determining regions was the same between groups (Fig 4.7c-e). Furthermore, there was no significant difference between groups in the rate of unproductive immunoglobulin mutations (Fig 4.7f). In WT GC cycles, there are relatively fixed, deterministic relationships between selection, proliferation, and SHM (Gitlin et al., 2014; Ersching et al., 2017; Long et al., 2022; Finkin et al., 2019; Pae et al., 2020). Our results suggest that upon loss of *Brwd1*, these tight relationships are uncoupled and the degree of proliferation following SHM and selection becomes stochastic.

We also measured affinity maturation by comparing the frequency of mutations known to increase affinity toward NP including W33L and K59R (Weiser et al., 2011). KO and Het GC B cells had an approximately two-fold decrease in the frequency of high affinity mutations relative to control GC B cells (Fig 4.6d). These results demonstrate that BRWD1 is necessary for optimal affinity maturation of GC B cells. Furthermore, decreased high affinity mutations in the Het GC B cells shows that the amount of BRWD1 is important for affinity maturation.

4.2.5 BRWD1 is involved in plasma cell selection from the germinal center

We also measured SHM in the splenic PCs of $Aicda^{Cre/wt}$ $Brwd1^{fl/wt}$ Het mice by comparing tdT^+ and tdT^- PCs from the same mice, which were immunized as above. Both total SHM and silent SHM were lower in tdT^+ Het PCs compared to tdT^- Het PCs (Fig 4.8a-b). Because deletion of *Brwd1* did not affect the rate of SHM in GC B cells, this suggests that tdT^+ PCs were exiting the GC reaction earlier than tdT^- PCs and thereby accumulating fewer mutations. There was no difference in affinity maturation between tdT^+ and tdT^-

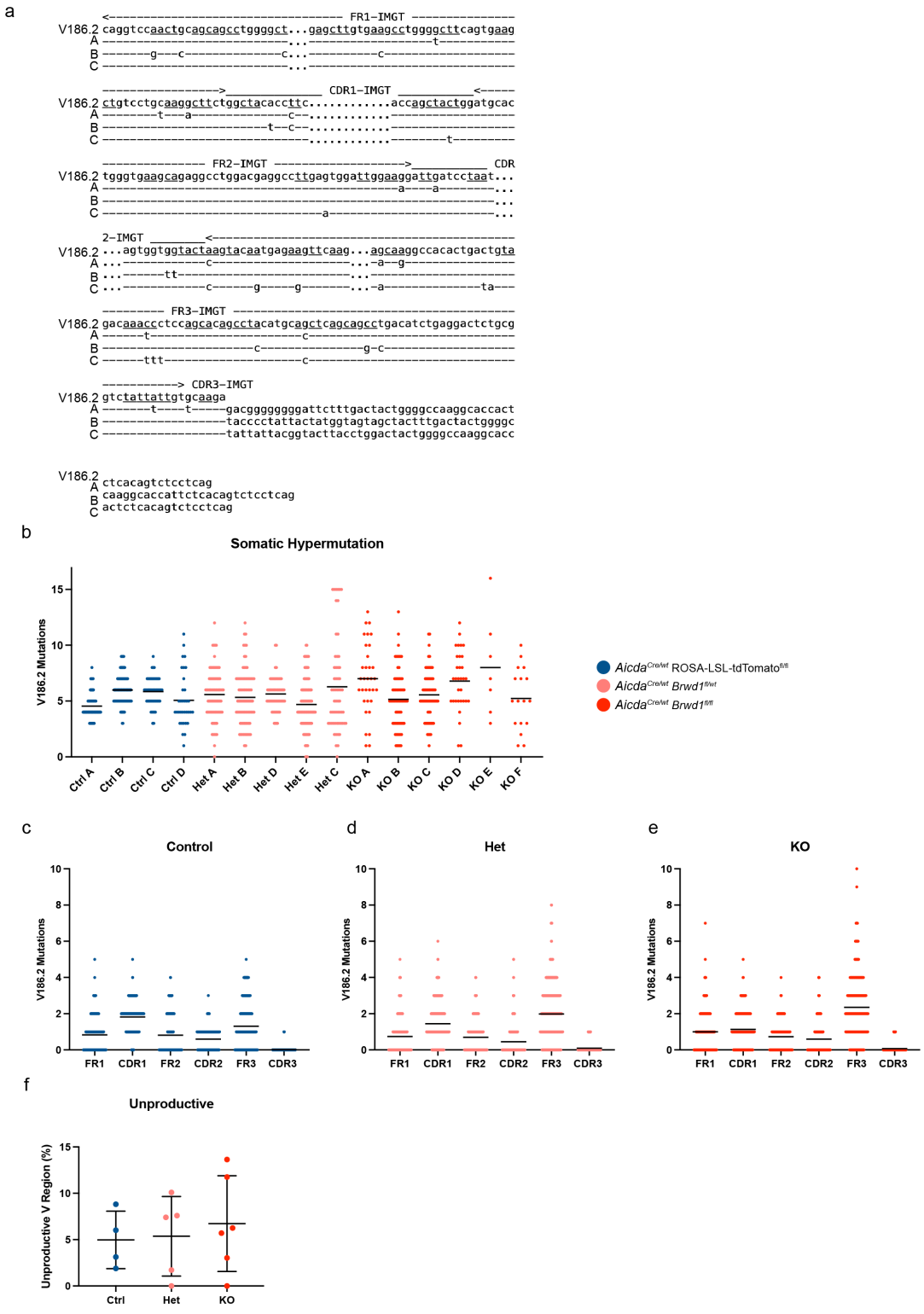

Figure 4.7: *Brwd1*$^{-/-}$germinal center B cells manifest wide distributions in somatic hypermutation frequencies. *Caption continued on the next page.*

Figure 4.7: **(a)** Example distribution of SHM in three representative *Aicda*$^{Cre/wt}$ *Brwd1*$^{fl/fl}$ (KO) tdT^{+} GC B cells with a relatively high level of mutations. The V$_H$186.2 nucleotide sequence is shown above. **(b)** Frequency of mutations within V$_H$186.2 in GC B cells per mouse. Lines show mean (Ctrl n = 4 mice, Het n = 5 mice, KO n = 6 mice). **(c-e)** Distribution of V$_H$186.2 mutations within framework regions (FR) and complementarity-determining regions (CDR) for *Aicda*$^{Cre/wt}$ ROSA26-LSL-tdTomato$^{fl/fl}$ (Ctrl) GC B cells (c), *Aicda*$^{Cre/wt}$ *Brwd1*$^{fl/wt}$ (Het) GC B cells (d), and *Aicda*$^{Cre/wt}$ *Brwd1*$^{fl/fl}$ (KO) GC B cells (e). Mutations in CDR3 introduced by junctional diversity were not counted. **(f)** Frequency of clones with an unproductive V region. Lines show mean ± standard deviation.

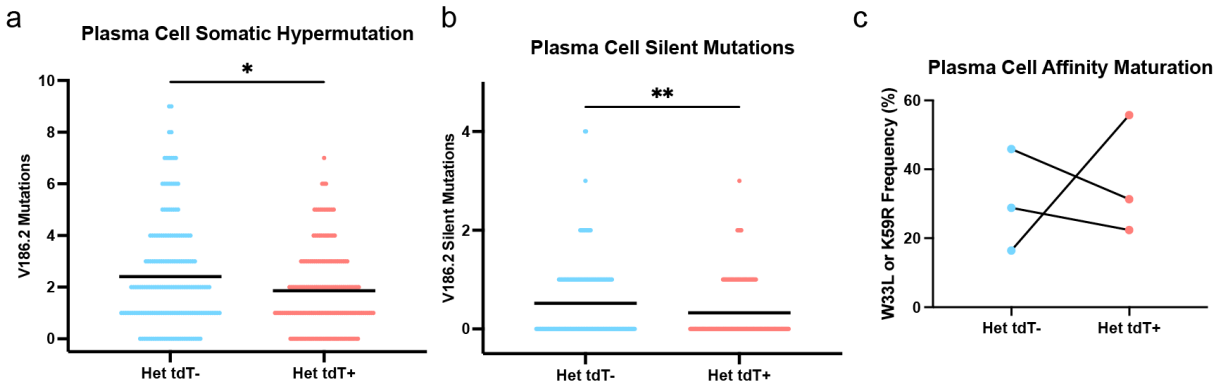

Figure 4.8: Plasma cells from heterozygous *Aicda*$^{Cre/wt}$ *Brwd1*$^{fl/wt}$ mice have decreased somatic hypermutation. *Aicda*$^{Cre/wt}$ *Brwd1*$^{fl/wt}$ (Het) mice were immunized wit NP-KLH and tdT^{+} and tdT^{-} PCs were sorted from the same mice. **(a)** Frequency of mutations within V$_H$186.2 in PCs. **(b)** Frequency of silent mutations within V$_H$186.2 in PCs. **(c)** Frequency of W33L or K59R amino acid substitutions in PCs. (*p<0.05, **p<0.01, two-sided Mann-Whitney, bars show means)

PCs by comparing the frequencies of affinity enhancing amino acid substitutions (Fig 4.8c).

4.2.6 BRWD1 prevents breaks in tolerance

In addition to selection for higher affinity, GCs also eliminate autoreactive clones that arise from SHM (Burnett et al., 2018; Mayer et al., 2017; Butt et al., 2015; Chan et al., 2012). To test GC negative selection, we collected sera from mice immunized with SRBCs or NP-KLH and tested reactivity to HEp-2 cells (Fig 4.9a). Prior to immunization, sera from all mice did not bind HEp-2 cells. Likewise, there was no detectable HEp-2 reactivity in control mouse serum after immunization. In contrast, sera from *Aicda*$^{Cre/wt}$ *Brwd1*$^{fl/fl}$ mice immunized

with either SRBCs or NP-KLH bound to HEp-2 cell nuclei, indicating self-reactivity. Approximately 40% of *Aicda*$^{Cre/wt}$ *Brwd1*$^{fl/fl}$ mice demonstrated HEp-2 reactivity (Fig 4.9b). These results suggest that *Aicda*$^{Cre/wt}$ *Brwd1*$^{fl/fl}$ mice are beginning to break tolerance following immunization, although the self-reactive sera may not be pathologically significant.

4.2.7 BRWD1 is required for germinal center B cell subset transcriptional identity

We next performed RNA-seq on GC B cells from the LZ, DZp, and DZd of *Aicda*$^{Cre/wt}$ *Brwd1*$^{fl/fl}$ mice and compared with WT GC B cell subsets. PCA of these populations revealed that *Brwd1*$^{-/-}$ GC B cells were transcriptionally distinct from WT GC B cells (Fig 4.10a-b). Comparison of WT and KO GC B cells within the same subset revealed a large transcriptional increase within the *Brwd1*$^{-/-}$ KO LZ, DZp, and DZd (Fig 4.10c-e). Interestingly, many of the same genes were upregulated across subsets (Fig 4.10f, Fig 4.11a-f). For example, 57% of genes increased in *Brwd1*$^{-/-}$ LZ cells were also increased in *Brwd1*$^{-/-}$ DZp and DZd cells (Fig 4.11b). A heatmap of differential expression between all groups revealed many genes with similar expression in each *Brwd1*$^{-/-}$ GC B cell subset (Fig 4.11g). This was especially true of *Brwd1*$^{-/-}$ DZp and DZd cells. Together, these results demonstrate that BRWD1 represses a large transcriptional program that is shared across *Brwd1*$^{-/-}$ GC B cell subsets.

In WT GC B cell subsets, RNA expression clustered into 8 groups, which previously revealed a transcriptional program unique to each GC subset, most notably the DZp (Fig 4.10g) (Kennedy et al., 2020). Surprisingly, *Brwd1*$^{-/-}$ DZp cells lost this unique transcriptional program and instead had intermediate expression between *Brwd1*$^{-/-}$ LZ and DZd cells. For example, WT DZp cells had the greatest expression of genes in clusters 5 and 6 and the lowest expression of genes in clusters 1 and 2 (Fig 4.11h). Yet *Brwd1*$^{-/-}$ DZp cells had gene expression intermediate that of *Brwd1*$^{-/-}$ LZ and DZd cells for genes in these

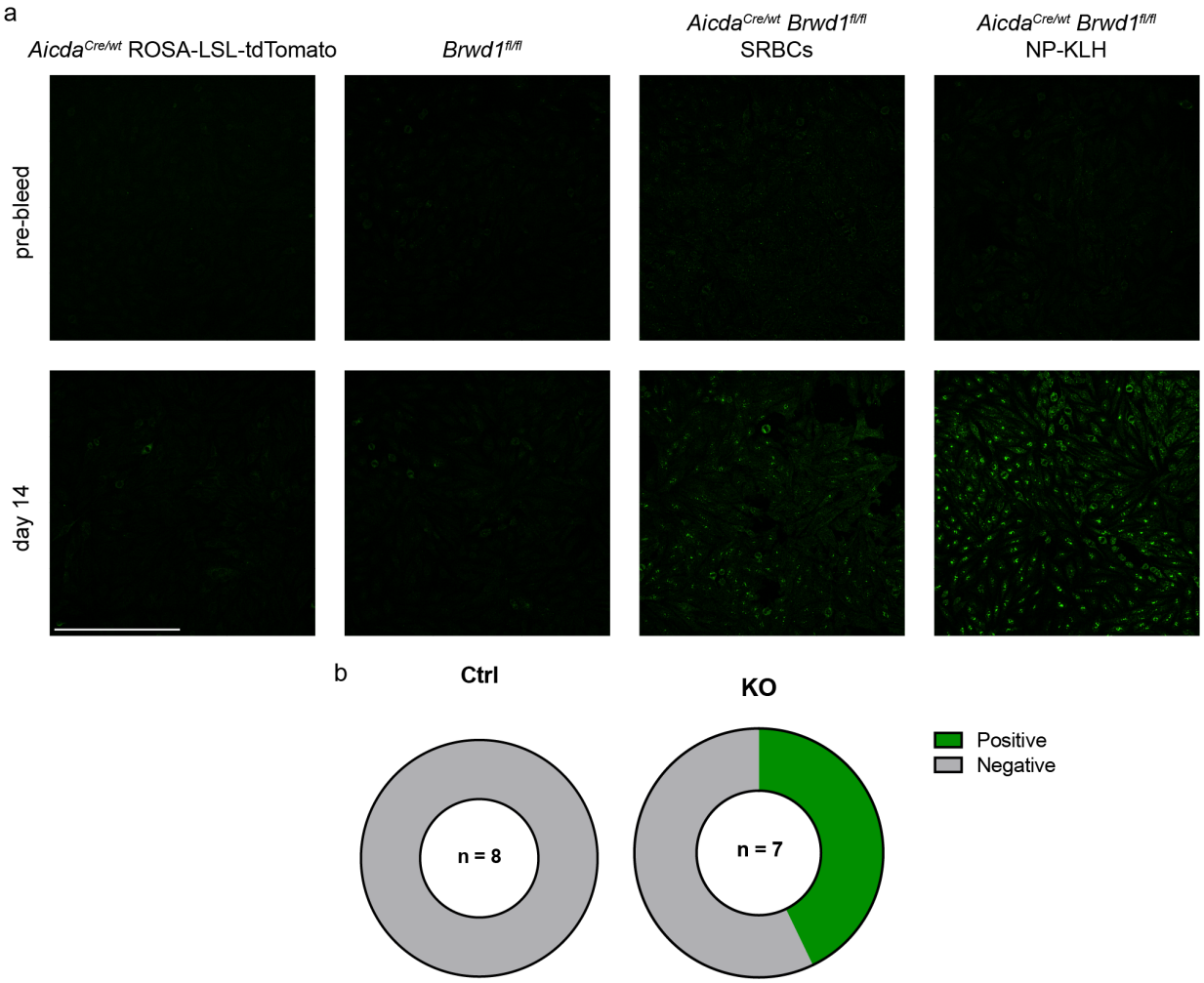

Figure 4.9: BRWD1 prevents self-reactive sera. Control and knockout mice were immunized with NP-KLH in CFA or with SRBCs. Sera was collected before immunization or at day 14 post-immunization and used to stain HEp-2 cells. **(a)** Representative images from a control *Aicda*$^{Cre/wt}$ ROSA-LSL-tdTomato$^{fl/fl}$ mouse, a control *Brwd1*$^{fl/fl}$ mouse, a knockout *Aicda*$^{Cre/wt}$ *Brwd1*$^{fl/fl}$ mouse immunized with SRBCs, and a knockout *Aicda*$^{Cre/wt}$ *Brwd1*$^{fl/fl}$ mouse immunized with NP-KLH with CFA. Scale bar = 300 μm. **(b)** Proportion of mice with positive anti-nuclear antibody tests. Control *Brwd1*$^{fl/fl}$ and *Aicda*$^{Cre/wt}$ ROSA-LSL-tdTomato$^{fl/fl}$ mice are grouped. Mice immunized with either SRBCs or NP-KLH are grouped.

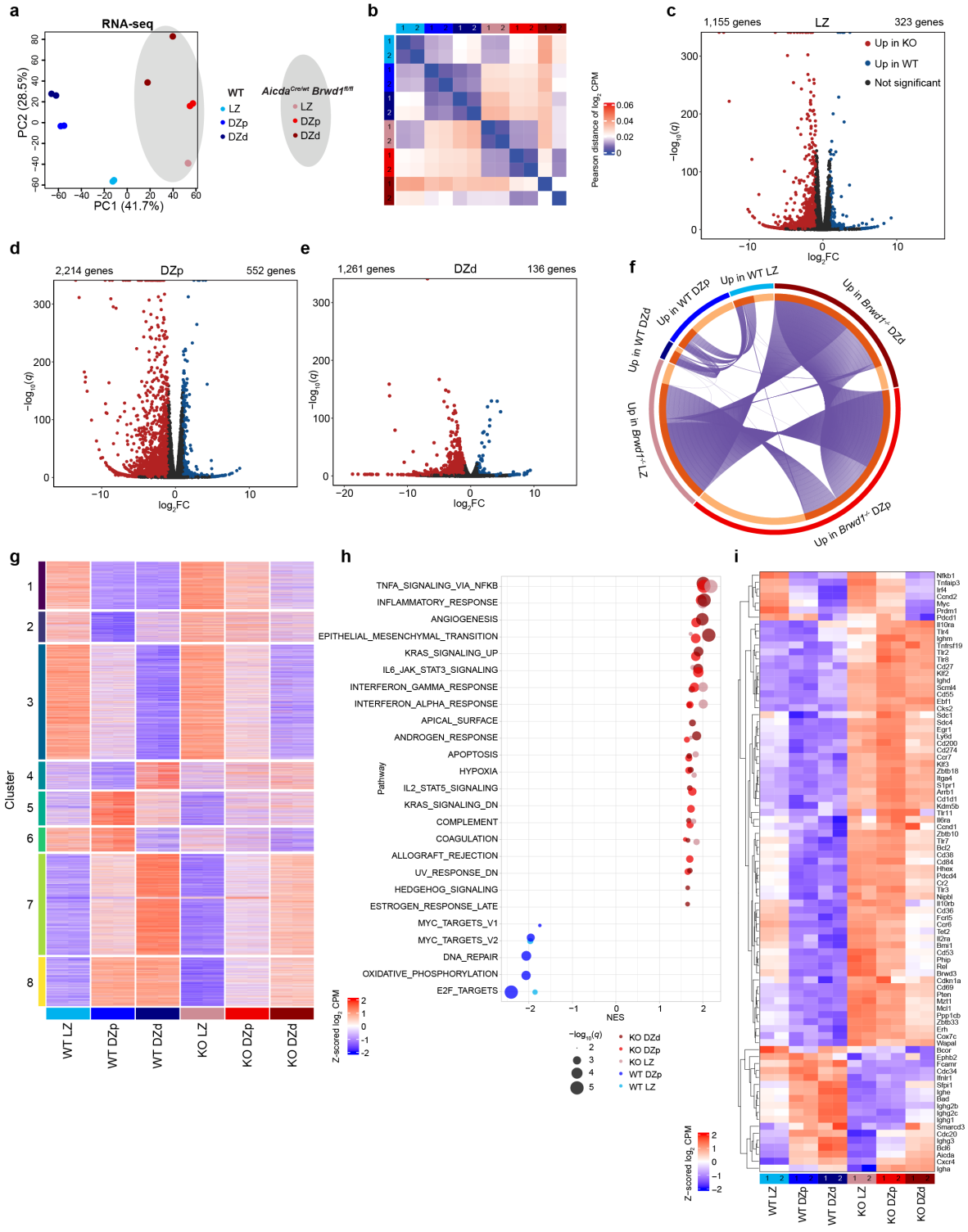

Figure 4.10: BRWD1 is required for germinal center B cell subset transcriptional identity. *Caption continued on the next page.*

Figure 4.10: **(a)** PCA plot of RNA-seq of each GC subset in WT and *Aicda*$^{Cre/wt}$ *Brwd1*$^{fl/fl}$ (KO) mice. n = 2 per cell type. Each n represents cells pooled from 20 mice. WT GC B cell RNA-seq was previously published (Kennedy et al., 2020). **(b)** Heatmap of Pearson correlation of RNA-seq. **(c-e)** Volcano plots of differentially expressed genes ($\log_2$ fold change > 1, $q < 0.05$) between KO and WT GC B cells from the LZ (c), DZp (d), and DZd (e). **(f)** Differentially expressed genes between *Brwd1*$^{-/-}$ and WT GC B cells from the LZ, DZp, or DZd. Purple lines show genes shared between groups. Dark orange signifies genes in the group that are shared with another group. **(g)** Gene expression of WT and KO GC subsets at clusters generated by unsupervised K-means clustering of WT GC subsets, performed previously (Kennedy et al., 2020). Z-scored $\log_2$ counts per million (CPM) are plotted. **(h)** Gene set enrichment analysis (GSEA) using the Molecular Signatures Database hallmark genes sets for each GC subpopulation. Pathways are ordered by normalized enrichment score (NES). Pathways with $q < 0.01$ are shown. **(i)** Z-scored $\log_2$ CPM of notable genes expressed across the LZ, DZp, and DZd of WT and KO mice.

same clusters. Thus, BRWD1 specifically maintains the DZp transcriptional program.

To understand the function of dysregulated genes in *Brwd1*$^{-/-}$ GC B cells, we performed a gene set enrichment analysis (GSEA) comparing WT and *Brwd1*$^{-/-}$ GC B cells from each GC subset. GSEA revealed a significant enrichment of many pathways in *Brwd1*$^{-/-}$ GC B cells including TNFα signaling via NFκB and the inflammatory response (Fig 4.10h, Fig 4.11i-n). Similarly, a gene ontology (GO) pathway analysis of genes significantly upregulated in WT or *Brwd1*$^{-/-}$ GC B cells from each GC subset also revealed shared transcriptional pathways in *Brwd1*$^{-/-}$ GC B cells, including multiple immune and inflammatory response GO pathways (Fig 4.11o). Within these pathways were many differentially expressed genes important for GC B cell biology (Fig 4.10i). Taken together, these results demonstrate that within the genes upregulated in each *Brwd1*$^{-/-}$ GC B cell subset are inflammatory transcriptional programs not expressed in WT GC B cells.

RNA-seq revealed increased expression of the *Brwd1* homologs *Phip* (also known as *Brwd2*) and *Brwd3* in the *Brwd1*$^{-/-}$ GC subsets (Fig 4.11p). These genes could partially compensate for *Brwd1* deletion in *Aicda*$^{Cre/wt}$ *Brwd1*$^{fl/fl}$ mice, thereby mitigating the observed phenotype.

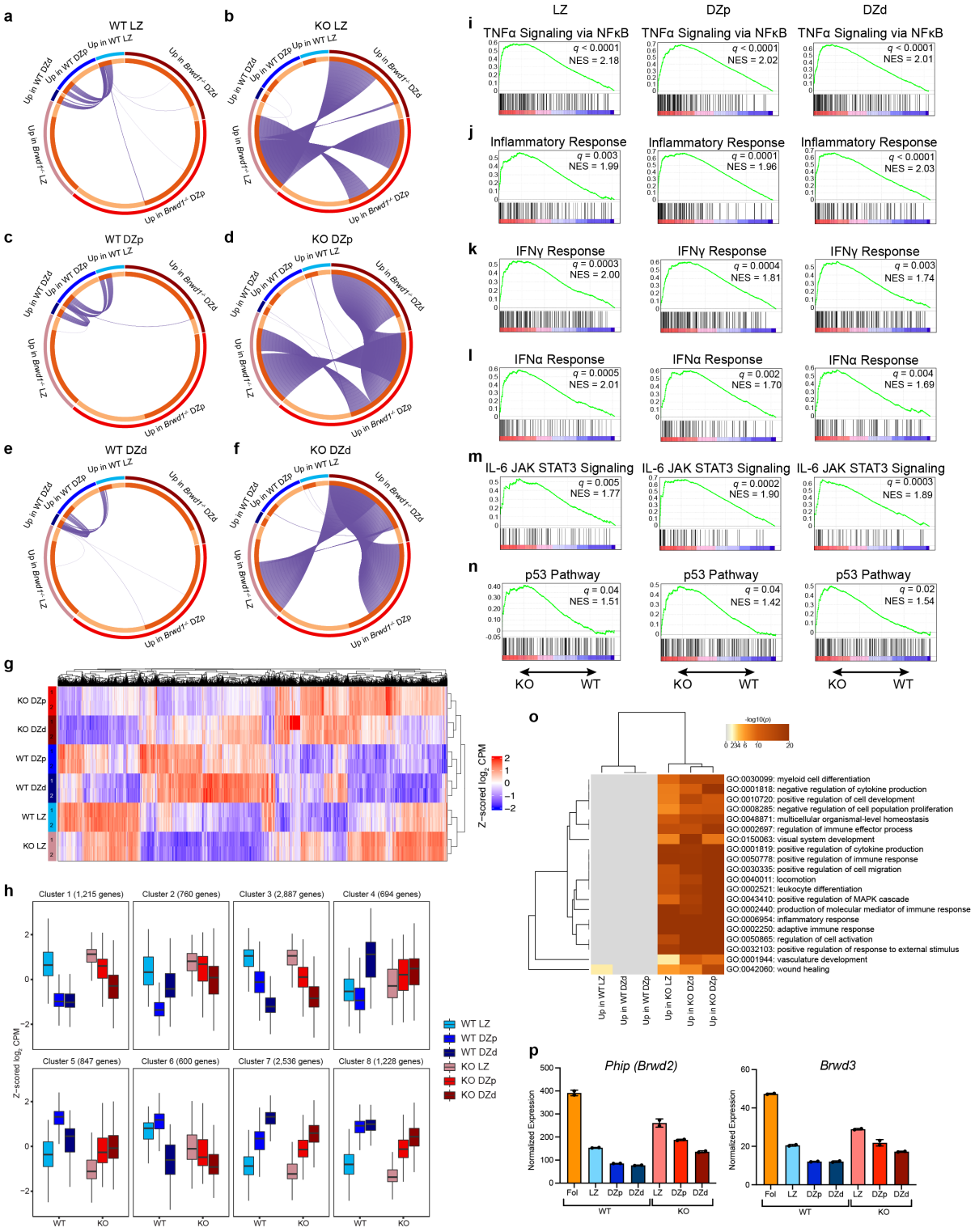

Figure 4.11: BRWD1 maintains germinal center B cell subset transcriptional identity. *Caption continued on the next page.*

Figure 4.11: **(a-f)** Differentially expressed genes between *Brwd1*$^{-/-}$ and WT GC B cells from the LZ, DZp, or DZd. Purple lines show genes shared between groups. Dark orange signifies genes in the group that are shared with another group. Each plot shows shared genes from the perspective of the WT LZ (a), KO LZ (b), WT DZp (c), KO DZp (d), WT DZd (e), or KO DZd (f). n = 2 per cell type. Each n represents cells pooled from 20 mice. **(g)** Heatmap of 11,998 differentially expressed genes (one-way ANOVA, $q < 0.05$) between KO and WT GC B cells from the LZ, DZp, or DZd. Z-scored $\log_2$ counts per million (CPM) are plotted. **(h)** Gene expression of WT and KO GC subsets at clusters generated by unsupervised K-means clustering of WT GC subsets, performed previously (Kennedy et al., 2020). Z-scored $\log_2$ CPM are plotted. Box limits show interquartile range (IQR), and center lines show median. Maximum and minimum values (whiskers) are defined as Q3 + 1.5 x IQR and Q1 − 1.5 x IQR, respectively. **(i-n)** Gene set enrichment analyses for the TNFα signaling via NFκB (i), inflammatory response (j), IFNγ response (k), IFNα response (l), IL-6 JAK-STAT3 signaling (m), and p53 (n) pathways for each GC subpopulation. **(o)** Gene Ontology (GO) pathways enriched in differentially expressed genes between *Brwd1*$^{-/-}$ and WT cells from the LZ, DZp, or DZd. The top 20 pathways by p value are listed. **(p)** RNA-seq expression of *Phip* (also known as *Brwd2*) and *Brwd3*. Bar plots show mean ± standard deviation.

4.2.8 BRWD1 maintains chromatin accessibility differences across germinal center subsets

Finally, we performed ATAC-seq on LZ, DZp, and DZd GC B cells from *Aicda*$^{Cre/wt}$ *Brwd1*$^{fl/fl}$ and WT mice to understand the effects of deleting *Brwd1* in GC B cells. Comparison with WT GC B cells revealed that *Brwd1*$^{-/-}$ GC B cells were epigenetically distinct in the PCA space (Fig 4.12a). In *Brwd1*$^{-/-}$ GC B cells, differences in chromatin accessibility were diminished as shown by PCA where *Brwd1*$^{-/-}$ samples clustered more closely together. Indeed, the biological coefficient of variation (BCV) was lower across *Brwd1*$^{-/-}$ GC subsets (12.7%) compared to WT GC subsets (25.2%). In WT GC B cells, many accessibility peaks significantly changed during transitions between subsets; however, these changes were diminished in *Brwd1*$^{-/-}$ GC B cells (Fig 4.12b). For example, transition between the DZd and LZ involves 61,451 differential accessibility peaks in WT cells but only 15,522 differential accessibility peaks in *Brwd1*$^{-/-}$ GC B cells. A striking example of this occurred at the *Myc* locus. In WT cells, accessibility peaks at *Myc* and downstream enhancers in the LZ were

closed in DZd GC B cells. In contrast in *Brwd1*$^{-/-}$ GC B cells, chromatin accessibility was unchanged at the *Myc* locus across GC B cell subsets (Fig 4.12c).

In WT GC B cells, accessibility peaks clustered into eight groups each with a different distribution pattern across GC subsets (Fig 4.12d) (Kennedy et al., 2020). In contrast, *Brwd1*$^{-/-}$ GC subsets had decreased variability within these groups compared to WT. Accessibility was especially dysregulated in *Brwd1*$^{-/-}$ DZp and DZd cells. For example, at sites in cluster 5, WT DZd cells have low accessibility; however, *Brwd1*$^{-/-}$ DZd cells had greater accessibility than *Brwd1*$^{-/-}$ LZ or DZp cells at these same sites. In a similar manner for cluster 6, WT DZp cells have the greatest accessibility; however, these sites were accessible in both *Brwd1*$^{-/-}$ DZp and DZd cells. Generally, sites uniquely accessible in WT LZ cells were also accessible in *Brwd1*$^{-/-}$ LZ cells (clusters 3, 4, and 8), yet these clusters also showed a blending across *Brwd1*$^{-/-}$ subsets. These results demonstrate that BRWD1 is necessary for polarizing the chromatin accessibility states of GC B cells.

Comparison of WT and *Brwd1*$^{-/-}$ cells within the same GC B cell subset revealed large differences in chromatin accessibility (Fig 4.12e). Analysis of the chromatin accessibility peaks that were increased in *Brwd1*$^{-/-}$ cells in each subset revealed similar TF motifs across subsets (Fig 4.12f). We previously reported that each GC subset is associated with unique TF motif accessibility (Fig 4.12g) (Kennedy et al., 2020); however, *Brwd1*$^{-/-}$ GC B cell subsets were enriched for many of the same TF motifs. For example, in WT cells CTCF is most enriched in DZd cells (Kennedy et al., 2020), yet in *Brwd1*$^{-/-}$ GCs the CTCF motif was enriched in LZ and DZp cells. Similarly, OCT2 is the top enriched motif in WT DZp cells (Kennedy et al., 2020), yet this motif was enriched in *Brwd1*$^{-/-}$ cells in the LZ and DZd. Across all three KO GC subsets, the accessibility at motifs for PU.1, SPIB, PRDM1, and IRF4 was shared while in WT cells, accessibility at each site was restricted to one GC subset. In total, we conclude that BRWD1 is necessary for maintaining the unique transcriptional and epigenetic states of each GC subset.

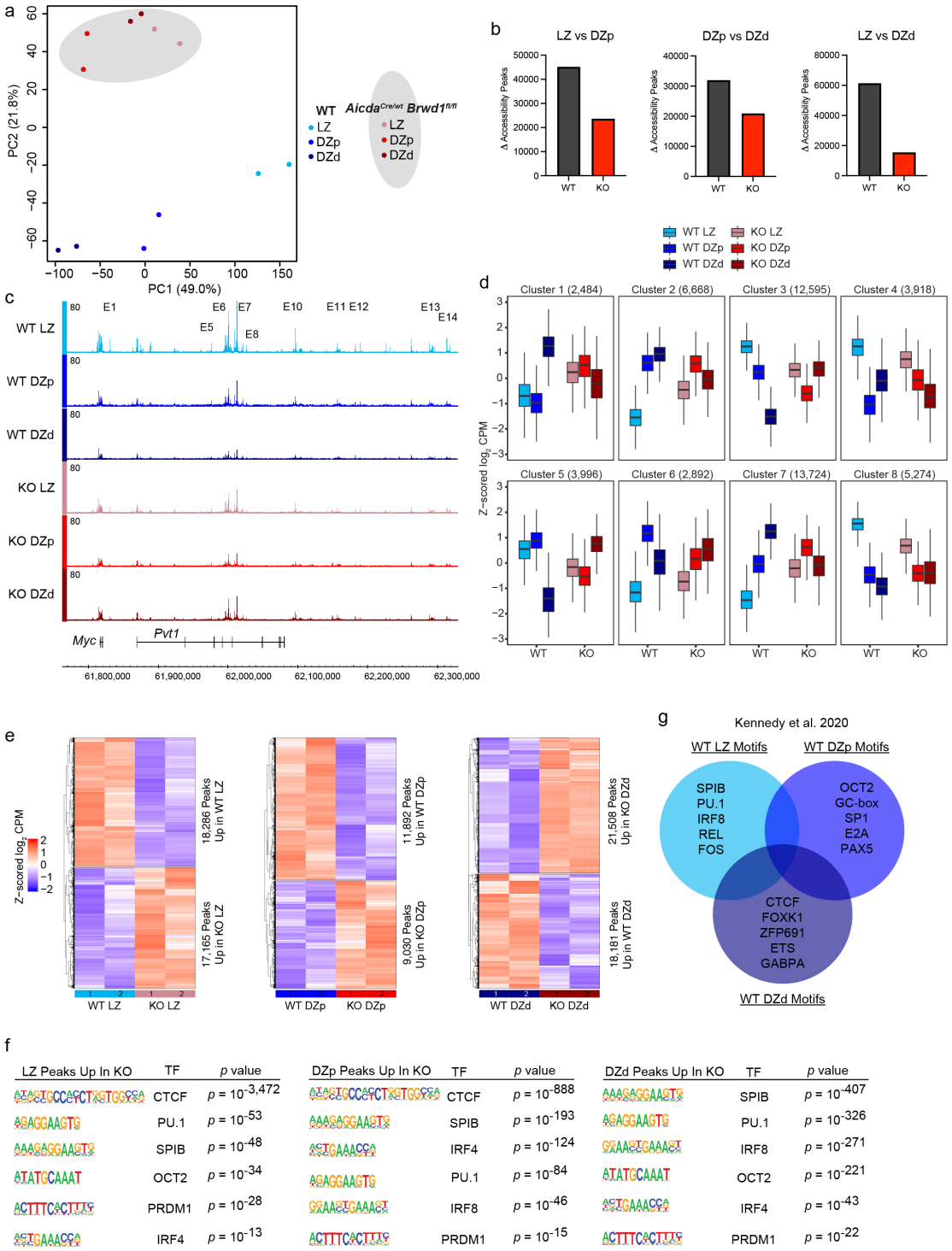

Figure 4.12: BRWD1 maintains the distinct epigenetic states of each germinal center subset. *Caption continued on the next page.*

Figure 4.12: **(a)** PCA plot of ATAC-seq of each GC subset in WT and *Aicda*$^{Cre/wt}$ *Brwd1*$^{fl/fl}$ (KO) mice. n = 2 per cell type. Each n represents cells pooled from 20 mice. WT GC B cell ATAC-seq was previously published (Kennedy et al., 2020). **(b)** Number of differentially regulated accessibility peaks ($q < 0.05$) between GC subsets in WT and KO mice. **(c)** Chromatin accessibility tracks at the *Myc* locus (mm9, chromosome 15) for each GC subset in WT and KO. *Myc* enhancers (E1-14) were previously characterized (Kieffer-Kwon et al., 2013). **(d)** Chromatin accessibility of WT and KO GC subsets at clusters generated by unsupervised K-means clustering of WT GC subsets, performed previously (Kennedy et al., 2020). Z-scored $\log_2$ counts per million (CPM) are plotted. Box limits show interquartile range (IQR), and center lines show median. Maximum and minimum values (whiskers) are defined as Q3 + 1.5 x IQR and Q1 – 1.5 x IQR, respectively. **(e)** Heatmaps of differentially accessible peaks ($q < 0.05$) between KO and WT GC B cells from the LZ, DZp, or DZd. Z-scored $\log_2$ CPM are plotted. **(f)** TF motifs enriched in accessible regions that are up in KO GC B cell subsets ($q < 0.05$) generated using HOMER. **(g)** Venn diagram of enriched TF motifs in each WT GC subset previously described (Kennedy et al., 2020)
.

4.2.9 BRWD1 may prevent accumulation of debris within germinal centers

The inflammatory transcriptional signature and the increased self-reactivity resulting from the GC suggested greater defects within the GC environment. To examine potential signs of inflammation, we stained spleen sections from immunized mice with hematoxylin and eosin (H&E). We observed a striking accumulation of nuclear debris, defined as small hematoxylin$^+$ objects, within the GCs of *Aicda*$^{Cre/wt}$ *Brwd1*$^{fl/fl}$ mice that was not observed in control mice (Fig 4.13a). Nuclear debris and apoptotic cells were found adjacent to TBMs in all mice; however, the accumulated debris was located away from TBMs. Scoring of this observation by a pathologist revealed that 3 of 4 *Aicda*$^{Cre/wt}$ *Brwd1*$^{fl/fl}$ mice had this phenotype (Fig 4.13b). We next quantified objects less than 5 μm^2 in GCs using Cellpose to segment objects. This analysis revealed no difference in the density of debris between control and *Aicda*$^{Cre/wt}$ *Brwd1*$^{fl/fl}$ mice (Fig 4.13c). Cellpose is designed to segment larger H&E objects such as cell nuclei and for this analysis Cellpose segmented more than just the debris of interest. Therefore, additional replicates or an alternative H&E analysis method will be needed to fully understand the accumulation of nuclear debris within the GCs of *Aicda*$^{Cre/wt}$ *Brwd1*$^{fl/fl}$ mice.

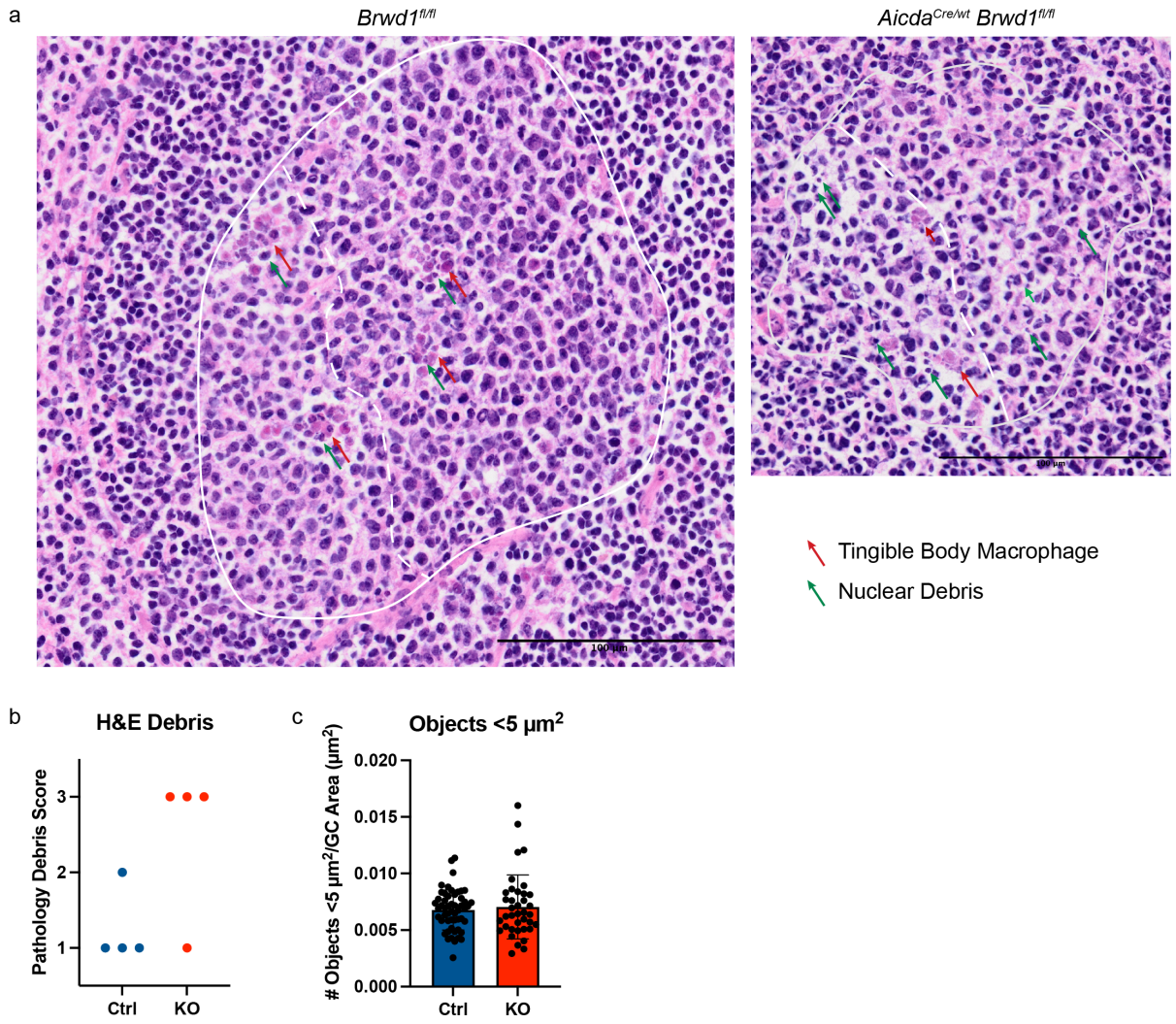

Figure 4.13: BRWD1 may prevent accumulation of debris within germinal centers. (a) Representative H&E images of splenic GCs from $Brwd1^{fl/fl}$ (Ctrl) and $Aicda^{Cre/wt}$ $Brwd1^{fl/fl}$ (KO) mice immunized with SRBCs day 14 post-immunization. Tingible body macrophages (TBMs, red arrows) and nuclear debris (green arrows) are labeled. GCs, LZ, and DZ are outlined in white (Scale bar = 100 μm, Ctrl n = 4, KO n = 4). **(b)** Pathology debris score of spleen sections with 3 being the greatest degree of debris accumulation away from TBMs and 1 being the least. **(c)** Quantification of objects <0.5 μm^2 per GC area (μm^2) using Cellpose 2.0. Bar plot shows mean ± standard deviation

Apoptosis within the GC (measured by terminal deoxynucleotidyl transferase dUTP nick end-labeling, TUNEL) occurs proximal to or within TBMs (Kennedy et al., 2020; Gurwicz et al., 2023; Grootveld et al., 2023). We stained spleens from *Aicda*$^{Cre/wt}$ *Brwd1*$^{fl/fl}$ mice with TUNEL and observed a normal spatial distribution of TUNEL^{+} cells clustered next to TBMs (Fig 4.14). Thus, the spatial distribution of apoptosis in the GC is not disrupted by *Brwd1* deletion.

4.2.10 BRWD1 is not important for LCMV clone 13 disease course

We infected *Aicda*$^{Cre/wt}$ *Brwd1*$^{fl/fl}$ mice with lymphocytic choriomeningitis virus (LCMV) clone 13, which causes a chronic infection in mice. As a control, we used *Brwd1*$^{fl/fl}$ littermates because differences in age and the microbiome effect the course of LCMV clone 13 infection. While many different immune cell types are required, a polyclonal B cell response is necessary to clear LCMV clone 13 infection (Bergthaler et al., 2009).

Both *Aicda*$^{Cre/wt}$ *Brwd1*$^{fl/fl}$ and control mice had the same survival following infection (Fig 4.15a). LCMV infection occurs in multiple tissues. The highest viral load is found in the kidney, which is among the last tissues to clear an LCMV infection. At day 42 post-infection, *Aicda*$^{Cre/wt}$ *Brwd1*$^{fl/fl}$ mice had a nonsignificant increase in viral load within the kidney (fold change = 7.7, $p = 0.0718$) (Fig 4.15b). In the spleen, both groups had undetectable virus and had cleared the infection in most animals (Fig 4.15c). These results demonstrate that BRWD1 is likely necessary for an optimal immune response against LCMV clone 13; however, the course of infection is largely unchanged in *Aicda*$^{Cre/wt}$ *Brwd1*$^{fl/fl}$ mice.

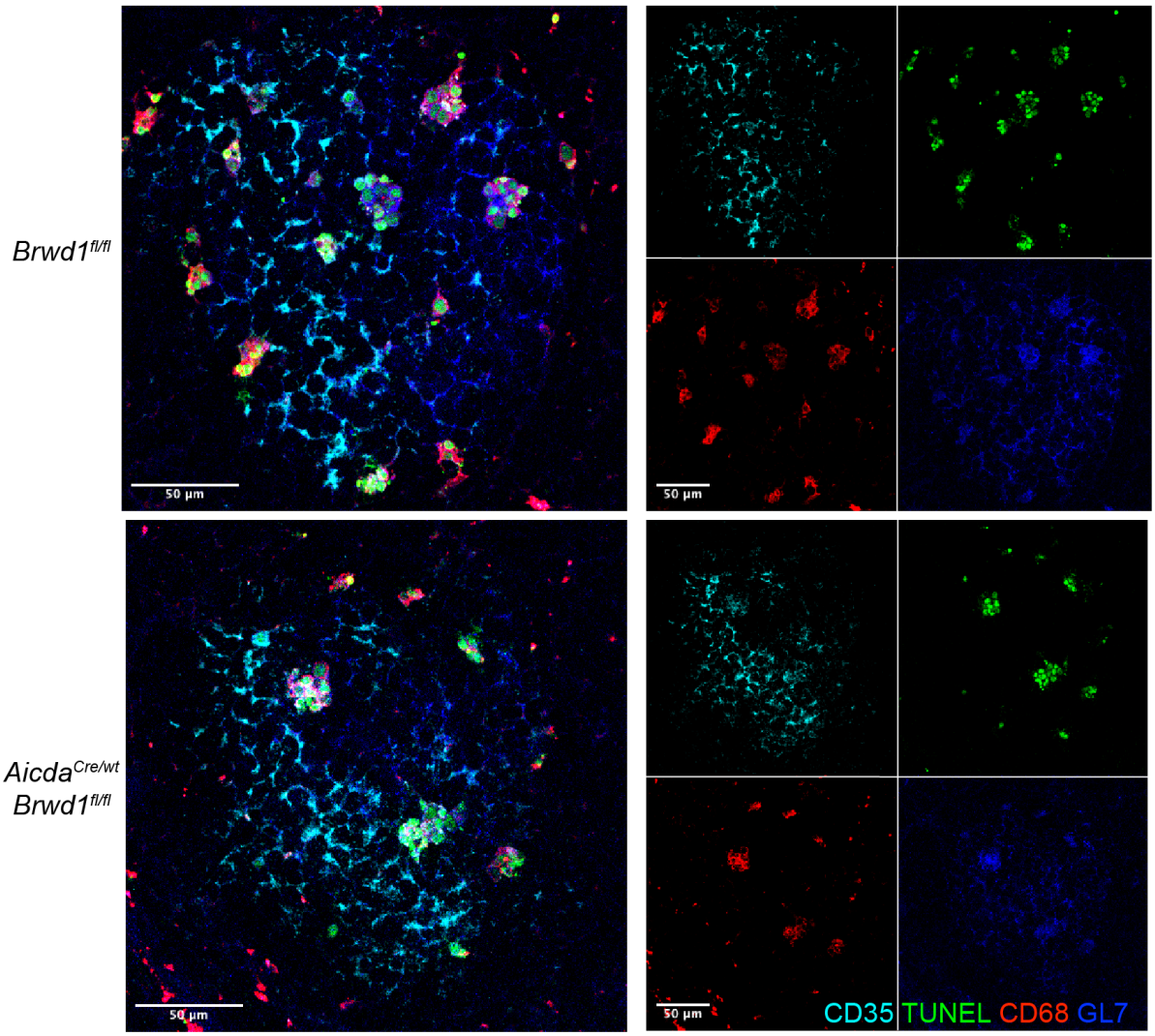

Figure 4.14: BRWD1 does not regulate the spatial distribution of early apoptotic cells. Representative immunofluorescence microscopy of splenic GCs from *Aicda*$^{Cre/wt}$ *Brwd1*$^{fl/fl}$ and *Brwd1*$^{fl/fl}$ mice immunized with SRBCs 14 days post-immunization using anti-CD35, TUNEL, anti-CD68, and GL7. (Scale bar = 50 μm, n = 4 for both groups)

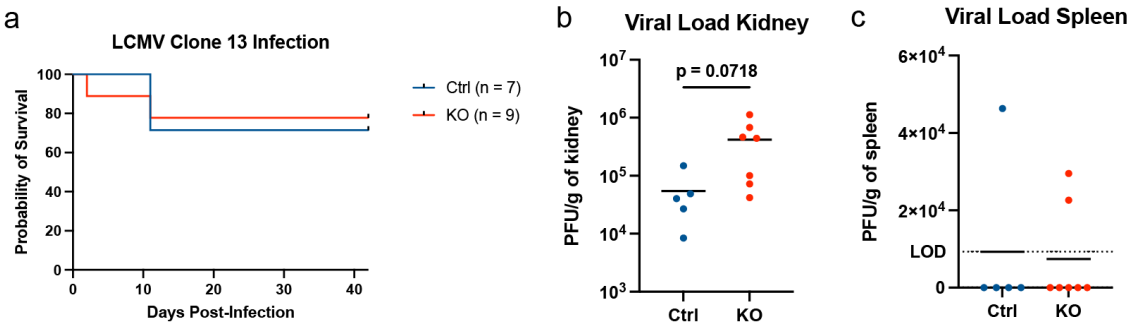

Figure 4.15: BRWD1 is not important for LCMV clone 13 disease course. *Aicda*$^{Cre/wt}$ *Brwd1*$^{fl/fl}$ and *Brwd1*$^{fl/fl}$ mice were infected with LCMV clone 13. **(a)** Kaplan-Meier survival curve to experimental endpoint of day 42 post-infection. **(b-c)** LCMV clone 13 viral loads in the kidney (b) and spleen (c) measured by plaque assay and normalized by weight of the tissue. LOD = limit of detection. (two-sided unpaired *t*-test, lines show means)

4.3 Discussion

4.3.1 Role of BRWD1 in germinal center cellular regulation

While in the prior chapter we described how BRWD1 is important for initiation of the GC response, here we demonstrate that BRWD1 has additional roles in the maintenance and function of GC B cells. Using *Aicda*^{Cre} mice to delete *Brwd1* in GC B cells after GC initiation, we discover an entirely different phenotype than that from using *Cd23*^{Cre} mice. Together, these and prior results show that BRWD1 is important throughout the B cell lineage from development and light chain recombination in the bone marrow to differentiation of activated B cells and the cycling of GC B cells in the periphery (Mandal et al., 2015, 2018).

In contrast to the results of the prior chapter, deletion of *Brwd1* in GC B cells resulted in increased GC B cells by flow cytometry. Similar results were also obtained with heterozygous mice, demonstrating a dose effect of BRWD1 in GC B cells. The increased cell number also resulted in larger GCs on average compared to controls.

The increased GC B cell number was due to increased proliferation. In small pre-B cells, we previously demonstrated that BRWD1 directly inhibits *Myc* and genes downstream of

Myc (Mandal et al., 2018). Furthermore, MYC is essential for the proliferation of positively selected GC B cells (Calado et al., 2012; Dominguez-Sola et al., 2012; Finkin et al., 2019). Thus, BRWD1 may directly inhibit *Myc* in GC B cells. ATAC-seq at the *Myc* locus in $Aicda^{Cre/wt}$ $Brwd1^{fl/fl}$ mice supported this. While in WT mice chromatin accessibility at *Myc* and downstream enhancers varies across the three GC subsets, these changes in chromatin accessibility were lost in $Brwd1^{-/-}$ GC B cells.

Throughout their lineage, B cells use separate cell stages to insulate proliferation and mutation from V(D)J recombination or SHM. We previously demonstrated that mitosis occurs in the DZp proximal to TBMs, describing both a spatial and cellular separation between proliferation and SHM in the GC (Kennedy et al., 2020). Here we showed that the increase in proliferation is greatest among cells within the DZp; however, we also observed increased proliferation among cells in the DZd. This result suggests a weakening of the division between proliferation and SHM in the GC. It would be interesting to explore whether the proliferating DZd cells are located next to TBMs. Furthermore, it is unknown whether this phenotype increases the risk for oncogenesis in GC B cells.

Not all characteristics of the GC response were abnormal in $Aicda^{Cre/wt}$ $Brwd1^{fl/fl}$ mice. For example, Tfh cells increased proportionally to the increased GC B cells. Because Tfh cells expand in response to antigen presentation by GC B cells, these results suggest that antigen presentation was normal in $Brwd1^{-/-}$ GC B cells (Merkenschlager et al., 2021). Furthermore, the LZ and DZ were both intact and in a normal ratio to one another by immunofluorescence microscopy and there were no major shifts in the LZ, DZp, or DZd of $Brwd1^{-/-}$ GC B cells by flow cytometry. This shows that $Brwd1^{-/-}$ GC B cells were still cycling through the GC zones.

Deletion of *Brwd1* had minor effects on the cellular products of the GC, namely MBCs. While we observed no differences in the number of mature MBCs, there was a decrease in the frequency of pre-MBCs within the GC following both homozygous and heterozygous

deletion of *Brwd1*. However, this had no effect on the number of pre-MBCs. We focused our studies on MBC populations that differentiated from the GC by using cell surface markers enriched in these populations. However, MBCs also differentiate directly from activated B cells, and BRWD1 may be important for these cells. Indeed, a single cell RNA-seq analysis of MBCs described two clusters of mature B cells, which corresponded with CD80^{+}PD-L2^{+} and CD80^{-}PD-L2^{-} MBC populations (Laidlaw et al., 2020). The CD80^{-}PD-L2^{-} MBC population, which is predominantly GC-independent, had *Brwd1* as a top differentially increased gene compared to the CD80^{+}PD-L2^{+} MBC population. Development of an MBC-specific Cre mouse model would allow our *Brwd1*-floxed mouse model to be used to study whether *Brwd1* is important for this GC-independent MBC subpopulation.

BRWD1 was also not necessary for establishing long-term memory responses in a 61 day recall experiment. GC B cells, plasmablasts, and PCs in both the spleen and bone marrow showed no difference in $Aicda^{Cre/wt}$ $Brwd1^{fl/fl}$ mice following recall compared with controls. These results further confirm that there are no major differences in MBC production in $Aicda^{Cre/wt}$ $Brwd1^{fl/fl}$ mice.

We also observed no differences in PC numbers following *Brwd1* deletion. In heterozygous mice, tdT^{+} PCs had decreased SHM compared with tdT^{-} PCs. Because SHM occurs within the GC, these results suggest that $Brwd1^{+/-}$ PCs exit the GC earlier than $Brwd1^{+/+}$ PCs and that $Brwd1^{+/-}$ GC B cells are more likely to differentiate into PCs.

We also studied the role of BRWD1 in SHM. While $Brwd1^{-/-}$ GCs had normal SHM rates, the distribution of SHM in GC B cells was greater such that some clones had few if any mutations while others had 10 or more mutations at 14 days post-immunization. Normally, there is a stringent relationship between SHM, selection, and proliferation with B cells proliferating once or twice following LZ selection (Gitlin et al., 2014; Ersching et al., 2017; Long et al., 2022; Finkin et al., 2019; Pae et al., 2020). In contrast, our data are consistent with $Brwd1^{-/-}$ GC B cells proliferating chaotically following selection. Together

with the increased proliferation observed among DZd cells, these results show a weakening of the separation between proliferation and SHM.

Furthermore, *Brwd1*$^{-/-}$ GC B cells had decreased affinity maturation. This could be due to dysregulation of either positive or negative selection of *Brwd1*$^{-/-}$ GC B cells. For example, *Brwd1*$^{-/-}$ GC B cells with a low affinity for NP may still be able to proliferate and cycle through the GC with diminished or no positive selection signals. Alternatively, it is possible that the negative selection signals to either exit the GC or undergo apoptosis are not properly received in these cells.

The model we used to measure affinity maturation only requires a single amino acid substitution to enhance B cell receptor affinity (Heise and Klein, 2017). Thus, it would be interesting to test affinity maturation using a more complex model antigen that requires multiple mutations to enhance affinity. We also tested the importance of *Brwd1* in a more complex infection model by infecting mice with LCMV clone 13. We observed no significant differences in the disease course of *Aicda*$^{Cre/wt}$ *Brwd1*$^{fl/fl}$ mice. While clearance of LCMV clone 13 does require a polyclonal B cell response, it would be interesting to use a disease model that is more dependent on B cell responses such as influenza in the future (Bergthaler et al., 2009; Guthmiller et al., 2021). In our experiments we also did not track antibody production or the neutralizing ability of antibodies in our mice. While affinity maturation is decreased in *Aicda*$^{Cre/wt}$ *Brwd1*$^{fl/fl}$ mice, it is possible that the antibody output of these mice is more normal.

We also characterized SHM in tdT^{-} GC B cells from *Aicda*$^{Cre/wt}$ *Brwd1*$^{fl/fl}$ mice (data not shown). These cells had the same rate of SHM as tdT^{+} GC B cells, demonstrating that they are genuine GC B cells and as a population are within the GC for the same duration as tdT^{+} GC B cells that have deleted *Brwd1*. Surprisingly, tdT^{-} GC B cells also had decreased affinity maturation relative to control mice (data not shown). These results suggest that the observed defect in affinity maturation is extrinsic from *Brwd1* deletion. In the future, this

phenomenon could be studied with a mixed bone marrow chimera to determine the intrinsic and extrinsic effects of *Brwd1* deletion on the GC.

We also observed in a portion of $Aicda^{Cre/wt}$ $Brwd1^{fl/fl}$ mice an initial break in tolerance as measured by anti-nuclear antibody tests. Remarkably, self-reactive sera was only detected in response to immunization and as soon as 14 days following immunization of $Aicda^{Cre/wt}$ $Brwd1^{fl/fl}$ mice. Notably, one study found autoreactive B cells that were associated with lymphoma driver mutations and excessive GC B cell proliferation (Singh et al., 2020). Thus, dysregulated GC B cell proliferative programs may contribute to the production of self-reactive clones in the GC.

How autoreactive clones were selected in $Aicda^{Cre/wt}$ $Brwd1^{fl/fl}$ mice is unclear. One possibility is that self-antigens were in the GCs of $Aicda^{Cre/wt}$ $Brwd1^{fl/fl}$ mice, allowing for selection of self-reactive clones. For example, an inability to clear apoptotic cells in the GC leads to lupus-like autoimmunity (Cohen et al., 2002; Baumann et al., 2002; A-Gonzalez et al., 2009; Rahman, 2011). We investigated this possibility by measuring apoptotic debris in the GC by H&E staining and found that some $Aicda^{Cre/wt}$ $Brwd1^{fl/fl}$ mice had a greater debris score assigned by a blinded pathologist. While still inconclusive, these results support a model whereby aberrant apoptosis in the GC introduces cellular debris. This debris could then allow positive selection of self-reactive clones while directing affinity maturation away from the immunized model antigen. However, staining GCs with TUNEL to measure GC B cells still completing apoptosis revealed that these apoptotic cells were found next to or within TBMs as expected (Kennedy et al., 2020; Gurwicz et al., 2023; Grootveld et al., 2023). Differences in apoptosis and self-antigens within the GC may be subtle but could have large effects on tolerance.

The decreased affinity maturation and breaks in tolerance following *Brwd1* deletion show that the BCR repertoire of $Brwd1^{-/-}$ GC B cells is altered. Chaotic proliferation or permissive selection may allow the expansion of clones that are not specific to antigens within

the GC. To test the repertoires of *Aicda*$^{Cre/wt}$ *Brwd1*$^{fl/fl}$ mice, we could use a cocktail of degenerate primers specific to different V families to see whether the repertoires are skewed toward specific V families. Alternatively, V(D)J-seq could be used to measure the repertoire of *Aicda*$^{Cre/wt}$ *Brwd1*$^{fl/fl}$ mice.

4.3.2 Role of BRWD1 in germinal center molecular regulation

Deletion of *Brwd1* resulted in dysregulated GC B cell transcription with two major characteristics. First, we observed a blending of transcriptional programs especially in *Brwd1*$^{-/-}$ DZp cells. Second, all *Brwd1*$^{-/-}$ GC subsets shared an inflammatory transcriptional program compared to WT GC subsets.

Regarding the blending of transcriptional programs, we used K-means clustering of differentially expressed genes in WT GC B cells to focus on how WT transcriptional programs are altered in *Brwd1*$^{-/-}$ GC B cells. Remarkably, *Brwd1*$^{-/-}$ DZp cells lacked the unique WT DZp transcriptional programs and instead had transcription intermediate that of LZ and DZd cells for these gene clusters. Thus, BRWD1 was necessary for the transcriptional integrity of the DZp proliferative programs. These results support the dysregulated proliferation of *Brwd1*$^{-/-}$ GC B cells.

Deletion of *Brwd1* also induced novel inflammatory gene signatures across *Brwd1*$^{-/-}$ GC subsets. These novel transcriptional programs were identified by comparing WT and *Brwd1*$^{-/-}$ cells from each GC subset and revealed over 1,000 genes with increased expression in *Brwd1*$^{-/-}$ LZ, DZp, and DZd cells. Many of these genes upregulated in each GC zone were shared between zones and were involved in immune cell signaling or inflammatory pathways. Inflammatory signals may explain the observed defects in affinity maturation and tolerance in *Aicda*$^{Cre/wt}$ *Brwd1*$^{fl/fl}$ mice. They could subvert both GC positive and negative selection by providing activation signals not determined by antigen avidity.

The exact mechanism behind this induction of transcriptional programs is unclear. It

could represent aberrant transcriptional activation in *Brwd1*$^{-/-}$ GC B cells. If BRWD1 directly regulates these genes, then BRWD1 would appear to act primarily as a transcriptional repressor in GC B cells. We previously demonstrated in small pre-B cells how BRWD1 controls chromatin looping and transcription through cohesin conversion (Mandal et al., 2024); however, this mechanism mostly explains gene activation. Thus, it is unclear which BRWD1-mediated mechanism or if an unknown mechanism could inhibit these genes in GC B cells. Alternatively, the aberrant transcriptional activation may be the effects of an environmental defect within the GC as described above. In this case, we did not consistently observe an upregulation of apoptotic pathways, and we failed to detect an increase in apoptotic cells within the GC.

BRWD1 also maintained GC epigenetic identity by polarizing chromatin accessibility differences between GC subsets. *Brwd1*$^{-/-}$ GC B cell subsets had a striking collapse of both chromatin accessibility differences and unique TF binding site accessibility toward a common state. Given the functions of BRWD1 in other contexts, we postulate that this epigenetic blending reflected a failure to prime transitions between GC B cell subset states. This epigenetic blending did not precisely map to transcriptional changes and was observed across all *Brwd1*$^{-/-}$ GC B cell subsets, unlike the transcriptional blending that was primarily observed in the DZp. Together these results demonstrate how the epigenetic regulation of GC B cells is necessary for specific GC functions.

Notably, *Myc* expression was relatively unchanged across *Brwd1*$^{-/-}$ GC B cell subsets, although there was a small increase in *Myc* expression in the *Brwd1*$^{-/-}$ DZp and DZd cells. This was unsurprising as *Myc* is expressed in a small number of positively selected GC B cells within the LZ (Dominguez-Sola et al., 2012). Our bulk gating strategy for LZ GC B cells includes cells at various stages of selection, so *Myc* expression is an average of these populations. Furthermore, while MYC is necessary for initiating the proliferative program, MYC activity is mostly restricted to the LZ and *Myc* expression decreases once

cells transition to the DZp (Finkin et al., 2019). Different cell cycle regulators, such as cyclin D3, are instead important for driving and completing the proliferative program (Pae et al., 2020). Our bulk gating strategy does reveal how chromatin accessibility at *Myc* and its downstream enhancers is tightly regulated in all GC B cell subsets. We postulate that regulation of *Myc* accessibility across all GC B cell subsets is necessary to allow for the rapid and transient *Myc* expression in a small population of GC B cells following Tfh cell-mediated selection.

In total, our results show how BRWD1 is necessary for GC integrity. Deletion of *Brwd1* in GC B cells resulted in major transcriptional and epigenetic disruption, which had specific effects on GC function, namely proliferation, affinity maturation, and tolerance. While we previously proposed a three-zone model of the GC that illuminates the transcriptional and epigenetic variation throughout the GC cycle (Kennedy et al., 2020), our data here validate this model and demonstrate that the molecular distinctions between the three GC zones are essential for GC function (Fig 4.16).

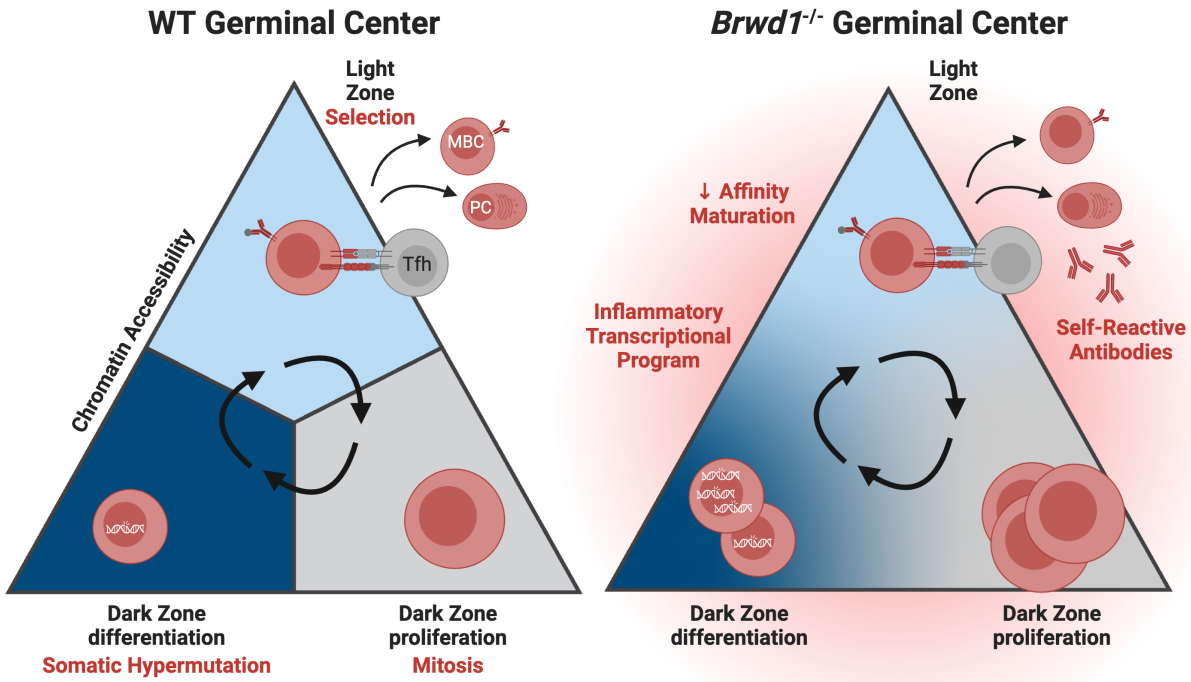

Figure 4.16: Model of BRWD1 in germinal center B cells. In WT GCs, B cells cycle between selection in the light zone, mitosis in the dark zone proliferation, and somatic hypermutation in the dark zone differentiation. Selection is mediated by T follicular helper (Tfh) cells and results in some B cells differentiating into memory B cells (MBCs) or plasma cells (PCs). Cycling between these three zones involves large changes in chromatin accessibility so that each cell subset is molecularly distinct (represented by the tricolored triangle). In contrast, deletion of *Brwd1* in GC B cells results in a blending of chromatin accessibility between GC subsets. *Brwd1* deletion also results in blending of transcriptional proliferative programs as well as an inflammatory transcriptional program shared across GC subsets. This is associated with specific defects including increased proliferation, chaotic somatic hypermutation, decreased affinity maturation, and production of self-reactive antibodies. Meanwhile, Tfh cells, MBCs, and PCs are mostly normal. This figure was created using BioRender.com.

CHAPTER 5

DISCUSSION

5.1 Molecular mechanisms regulating the germinal center

There are four stages of B cell development and activation in which the molecular necessities of diversity must be insulated from, and coordinated with, proliferation and selection (Wright et al., 2023). The precise cellular states to which light chain recombination and SHM are restricted have been defined (Kennedy et al., 2020; Mandal et al., 2018, 2015). In contrast, we only know the general developmental windows in which heavy chain recombination and CSR occur. BRWD1, which is first highly expressed in small pre-B cells, orchestrates the large epigenetic and transcriptional transitions that enable and insulate light chain recombination, CSR, and SHM from proliferation (Mandal et al., 2015, 2018). Therefore, BRWD1 is essential for most of the defining molecular events of B cell adaptive immunity.

The GC presents unique challenges for transcriptional and epigenetic regulation. Rapid cycling through the GC presents one such challenge. These transitions between GC B cell subsets are so rapid that gene transcription occurs in the GC B cell subset preceding the subset in which the translated protein is needed (Kennedy et al., 2020). These transitions are also impermanent, because as long as GC B cells are cycling they do not terminally differentiate. Furthermore, GC B cells proliferate more rapidly than other cell types with cell cycles as short as 5 to 6 hours depending on the degree of T cell help (Gitlin et al., 2015). This rapid proliferation, which precedes SHM, inevitably requires greater protection to prevent oncogenesis. Lastly, GC B cells must integrate multiple cell signaling inputs from the B cell receptor and Tfh cells to differentiate down multiple pathways to either recycle through the GC, differentiate as MBCs or PCs, or undergo apoptosis. Each of these pathways require their own unique molecular programs.

We propose that epigenetic chromatin regulation acting upstream of TF networks and

their transcriptional programs is essential for GC B cell transitions. Although many TFs are essential for GC B cell activity and differentiation, regulating the expression of these TFs may be too slow for GC B cells. Instead, we propose that the opening and closing of TF binding sites allows for different TF programs to manifest without large changes in TF expression levels. Furthermore, chromatin looping allows for rapid changes in promoter-enhancer interactions to quickly turn transcription on and off. We propose that BRWD1, in relationship with other epigenetic regulators, mediates many of these epigenetic changes through cohesin conversion or nucleosome positioning.

We have demonstrated that BRWD1 mediates important B cell fate transitions. In both B cell development and the GC, BRWD1 represses *Myc* (Mandal et al., 2018). However, the genetic programs regulated by BRWD1 at each stage are not identical. An obvious example is that BRWD1 mediates *Igk* contraction in small pre-B cells yet contributes to CSR in the periphery. BRWD1 is recruited to specific histone modifications downstream of signaling pathways (McLean and Mandal, 2020; Mandal et al., 2015). Therefore, it is likely that signaling and developmental contexts dictate where BRWD1 is recruited in the genome and which TADs and genes it acts on.

Considering BRWD1's essential role in chromatin loop extrusion, it was surprising that $Cd23^{Cre/wt}$ $Brwd1^{fl/fl}$ and $Aicda^{Cre/wt}$ $Brwd1^{fl/fl}$ mice still formed GCs. One possibility is that *Brwd1* homologs *Phip* and *Brwd3* compensated for *Brwd1* loss, although these homologs may lack functional domains unique to *Brwd1* (data not shown). Alternatively, our results may reveal the degree to which loop extrusion is necessary for cell differentiation. Disruption of loop extrusion by depleting cohesin in embryonic stem cells only modestly effects transcription (Davidson and Peters, 2021; Busslinger et al., 2017). However, loop extrusion by cohesin is required for many promoter-enhancer interactions, especially those occurring over longer distances in differentiated cells (Thiecke et al., 2020; Khattabi et al., 2019). Our results suggest that BRWD1-mediated changes in chromatin topology allow GC

B cell subsets to fully polarize as they rapidly cycle through the GC.

GC spatial organization into a LZ and DZ is dependent on the chemokine receptor CXCR4 expressed by B cells, which recognizes the ligand CXCL12 expressed by DZ reticular cells (Allen et al., 2004). However, disruption of either CXCR4 or its ligand CXCL12 only mildly affects SHM or affinity maturation despite the loss of spatial separation between the LZ and DZ (Bannard et al., 2013; Pikor et al., 2020). Thus, while spatial polarization is not necessary for GC function, the fidelity of molecular programs within each GC B cell subset is necessary.

5.2 Germinal center evolution

Our results reveal the role of the GC in the evolution of the humoral immune response. BRWD1 was only necessary for GC selection. In fact, many characteristics of the GC response, including zonal organization, MBC and PC differentiation, and Tfh cells, were normal in $Aicda^{Cre/wt}$ $Brwd1^{fl/fl}$ mice. These observations are consistent with what is known about GC evolutionary biology.

The adaptive humoral immune system evolved approximately 500 million years ago in ectothermic vertebrates (Flajnik, 2018). Jawless fish, such as the lamprey, evolved variable lymphocyte receptors (VLRs), while jawed vertebrates evolved immunoglobulin receptors (Pancer et al., 2004; Flajnik, 2018). Approximately 450 million years ago, SHM arose in cartilaginous fish, which can also generate MBCs and PCs (Matz and Dooley, 2023; Dooley and Flajnik, 2005; Castro et al., 2013). Furthermore, all jawed vertebrates have AID to mutate immunoglobulins (Barreto and Magor, 2011). In cartilaginous fish, SHM functions to diversify antibody responses and only modestly enhances affinity (Dooley et al., 2006; Matz et al., 2023). Furthermore, adaptive humoral immunity in ectotherms generally occurs more slowly with both the beginning of antibody production and the peak of the antibody response occurring later than in endotherms (Matz and Dooley, 2023). Thus in many ectotherms,

adaptive humoral immunity is less stringently selective and produces broad responses that are likely more important for a diverse memory responses.

GCs and affinity maturation convergently evolved only in endothermic jawed vertebrates, mammals and birds, approximately 200 million years ago (Matz and Dooley, 2023). Notably, mammalian and avian GCs both evolved FDCs to present antigen to B cells (Flajnik, 2018). In contrast, ectothermic frogs use a single hematopoietic antigen presenting cell, termed an XL cell, to present antigen to both T and B cells. Furthermore, mammalian and avian GCs both spatially separate the LZ and DZ, with the avian DZ situated as a ring surrounding a central LZ (Matz and Dooley, 2023). That both mammals and birds convergently evolved similar GC structures is likely important. Thus, evolution of the GC included separation of multiple immune functions into distinct cell types and locations. We posit that GC evolution also included separation of proliferation and mutation into distinct GC B cell subsets.

The advent of GCs allowed for efficient affinity maturation. While SHM in ectothermic vertebrates can increase affinity about 10-fold maximally, GC-mediated affinity maturation in endothermic vertebrates can lead to 10,000-fold increases in affinity (Matz and Dooley, 2023). The structure of GCs allows for more stringent and efficient selective pressures that facilitate faster and more specific antibody responses. Presumably, the potential for greater affinity maturation against foreign antigens also increased the risk for affinity maturation toward self antigens. It has been argued that GCs evolved to deal with the more rapid cell proliferation that accompanies the higher core body temperature of endotherms (Matz and Dooley, 2023). Indeed, we postulate that with higher proliferative rates, insulation between SHM and mitosis via specialization of GC subsets became an evolutionary imperative to diminish the risk of neoplastic transformation. These observations suggest that BRWD1 selectively mediates functions that were only acquired with the evolutionary advent of GCs.

5.3 Future directions

While we demonstrated that BRWD1 is important for GC initiation, differentiation of Fol B cells into GC B cells involves multiple stages across four days following antigen encounter. It would be interesting to determine which specific stage of differentiation BRWD1 is necessary for. Because differentiating activated B cells are a small and transient population, single cell RNA-seq and ATAC-seq could reveal the precise transcriptional and epigenetic programs BRWD1 regulates for GC initiation. Furthermore, we demonstrate that BRWD1 establishes epigenetic states in Fol B cells for later GC differentiation. ChIP-seq of BRWD1 could reveal which of these chromatin accessibility states are regulated directly by BRWD1.

While we show that BRWD1 regulates the accessibility of important TF binding sites in both Fol and GC B cells, we have not proven whether these changes in chromatin accessibility actually change the binding patterns of the same TFs using ChIP-seq. In WT and *Brwd1*$^{-/-}$ Fol B cells, we will perform ChIP-seq for the TFs IRF4 and OCT2, which are important for GC initiation and have BRWD1-regulated chromatin binding sites (Zhang et al., 2017b; Doane et al., 2021). Similarly, we will perform ChIP-seq in WT and *Brwd1*$^{-/-}$ GC B cell subsets for IRF4, SPIB, and PU.1, which had increased open binding sites across all *Brwd1*$^{-/-}$ GC B cell subsets.

Because BRWD1 is necessary to polarize the epigenetic states of GC B cell subsets, BRWD1 is likely differentially recruited throughout the genome in each GC B cell subset. Furthermore, specific histone marks (H3S10p, H3K9ac, and H3K14ac) recruit BRWD1 in small pre-B cells (Mandal et al., 2015). Thus, we predict that these specific histone marks are added and removed throughout the genome to control BRWD1 binding. Because H3S10p marks are deposited downstream of ERK signaling, B cell signaling may direct the activity of BRWD1 in GC B cells (McLean and Mandal, 2020). Furthermore, BRWD1 likely regulates GC B cells through cohesin conversion to control 3D chromatin structure. We predict that ChIP-seq of cohesin, NIPBL, and WAPL would reveal dynamic cohesin complexes

that explain variable chromatin accessibility across the GC B cell subsets. Measuring both BRWD1 binding and the hallmarks of cohesin conversion with ChIP-seq would allow us to determine which chromatin accessibility sites are regulated directly by BRWD1 and which are secondary effects of BRWD1 activity.

We would also like to understand the degree by which chromatin accessibility differences in *Brwd1*$^{-/-}$ GC B cells determine transcriptional differences in *Brwd1*$^{-/-}$ GC B cells. One possibility is that BRWD1 regulates enhancer activity by controlling chromatin accessibility and looping. To identify enhancers and their status, we could perform ChIP-seq to identify active enhancers with H3K27ac and H3K4me1 marks and repressed enhancers with H3K27me3 marks. We could also identify poised enhancers with just H3K4me1 marks, bivalent enhancers with H3K4me1 and H3K27me3 marks, and active promoters with H3K4me3 (Creyghton et al., 2010; Rada-Iglesias et al., 2011; Blanco et al., 2020; Heintzman et al., 2007). We predict that active and repressed enhancers will change between GC B cell subsets in a BRWD1-dependent manner.

Considering BRWD1's role in organizing 3D chromatin structure (Mandal et al., 2024), we predict that regulation of chromatin loop extrusion is a major contributor to the chromatin accessibility differences observed between GC B cell subsets. We would like to perform Hi-C across GC B cell subsets both in WT and *Aicda*$^{Cre/wt}$ *Brwd1*$^{fl/fl}$ mice to measure how chromatin contacts change across GC B cell subsets. We predict BRWD1 will be essential for maintaining long-range chromatin contacts and that without BRWD1 each GC B cell subset will have similar 3D chromatin structures.

Brwd1$^{-/-}$ GC B cells had greater *Ighm* expression and decreased *Ighg1* expression relative to WT GC B cells. This was consistent with the decreased antibody class switching in *Cd23*$^{Cre/wt}$ *Brwd1*$^{fl/fl}$ mice. To study SHM, we focused on B cell clones expressing IgG1 because the antibody response to the hapten NP is predominantly IgG1 (Heise and Klein, 2017). Because of the different antibody isotype usages between mice, we will also measure

SHM in IgM^+ clones.

Lastly, we observed an inflammatory transcriptional program in *Brwd1*$^{-/-}$ GC B cells, yet it was unclear whether this was a direct or indirect effect from *Brwd1* deletion. This could be tested with a mixed bone marrow chimera of WT and *Brwd1*$^{-/-}$ cells. If a direct effect from *Brwd1* deletion, then only *Brwd1*$^{-/-}$ cells should display the inflammatory transcriptional program. In this case, ChIP-seq of BRWD1 could reveal whether BRWD1 binds near the inflammatory genes and directly represses them. Alternatively, if the inflammatory transcriptional program is caused by an inflammatory environment indirect from *Brwd1* deletion, then WT GC B cells should express the same genes. In this case, other cell types within the GC such as Tfh cells may also show transcriptional signs of inflammation.

5.4 Conclusion

The GC is one of evolution's greatest accomplishments. While the natural selection of species occurs across generations, the selection of B cell clones within the GC occurs over days to produce antibodies perfectly adapted for their cognate antigen. These antibodies can be highly mutated with remarkable affinities. Because of the GC, these antibodies mediate potent and lasting immune responses following infection and vaccination. The converse to this ability is that GCs are capable of causing terrible diseases in autoimmunity and lymphoma.

Throughout the 2010's, immunologists discovered the complex cell networks and cell regulators that drive the GC reaction. Now as a field, we are continually gaining a better understanding of the molecular systems behind GC biology. Here I have shown how the epigenetic reader BRWD1 controls molecular programs for proper GC function. Continuing to understand how BRWD1 and the many other epigenetic and cell regulators of the GC work in complex together will allow us to better leverage the power of the GC for health and medicine.

REFERENCES

Noelia A-Gonzalez, Steven J. Bensinger, Cynthia Hong, Susana Beceiro, Michelle N. Bradley, Noam Zelcer, Jose Deniz, Cristina Ramirez, Mercedes Díaz, German Gallardo, Carlos Ruiz de Galarreta, Jon Salazar, Felix Lopez, Peter Edwards, John Parks, Miguel Andujar, Peter Tontonoz, and Antonio Castrillo. Apoptotic cells promote their own clearance and immune tolerance through activation of the nuclear receptor LXR. *Immunity*, 31(2):245–258, 2009. doi:10.1016/j.immuni.2009.06.018.

Christopher D C Allen, K Mark Ansel, Caroline Low, Robin Lesley, Hirokazu Tamamura, Nobutaka Fujii, and Jason G Cyster. Germinal center dark and light zone organization is mediated by CXCR4 and CXCR5. *Nature Immunology*, 5(9):943–952, 2004. doi:10.1038/ni1100.

Zhaoqing Ba, Jiangman Lou, Adam Yongxin Ye, Hai-Qiang Dai, Edward W. Dring, Sherry G. Lin, Suvi Jain, Nia Kyritsis, Kyong-Rim Kieffer-Kwon, Rafael Casellas, and Frederick W. Alt. CTCF orchestrates long-range cohesin-driven V(D)J recombinational scanning. *Nature*, 586(7828):305–310, 2020. doi:10.1038/s41586-020-2578-0.

Peter Bankhead, Maurice B. Loughrey, José A. Fernández, Yvonne Dombrowski, Darragh G. McArt, Philip D. Dunne, Stephen McQuaid, Ronan T. Gray, Liam J. Murray, Helen G. Coleman, Jacqueline A. James, Manuel Salto-Tellez, and Peter W. Hamilton. QuPath: open source software for digital pathology image analysis. *Scientific Reports*, 7(1):16878, 2017. doi:10.1038/s41598-017-17204-5.

Oliver Bannard, Robert M. Horton, Christopher D.C. Allen, Jinping An, Takashi Nagasawa, and Jason G. Cyster. Germinal Center Centroblasts Transition to a Centrocyte Phenotype According to a Timed Program and Depend on the Dark Zone for Effective Selection. *Immunity*, 39(5):912–924, 2013. doi:10.1016/j.immuni.2013.08.038.

Vasco M. Barreto and Brad G. Magor. Activation-induced cytidine deaminase structure and functions: a species comparative view. *Developmental & Comparative Immunology*, 35(9): 991–1007, 2011. doi:10.1016/j.dci.2011.02.005.

Katia Basso, Masumichi Saito, Pavel Sumazin, Adam A. Margolin, Kai Wang, Wei-Keat Lim, Yukiko Kitagawa, Christof Schneider, Mariano J. Alvarez, Andrea Califano, and Riccardo Dalla-Favera. Integrated biochemical and computational approach identifies BCL6 direct target genes controlling multiple pathways in normal germinal center B cells. *Blood*, 115 (5):975–984, 2010. doi:10.1182/blood-2009-06-227017.

Benedikt W. Bauer, Iain F. Davidson, Daniel Canena, Gordana Wutz, Wen Tang, Gabriele Litos, Sabrina Horn, Peter Hinterdorfer, and Jan-Michael Peters. Cohesin mediates DNA loop extrusion by a "swing and clamp" mechanism. *Cell*, 184(21):5448–5464.e22, 2021. doi:10.1016/j.cell.2021.09.016.

Irith Baumann, Wasilis Kolowos, Reinhard E. Voll, Bernhard Manger, Udo Gaipl, Winfried L. Neuhuber, Thomas Kirchner, Joachim R. Kalden, and Martin Herrmann. Impaired uptake of apoptotic cells into tingible body macrophages in germinal centers of patients with systemic lupus erythematosus. *Arthritis & Rheumatism*, 46(1):191–201, 2002. doi:10.1002/1529-0131(200201)46:1<191::aid-art10027>3.0.co;2-k.

Andreas Bergthaler, Lukas Flatz, Admar Verschoor, Ahmed N. Hegazy, Martin Holdener, Katja Fink, Bruno Eschli, Doron Merkler, Rami Sommerstein, Edit Horvath, Marylise Fernandez, André Fitsche, Beatrice M Senn, J. Sjef Verbeek, Bernhard Odermatt, Claire-Anne Siegrist, and Daniel D. Pinschewer. Impaired antibody response causes persistence of prototypic T cell–contained virus. *PLoS Biology*, 7(4):e1000080, 2009. doi:10.1371/journal.pbio.1000080.

Enrique Blanco, Mar González-Ramírez, Anna Alcaine-Colet, Sergi Aranda, and Luciano Di Croce. The bivalent genome: characterization, structure, and regulation. *Trends in Genetics*, 36(2):118–131, 2020. doi:10.1016/j.tig.2019.11.004.

Paola Bonetti, Monica Testoni, Marta Scandurra, Maurilio Ponzoni, Roberto Piva, Afua A. Mensah, Andrea Rinaldi, Ivo Kwee, Maria Grazia Tibiletti, Javeed Iqbal, Timothy C. Greiner, Wing-Chung Chan, Gianluca Gaidano, Miguel A. Piris, Franco Cavalli, Emanuele Zucca, Giorgio Inghirami, and Francesco Bertoni. Deregulation of ETS1 and FLI1 contributes to the pathogenesis of diffuse large B-cell lymphoma. *Blood*, 122(13):2233–2241, 2013. doi:10.1182/blood-2013-01-475772.

Xavier Brochet, Marie-Paule Lefranc, and Véronique Giudicelli. IMGT/V-QUEST: the highly customized and integrated system for IG and TR standardized V-J and V-D-J sequence analysis. *Nucleic Acids Research*, 36(suppl_2):W503–W508, 2008. doi:10.1093/nar/gkn316.

Karen L. Bunting, T. David Soong, Rajat Singh, Yanwen Jiang, Wendy Béguelin, David W. Poloway, Brandon L. Swed, Katerina Hatzi, William Reisacher, Matt Teater, Olivier Elemento, and Ari M. Melnick. Multi-tiered reorganization of the genome during B cell affinity maturation anchored by a germinal center-specific locus control region. *Immunity*, 45(3):497–512, 2016. doi:10.1016/j.immuni.2016.08.012.

Deborah L. Burnett, David B. Langley, Peter Schofield, Jana R. Hermes, Tyani D. Chan, Jennifer Jackson, Katherine Bourne, Joanne H. Reed, Kate Patterson, Benjamin T. Porebski, Robert Brink, Daniel Christ, and Christopher C. Goodnow. Germinal center antibody mutation trajectories are determined by rapid self/foreign discrimination. *Science*, 360 (6385):223–226, 2018. doi:10.1126/science.aao3859.

Georg A. Busslinger, Roman R. Stocsits, Petra van der Lelij, Elin Axelsson, Antonio Tedeschi, Niels Galjart, and Jan-Michael Peters. Cohesin is positioned in mammalian genomes by transcription, CTCF and Wapl. *Nature*, 544(7651):503–507, 2017. doi:10.1038/nature22063.

Danyal Butt, Tyani D. Chan, Katherine Bourne, Jana R. Hermes, Akira Nguyen, Aaron Statham, Lorraine A. O'Reilly, Andreas Strasser, Susan Price, Peter Schofield, Daniel Christ, Antony Basten, Cindy S. Ma, Stuart G. Tangye, Tri Giang Phan, V. Koneti Rao, and Robert Brink. FAS inactivation releases unconventional germinal center B cells that escape antigen control and drive IgE and autoantibody production. *Immunity*, 42(5): 890–902, 2015. doi:10.1016/j.immuni.2015.04.010.

Wendy Béguelin, Relja Popovic, Matt Teater, Yanwen Jiang, Karen L. Bunting, Monica Rosen, Hao Shen, Shao Ning Yang, Ling Wang, Teresa Ezponda, Eva Martinez-Garcia, Haikuo Zhang, Yupeng Zheng, Sharad K. Verma, Michael T. McCabe, Heidi M. Ott, Glenn S. Van Aller, Ryan G. Kruger, Yan Liu, Charles F. McHugh, David W. Scott, Young Rock Chung, Neil Kelleher, Rita Shaknovich, Caretha L. Creasy, Randy D. Gascoyne, Kwok-Kin Wong, Leandro Cerchietti, Ross L. Levine, Omar Abdel-Wahab, Jonathan D. Licht, Olivier Elemento, and Ari M. Melnick. EZH2 Is required for germinal center formation and somatic EZH2 mutations promote lymphoid transformation. *Cancer Cell*, 23(5):677–692, 2013. doi:10.1016/j.ccr.2013.04.011.

Wendy Béguelin, Martín A. Rivas, María T. Calvo Fernández, Matt Teater, Alberto Purwada, David Redmond, Hao Shen, Matt F. Challman, Olivier Elemento, Ankur Singh, and Ari M. Melnick. EZH2 enables germinal centre formation through epigenetic silencing of CDKN1A and an Rb-E2F1 feedback loop. *Nature Communications*, 8(1):877, 2017. doi:10.1038/s41467-017-01029-x.

Marieta Caganova, Chiara Carrisi, Gabriele Varano, Federica Mainoldi, Federica Zanardi, Pierre-Luc Germain, Laura George, Federica Alberghini, Luca Ferrarini, Asoke K. Talukder, Maurilio Ponzoni, Giuseppe Testa, Takuya Nojima, Claudio Doglioni, Daisuke Kitamura, Kai-M. Toellner, I-hsin Su, and Stefano Casola. Germinal center dysregulation by histone methyltransferase EZH2 promotes lymphomagenesis. *Journal of Clinical Investigation*, 123(12):5009–5022, 2013. doi:10.1172/jci70626.

Dinis Pedro Calado, Yoshiteru Sasaki, Susana A. Godinho, Alex Pellerin, Karl Köchert, Barry P. Sleckman, Ignacio Moreno de Alborán, Martin Janz, Scott Rodig, and Klaus Rajewsky. The cell-cycle regulator c-Myc is essential for the formation and maintenance of germinal centers. *Nature Immunology*, 13(11):1092–1100, 2012. doi:10.1038/ni.2418.

Derrick Callahan, Shuchi Smita, Stephen Joachim, Kenneth Hoehn, Steven Kleinstein, Florian Weisel, Maria Chikina, and Mark Shlomchik. Memory B cell subsets have divergent developmental origins that are coupled to distinct imprinted epigenetic states. *Nature Immunology*, 25(3):562–575, 2024. doi:10.1038/s41590-023-01721-9.

Renan V.H. de Carvalho, Jonatan Ersching, Alexandru Barbulescu, Alvaro Hobbs, Tiago B.R. Castro, Luka Mesin, Johanne T. Jacobsen, Brooke K. Phillips, Hans-Heinrich Hoffmann, Roham Parsa, Maria Cecilia C. Canesso, Carla R. Nowosad, Allan Feng, Sarah R. Leist, Ralph S. Baric, Emily Yang, P.J. Utz, and Gabriel D. Victora. Clonal replacement sustains long-lived germinal centers primed by respiratory viruses. *Cell*, 186 (1):131–146.e13, 2023. doi:10.1016/j.cell.2022.11.031.

Caitlin D. Castro, Yuko Ohta, Helen Dooley, and Martin F. Flajnik. Noncoordinate expression of J-chain and Blimp-1 define nurse shark plasma cell populations during ontogeny. *European Journal of Immunology*, 43(11):3061–3075, 2013. doi:10.1002/eji.201343416.

Matthew H. Cato, Irene W. Yau, and Robert C. Rickert. Magnetic-based purification of untouched mouse germinal center B cells for ex vivo manipulation and biochemical analysis. *Nature Protocols*, 6(7):953–960, 2011. doi:10.1038/nprot.2011.344.

Tyani D. Chan, Katherine Wood, Jana R. Hermes, Danyal Butt, Christopher J. Jolly, Antony Basten, and Robert Brink. Elimination of germinal-center-derived self-reactive B cells is governed by the location and concentration of self-antigen. *Immunity*, 37(5):893–904, 2012. doi:10.1016/j.immuni.2012.07.017.

Dianyu Chen, Yan Wang, Godhev K. Manakkat Vijay, Shujie Fu, Colt W. Nash, Di Xu, Danyang He, Nathan Salomonis, Harinder Singh, and Heping Xu. Coupled analysis of transcriptome and BCR mutations reveals role of OXPHOS in affinity maturation. *Nature Immunology*, 22(7):904—-913, 2021. doi:10.1038/s41590-021-00936-y.

Spencer T. Chen, Thiago Y. Oliveira, Anna Gazumyan, Melissa Cipolla, and Michel C. Nussenzweig. B cell receptor signaling in germinal centers prolongs survival and primes B cells for selection. *Immunity*, 56(3):547–561.e7, 2023. doi:10.1016/j.immuni.2023.02.003.

Darya Chetverina, Maksim Erokhin, and Paul Schedl. GAGA factor: a multifunctional pioneering chromatin protein. *Cellular and Molecular Life Sciences*, 78(9):4125–4141, 2021. doi:10.1007/s00018-021-03776-z.

Weimin Ci, Jose M. Polo, Leandro Cerchietti, Rita Shaknovich, Ling Wang, Shao Ning Yang, Kenny Ye, Pedro Farinha, Douglas E Horsman, Randy D. Gascoyne, Olivier Elemento, and Ari Melnick. The BCL6 transcriptional program features repression of multiple oncogenes in primary B cells and is deregulated in DLBCL. *Blood*, 113(22):5536–5548, 2009. doi:10.1182/blood-2008-12-193037.

Marcus R. Clark, Malay Mandal, Kyoko Ochiai, and Harinder Singh. Orchestrating B cell lymphopoiesis through interplay of IL-7 receptor and pre-B cell receptor signalling. *Nature Reviews Immunology*, 14(2):69–80, 2014. doi:10.1038/nri3570.

Philip L. Cohen, Roberto Caricchio, Valsamma Abraham, Todd D. Camenisch, J. Charles Jennette, Robert A.S. Roubey, H. Shelton Earp, Glenn Matsushima, and Elizabeth A. Reap. Delayed apoptotic cell clearance and lupus-like autoimmunity in mice lacking the c-mer membrane tyrosine kinase. *The Journal of Experimental Medicine*, 196(1):135–140, 2002. doi:10.1084/jem.20012094.

Laura J. Conter, Eunice Song, Mark J. Shlomchik, and Mary M. Tomayko. CD73 expression is dynamically regulated in the germinal center and bone marrow plasma cells are diminished in its absence. *PLoS ONE*, 9(3):e92009, 2014. doi:10.1371/journal.pone.0092009.

A. Byron Cooper, Catherine M. Sawai, Ewa Sicinska, Sarah E. Powers, Piotr Sicinski, Marcus R. Clark, and Iannis Aifantis. A unique function for cyclin D3 in early B cell development. *Nature Immunology*, 7(5):489–497, 2006. doi:10.1038/ni1324.

Menno P. Creyghton, Albert W. Cheng, G. Grant Welstead, Tristan Kooistra, Bryce W. Carey, Eveline J. Steine, Jacob Hanna, Michael A. Lodato, Garrett M. Frampton, Phillip A. Sharp, Laurie A. Boyer, Richard A. Young, and Rudolf Jaenisch. Histone H3K27ac separates active from poised enhancers and predicts developmental state. *Proceedings of the National Academy of Sciences*, 107(50):21931–21936, 2010. doi:10.1073/pnas.1016071107.

Elizabeth E. Crouch, Zhiyu Li, Makiko Takizawa, Stefan Fichtner-Feigl, Polyxeni Gourzi, Carolina Montaño, Lionel Feigenbaum, Patrick Wilson, Siegfried Janz, F. Nina Papavasiliou, and Rafael Casellas. Regulation of AID expression in the immune response. *The Journal of Experimental Medicine*, 204(5):1145–1156, 2007. doi:10.1084/jem.20061952.

Jason G. Cyster and Christopher D.C. Allen. B cell responses: cell interaction dynamics and decisions. *Cell*, 177(3):524–540, 2019. doi:10.1016/j.cell.2019.03.016.

Hai-Qiang Dai, Hongli Hu, Jiangman Lou, Adam Yongxin Ye, Zhaoqing Ba, Xuefei Zhang, Yiwen Zhang, Lijuan Zhao, Hye Suk Yoon, Aimee M. Chapdelaine-Williams, Nia Kyritsis, Huan Chen, Kerstin Johnson, Sherry Lin, Andrea Conte, Rafael Casellas, Cheng-Sheng Lee, and Frederick W. Alt. Loop extrusion mediates physiological Igh locus contraction for RAG scanning. *Nature*, 590(7845):338–343, 2021. doi:10.1038/s41586-020-03121-7.

Iain F. Davidson and Jan-Michael Peters. Genome folding through loop extrusion by SMC complexes. *Nature Reviews Molecular Cell Biology*, 22(7):445–464, 2021. doi:10.1038/s41580-021-00349-7.

Iain F. Davidson, Benedikt Bauer, Daniela Goetz, Wen Tang, Gordana Wutz, and Jan-Michael Peters. DNA loop extrusion by human cohesin. *Science*, 366(6471):1338–1345, 2019. doi:10.1126/science.aaz3418.

Alexander L. Dent, Arthur L. Shaffer, Xin Yu, David Allman, and Louis M. Staudt. Control of inflammation, cytokine expression, and germinal center formation by BCL-6. *Science*, 276(5312):589–592, 1997. doi:10.1126/science.276.5312.589.

Ashley S. Doane, Chi-Shuen Chu, Dafne Campigli Di Giammartino, Martín A. Rivas, Johannes C. Hellmuth, Yanwen Jiang, Nevin Yusufova, Alicia Alonso, Robert G. Roeder, Effie Apostolou, Ari M. Melnick, and Olivier Elemento. OCT2 pre-positioning facilitates cell fate transition and chromatin architecture changes in humoral immunity. *Nature Immunology*, 22(10):1327–1340, 2021. doi:10.1038/s41590-021-01025-w.

Alexander Dobin, Carrie A. Davis, Felix Schlesinger, Jorg Drenkow, Chris Zaleski, Sonali Jha, Philippe Batut, Mark Chaisson, and Thomas R. Gingeras. STAR: ultrafast universal RNA-seq aligner. *Bioinformatics*, 29(1):15–21, 2013. doi:10.1093/bioinformatics/bts635.

David Dominguez-Sola, Gabriel D. Victora, Carol Y. Ying, Ryan T. Phan, Masumichi Saito, Michel C. Nussenzweig, and Riccardo Dalla-Favera. The proto-oncogene MYC is required for selection in the germinal center and cyclic reentry. *Nature Immunology*, 13(11):1083–1091, 2012. doi:10.1038/ni.2428.

Helen Dooley and Martin F. Flajnik. Shark immunity bites back: affinity maturation and memory response in the nurse shark, Ginglymostoma cirratum. *European Journal of Immunology*, 35(3):936–945, 2005. doi:10.1002/eji.200425760.

Helen Dooley, Robyn L. Stanfield, Rebecca A. Brady, and Martin F. Flajnik. First molecular and biochemical analysis of in vivo affinity maturation in an ectothermic vertebrate. *Proceedings of the National Academy of Sciences*, 103(6):1846–1851, 2006. doi:10.1073/pnas.0508341103.

Lihui Duan, Dan Liu, Hsin Chen, Michelle A. Mintz, Marissa Y. Chou, Dmitri I. Kotov, Ying Xu, Jinping An, Brian J. Laidlaw, and Jason G. Cyster. Follicular dendritic cells restrict interleukin-4 availability in germinal centers and foster memory B cell generation. *Immunity*, 54(10):2256–2272.e6, 2021. doi:10.1016/j.immuni.2021.08.028.

Katherine L. Dunn and James R. Davie. Stimulation of the Ras-MAPK pathway leads to independent phosphorylation of histone H3 on serine 10 and 28. *Oncogene*, 24(21):3492–3502, 2005. doi:10.1038/sj.onc.1208521.

Cihangir Duy, J. Jessica Yu, Rahul Nahar, Srividya Swaminathan, Soo-Mi Kweon, Jose M. Polo, Ester Valls, Lars Klemm, Seyedmehdi Shojaee, Leandro Cerchietti, Wolfgang Schuh, Hans-Martin Jäck, Christian Hurtz, Parham Ramezani-Rad, Sebastian Herzog, Hassan Jumaa, H. Phillip Koeffler, Ignacio Moreno de Alborán, Ari M. Melnick, B. Hilda Ye, and Markus Müschen. BCL6 is critical for the development of a diverse primary B cell repertoire. *Journal of Experimental Medicine*, 207(6):1209–1221, 2010. doi:10.1084/jem.20091299.

Jonatan Ersching, Alejo Efeyan, Luka Mesin, Johanne T. Jacobsen, Giulia Pasqual, Brian C. Grabiner, David Dominguez-Sola, David M. Sabatini, and Gabriel D. Victora. Germinal center selection and affinity maturation require dynamic regulation of mTORC1 kinase. *Immunity*, 46(6):1045–1058.e6, 2017. doi:10.1016/j.immuni.2017.06.005.

Panagis Filippakopoulos, Sarah Picaud, Maria Mangos, Tracy Keates, Jean-Philippe Lambert, Dalia Barsyte-Lovejoy, Ildiko Felletar, Rudolf Volkmer, Susanne Müller, Tony Pawson, Anne-Claude Gingras, Cheryl H. Arrowsmith, and Stefan Knapp. Histone recognition and large-scale structural analysis of the human bromodomain family. *Cell*, 149(1):214–231, 2012. doi:10.1016/j.cell.2012.02.013.

Shlomo Finkin, Harald Hartweger, Thiago Y. Oliveira, Ervin E. Kara, and Michel C. Nussenzweig. Protein amounts of the MYC transcription factor determine germinal center B cell division capacity. *Immunity*, 51(2):324–336.e5, 2019. doi:10.1016/j.immuni.2019.06.013.

Martin F. Flajnik. A cold-blooded view of adaptive immunity. *Nature Reviews Immunology*, 18(7):438–453, 2018. doi:10.1038/s41577-018-0003-9.

Nowlan H. Freese, David C. Norris, and Ann E. Loraine. Integrated genome browser: visual analytics platform for genomics. *Bioinformatics*, 32(14):2089–2095, 2016. doi:10.1093/bioinformatics/btw069.

Tetsuya Fukuda, Takehiko Yoshida, Seiji Okada, Masahiko Hatano, Tohru Miki, Kazuki Ishibashi, Shinichiro Okabe, Haruhiko Koseki, Shinsaku Hirosawa, Masaru Taniguchi, Nobuyuki Miyasaka, and Takeshi Tokuhisa. Disruption of the Bcl6 gene results in an impaired germinal center formation. *The Journal of Experimental Medicine*, 186(3):439–448, 1997. doi:10.1084/jem.186.3.439.

Sasha L. Fulton, Wendy Wenderski, Ashley E. Lepack, Andrew L. Eagle, Tomas Fanutza, Ryan M. Bastle, Aarthi Ramakrishnan, Emma C. Hays, Arianna Neal, Jaroslav Bendl, Lorna A. Farrelly, Amni Al-Kachak, Yang Lyu, Bulent Cetin, Jennifer C. Chan, Tina N. Tran, Rachael L. Neve, Randall J. Roper, Kristen J. Brennand, Panos Roussos, John C. Schimenti, Allyson K. Friedman, Li Shen, Robert D. Blitzer, Alfred J. Robison, Gerald R. Crabtree, and Ian Maze. Rescue of deficits by Brwd1 copy number restoration in the Ts65Dn mouse model of Down syndrome. *Nature Communications*, 13(1):6384, 2022. doi:10.1038/s41467-022-34200-0.

Alexander D. Gitlin, Ziv Shulman, and Michel C. Nussenzweig. Clonal selection in the germinal centre by regulated proliferation and hypermutation. *Nature*, 509(7502):637–640, 2014. doi:10.1038/nature13300.

Alexander D. Gitlin, Christian T. Mayer, Thiago Y. Oliveira, Ziv Shulman, Mathew J. K. Jones, Amnon Koren, and Michel C. Nussenzweig. T cell help controls the speed of the cell cycle in germinal center B cells. *Science*, 349(6248):643–646, 2015. doi:10.1126/science.aac4919.

Thomas Gligoris and Jan Löwe. Structural insights into ring formation of cohesin and related Smc complexes. *Trends in Cell Biology*, 26(9):680–693, 2016. doi:10.1016/j.tcb.2016.04.002.

Monica Gostissa, Julia M. Bianco, Daniel J. Malkin, Jeffery L. Kutok, Scott J. Rodig, Herbert C. Morse, Craig H. Bassing, and Frederick W. Alt. Conditional inactivation of p53 in mature B cells promotes generation of nongerminal center-derived B-cell lymphomas. *Proceedings of the National Academy of Sciences*, 110(8):2934–2939, 2013. doi:10.1073/pnas.1222570110.

Abigail K. Grootveld, Wunna Kyaw, Veera Panova, Angelica W.Y. Lau, Emily Ashwin, Guillaume Seuzaret, Rama Dhenni, Nayan Deger Bhattacharyya, Weng Hua Khoo, Maté Biro, Tanmay Mitra, Michael Meyer-Hermann, Patrick Bertolino, Masato Tanaka, David A. Hume, Peter I. Croucher, Robert Brink, Akira Nguyen, Oliver Bannard, and Tri Giang Phan. Apoptotic cell fragments locally activate tingible body macrophages in the germinal center. *Cell*, 186(6):1144–1161.e18, 2023. doi:10.1016/j.cell.2023.02.004.

Zuguang Gu, Lei Gu, Roland Eils, Matthias Schlesner, and Benedikt Brors. Circlize implements and enhances circular visualization in R. *Bioinformatics*, 30(19):2811–2812, 2014. doi:10.1093/bioinformatics/btu393.

Zuguang Gu, Roland Eils, and Matthias Schlesner. Complex heatmaps reveal patterns and correlations in multidimensional genomic data. *Bioinformatics*, 32(18):2847–2849, 2016. doi:10.1093/bioinformatics/btw313.

Neta Gurwicz, Liat Stoler-Barak, Niklas Schwan, Arnab Bandyopadhyay, Michael Meyer-Hermann, and Ziv Shulman. Tingible body macrophages arise from lymph node–resident precursors and uptake B cells by dendrites. *Journal of Experimental Medicine*, 220(4): e20222173, 2023. doi:10.1084/jem.20222173.

Jenna J. Guthmiller, Henry A. Utset, and Patrick C. Wilson. B cell responses against influenza viruses: short-lived humoral immunity against a life-long threat. *Viruses*, 13(6): 965, 2021. doi:10.3390/v13060965.

Judith H.I. Haarhuis, Robin H. van der Weide, Vincent A. Blomen, J. Omar Yáñez-Cuna, Mario Amendola, Marjon S. van Ruiten, Peter H.L. Krijger, Hans Teunissen, René H. Medema, Bas van Steensel, Thijn R. Brummelkamp, Elzo de Wit, and Benjamin D. Rowland. The cohesin release factor WAPL restricts chromatin loop extension. *Cell*, 169(4): 693–707.e14, 2017. doi:10.1016/j.cell.2017.04.013.

Katerina Hatzi, Huimin Geng, Ashley S. Doane, Cem Meydan, Reed LaRiviere, Mariano Cardenas, Cihangir Duy, Hao Shen, Maria Nieves Calvo Vidal, Timour Baslan, Helai P. Mohammad, Ryan G. Kruger, Rita Shaknovich, Ann M. Haberman, Giorgio Inghirami, Scott W. Lowe, and Ari M. Melnick. Histone demethylase LSD1 is required for germinal center formation and BCL6-driven lymphomagenesis. *Nature Immunology*, 20(1):86–96, 2019. doi:10.1038/s41590-018-0273-1.

Nathaniel D Heintzman, Rhona K Stuart, Gary Hon, Yutao Fu, Christina W Ching, R David Hawkins, Leah O Barrera, Sara Van Calcar, Chunxu Qu, Keith A Ching, Wei Wang, Zhiping Weng, Roland D Green, Gregory E Crawford, and Bing Ren. Distinct and predictive chromatin signatures of transcriptional promoters and enhancers in the human genome. *Nature Genetics*, 39(3):311–318, 2007. doi:10.1038/ng1966.

Sven Heinz, Christopher Benner, Nathanael Spann, Eric Bertolino, Yin C. Lin, Peter Laslo, Jason X. Cheng, Cornelis Murre, Harinder Singh, and Christopher K. Glass. Simple combinations of lineage-determining transcription factors prime cis-regulatory elements required for macrophage and B cell identities. *Molecular Cell*, 38(4):576–589, 2010. doi:10.1016/j.molcel.2010.05.004.

Nicole Heise and Ulf Klein. Somatic hypermutation and affinity maturation analysis using the 4-hydroxy-3-nitrophenyl-acetyl (NP) system. *Methods in Molecular Biology*, 1623: 191–208, 2017. doi:10.1007/978-1-4939-7095-7_16.

Sebastian Herzog, Michael Reth, and Hassan Jumaa. Regulation of B-cell proliferation and differentiation by pre-B-cell receptor signalling. *Nature Reviews Immunology*, 9(3):195–205, 2009. doi:10.1038/nri2491.

Louisa Hill, Anja Ebert, Markus Jaritz, Gordana Wutz, Kota Nagasaka, Hiromi Tagoh, Daniela Kostanova-Poliakova, Karina Schindler, Qiong Sun, Peter Bönelt, Maria Fischer, Jan-Michael Peters, and Meinrad Busslinger. Wapl repression by Pax5 promotes V gene recombination by Igh loop extrusion. *Nature*, 584(7819):142–147, 2020. doi:10.1038/s41586-020-2454-y.

Daniel J. Hodson, Arthur L. Shaffer, Wenming Xiao, George W. Wright, Roland Schmitz, James D. Phelan, Yandan Yang, Daniel E. Webster, Lixin Rui, Holger Kohlhammer, Masao Nakagawa, Thomas A. Waldmann, and Louis M. Staudt. Regulation of normal B-cell differentiation and malignant B-cell survival by OCT2. *Proceedings of the National Academy of Sciences*, 113(14):E2039–E2046, 2016. doi:10.1073/pnas.1600557113.

Antony B. Holmes, Clarissa Corinaldesi, Qiong Shen, Rahul Kumar, Nicolo Compagno, Zhong Wang, Mor Nitzan, Eli Grunstein, Laura Pasqualucci, Riccardo Dalla-Favera, and Katia Basso. Single-cell analysis of germinal-center B cells informs on lymphoma cell of origin and outcome. *Journal of Experimental Medicine*, 217(10):e20200483, 2020. doi:10.1084/jem.20200483.

Chuanxin Huang, David G. Gonzalez, Christine M. Cote, Yanwen Jiang, Katerina Hatzi, Matt Teater, Kezhi Dai, Timothy Hla, Ann M. Haberman, and Ari Melnick. The BCL6 RD2 domain governs commitment of activated B cells to form germinal centers. *Cell Reports*, 8(5):1497–1508, 2014. doi:10.1016/j.celrep.2014.07.059.

Takeshi Inoue, Ryo Shinnakasu, Chie Kawai, Wataru Ise, Eiryo Kawakami, Nicolas Sax, Toshihiko Oki, Toshio Kitamura, Kazuo Yamashita, Hidehiro Fukuyama, and Tomohiro Kurosaki. Exit from germinal center to become quiescent memory B cells depends on metabolic reprograming and provision of a survival signal. *Journal of Experimental Medicine*, 218(1):e20200866, 2020. doi:10.1084/jem.20200866.

Yanwen Jiang, Ana Ortega-Molina, Huimin Geng, Hsia-Yuan Ying, Katerina Hatzi, Sara Parsa, Dylan McNally, Ling Wang, Ashley S. Doane, Xabier Agirre, Matt Teater, Cem Meydan, Zhuoning Li, David Poloway, Shenqiu Wang, Daisuke Ennishi, David W. Scott, Kristy R. Stengel, Janice E. Kranz, Edward Holson, Sneh Sharma, James W. Young, Chi-Shuen Chu, Robert G. Roeder, Rita Shaknovich, Scott W. Hiebert, Randy D. Gascoyne, Wayne Tam, Olivier Elemento, Hans-Guido Wendel, and Ari M. Melnick. CREBBP inactivation promotes the development of HDAC3-dependent lymphomas. *Cancer Discovery*, 7(1):38–53, 2017. doi:10.1158/2159-8290.cd-16-0975.

Sonja E. Johnson, Nisha Shah, Angela Panoskaltsis-Mortari, and Tucker W. LeBien. Murine and human IL-7 activate STAT5 and induce proliferation of normal human pro-B cells. *The Journal of Immunology*, 175(11):7325–7331, 2005. doi:10.4049/jimmunol.175.11.7325.

Michael H. Kagey, Jamie J. Newman, Steve Bilodeau, Ye Zhan, David A. Orlando, Nynke L. van Berkum, Christopher C. Ebmeier, Jesse Goossens, Peter B. Rahl, Stuart S. Levine, Dylan J. Taatjes, Job Dekker, and Richard A. Young. Mediator and cohesin connect gene expression and chromatin architecture. *Nature*, 467(7314):430–435, 2010. doi:10.1038/nature09380.

Tomohiro Kaji, Akiko Ishige, Masaki Hikida, Junko Taka, Atsushi Hijikata, Masato Kubo, Takeshi Nagashima, Yoshimasa Takahashi, Tomohiro Kurosaki, Mariko Okada, Osamu Ohara, Klaus Rajewsky, and Toshitada Takemori. Distinct cellular pathways select germline-encoded and somatically mutated antibodies into immunological memory. *Journal of Experimental Medicine*, 209(11):2079–2097, 2012. doi:10.1084/jem.20120127.

Domenick E. Kennedy and Marcus R. Clark. Compartments and connections within the germinal center. *Frontiers in Immunology*, 12:659151, 2021. doi:10.3389/fimmu.2021.659151.

Domenick E. Kennedy, Michael K. Okoreeh, Mark Maienschein-Cline, Junting Ai, Margaret Veselits, Kaitlin C. McLean, Yogesh Dhungana, Hong Wang, Junmin Peng, Hongbo Chi, Malay Mandal, and Marcus R. Clark. Novel specialized cell state and spatial compartments within the germinal center. *Nature Immunology*, 21(6):660–670, 2020. doi:10.1038/s41590-020-0660-2.

Steven M. Kerfoot, Gur Yaari, Jaymin R. Patel, Kody L. Johnson, David G. Gonzalez, Steven H. Kleinstein, and Ann M. Haberman. Germinal center B cell and T follicular helper cell development initiates in the interfollicular zone. *Immunity*, 34(6):947–960, 2011. doi:10.1016/j.immuni.2011.03.024.

Laila El Khattabi, Haiyan Zhao, Jens Kalchschmidt, Natalie Young, Seolkyoung Jung, Peter Van Blerkom, Philippe Kieffer-Kwon, Kyong-Rim Kieffer-Kwon, Solji Park, Xiang Wang, Jordan Krebs, Subhash Tripathi, Noboru Sakabe, Débora R. Sobreira, Su-Chen Huang, Suhas S.P. Rao, Nathanael Pruett, Daniel Chauss, Erica Sadler, Andrea Lopez, Marcelo A. Nóbrega, Erez Lieberman Aiden, Francisco J. Asturias, and Rafael Casellas. A pliable Mediator acts as a functional rather than an architectural bridge between promoters and enhancers. *Cell*, 178(5):1145–1158.e20, 2019. doi:10.1016/j.cell.2019.07.011.

Kyong-Rim Kieffer-Kwon, Zhonghui Tang, Ewy Mathe, Jason Qian, Myong-Hee Sung, Guoliang Li, Wolfgang Resch, Songjoon Baek, Nathanael Pruett, Lars Grøntved, Laura Vian, Steevenson Nelson, Hossein Zare, Ofir Hakim, Deepak Reyon, Arito Yamane, Hirotaka Nakahashi, Alexander L. Kovalchuk, Jizhong Zou, J. Keith Joung, Vittorio Sartorelli, Chia-Lin Wei, Xiaoan Ruan, Gordon L. Hager, Yijun Ruan, and Rafael Casellas. Interactome maps of mouse gene regulatory domains reveal basic principles of transcriptional regulation. *Cell*, 155(7):1507–1520, 2013. doi:10.1016/j.cell.2013.11.039.

Hamish W. King, Nara Orban, John C. Riches, Andrew J. Clear, Gary Warnes, Sarah A. Teichmann, and Louisa K. James. Single-cell analysis of human B cell maturation predicts how antibody class switching shapes selection dynamics. *Science Immunology*, 6(56): eabe6291, 2021. doi:10.1126/sciimmunol.abe6291.

Masahiro Kitano, Saya Moriyama, Yoshikazu Ando, Masaki Hikida, Yasuo Mori, Tomohiro Kurosaki, and Takaharu Okada. Bcl6 protein expression shapes pre-germinal center B cell dynamics and follicular helper T cell heterogeneity. *Immunity*, 34(6):961–972, 2011. doi:10.1016/j.immuni.2011.03.025.

Kyongrim Kwon, Caroline Hutter, Qiong Sun, Ivan Bilic, César Cobaleda, Stephen Malin, and Meinrad Busslinger. Instructive role of the transcription factor E2A in early B lymphopoiesis and germinal center B cell development. *Immunity*, 28(6):751–762, 2008. doi:10.1016/j.immuni.2008.04.014.

Brian J. Laidlaw, Timothy H. Schmidt, Jesse A. Green, Christopher D.C. Allen, Takaharu Okada, and Jason G. Cyster. The Eph-related tyrosine kinase ligand Ephrin-B1 marks germinal center and memory precursor B cells. *The Journal of Experimental Medicine*, 214(3):639–649, 2017. doi:10.1084/jem.20161461.

Brian J. Laidlaw, Lihui Duan, Ying Xu, Sara E. Vazquez, and Jason G. Cyster. The transcription factor Hhex cooperates with the corepressor Tle3 to promote memory B cell development. *Nature Immunology*, 21(9):1082–1093, 2020. doi:10.1038/s41590-020-0713-6.

Robin D. Lee, Sarah A. Munro, Todd P. Knutson, Rebecca S. LaRue, Lynn M. Heltemes-Harris, and Michael A. Farrar. Single-cell analysis identifies dynamic gene expression networks that govern B cell development and transformation. *Nature Communications*, 12(1):6843, 2021. doi:10.1038/s41467-021-27232-5.

Fubin Li, Yi Yan, Joyce Pieretti, Danielle A. Feldman, and Laurel A. Eckhardt. Comparison of identical and functional Igh alleles reveals a nonessential role for Eμ in somatic hypermutation and class-switch recombination. *The Journal of Immunology*, 185(10):6049–6057, 2010. doi:10.4049/jimmunol.0902992.

Heng Li. Aligning sequence reads, clone sequences and assembly contigs with BWA-MEM. *arXiv*, 2013. URL `https://arxiv.org/abs/1303.3997`.

Yang Liao, Gordon K. Smyth, and Wei Shi. featureCounts: an efficient general purpose program for assigning sequence reads to genomic features. *Bioinformatics*, 30(7):923–930, 2014. doi:10.1093/bioinformatics/btt656.

Arthur Liberzon, Chet Birger, Helga Thorvaldsdóttir, Mahmoud Ghandi, Jill P. Mesirov, and Pablo Tamayo. The molecular signatures database hallmark gene set collection. *Cell Systems*, 1(6):417–425, 2015. doi:10.1016/j.cels.2015.12.004.

Dan Liu, Heping Xu, Changming Shih, Zurong Wan, Xiaopeng Ma, Weiwei Ma, Dan Luo, and Hai Qi. T–B-cell entanglement and ICOSL-driven feed-forward regulation of germinal centre reaction. *Nature*, 517(7533):214–218, 2015. doi:10.1038/nature13803.

Ning Qing Liu, Michela Maresca, Teun van den Brand, Luca Braccioli, Marijne M. G. A. Schijns, Hans Teunissen, Benoit G. Bruneau, Elphège P. Nora, and Elzo de Wit. WAPL

maintains a cohesin loading cycle to preserve cell-type-specific distal gene regulation. *Nature Genetics*, 53(1):100–109, 2021. doi:10.1038/s41588-020-00744-4.

Ziqi Long, Bethan Phillips, Daniel Radtke, Michael Meyer-Hermann, and Oliver Bannard. Competition for refueling rather than cyclic reentry initiation evident in germinal centers. *Science Immunology*, 7(69):eabm0775, 2022. doi:10.1126/sciimmunol.abm0775.

Wei Luo, Jessica Mayeux, Toni Gutierrez, Lisa Russell, Andrew Getahun, Jennifer Müller, Thomas Tedder, Jane Parnes, Robert Rickert, Lars Nitschke, John Cambier, Anne B. Satterthwaite, and Lee Ann Garrett-Sinha. A balance between B cell receptor and inhibitory receptor signaling controls plasma cell differentiation by maintaining optimal Ets1 levels. *The Journal of Immunology*, 193(2):909–920, 2014. doi:10.4049/jimmunol.1400666.

Heather E. Machado, Emily Mitchell, Nina F. Øbro, Kirsten Kübler, Megan Davies, Daniel Leongamornlert, Alyssa Cull, Francesco Maura, Mathijs A. Sanders, Alex T. J. Cagan, Craig McDonald, Miriam Belmonte, Mairi S. Shepherd, Felipe A. Vieira Braga, Robert J. Osborne, Krishnaa Mahbubani, Iñigo Martincorena, Elisa Laurenti, Anthony R. Green, Gad Getz, Paz Polak, Kourosh Saeb-Parsy, Daniel J. Hodson, David G. Kent, and Peter J. Campbell. Diverse mutational landscapes in human lymphocytes. *Nature*, 608(7924):724–732, 2022. doi:10.1038/s41586-022-05072-7.

Malay Mandal, Sarah E. Powers, Kyoko Ochiai, Katia Georgopoulos, Barbara L. Kee, Harinder Singh, and Marcus R. Clark. Ras orchestrates exit from the cell cycle and light-chain recombination during early B cell development. *Nature Immunology*, 10(10): 1110–1117, 2009. doi:10.1038/ni.1785.

Malay Mandal, Sarah E. Powers, Mark Maienschein-Cline, Elizabeth T. Bartom, Keith M. Hamel, Barbara L. Kee, Aaron R. Dinner, and Marcus R. Clark. Epigenetic repression of the Igk locus by STAT5-mediated recruitment of the histone methyltransferase Ezh2. *Nature Immunology*, 12(12):1212–1220, 2011. doi:10.1038/ni.2136.

Malay Mandal, Keith M. Hamel, Mark Maienschein-Cline, Azusa Tanaka, Grace Teng, Jigyasa H. Tuteja, Jeffrey J. Bunker, Neil Bahroos, John J. Eppig, David G. Schatz, and Marcus R. Clark. Histone reader BRWD1 targets and restricts recombination to the Igk locus. *Nature Immunology*, 16(10):1094–1103, 2015. doi:10.1038/ni.3249.

Malay Mandal, Mark Maienschein-Cline, Patrick Maffucci, Margaret Veselits, Domenick E. Kennedy, Kaitlin C. McLean, Michael K. Okoreeh, Sophiya Karki, Charlotte Cunningham-Rundles, and Marcus R. Clark. BRWD1 orchestrates epigenetic landscape of late B lymphopoiesis. *Nature Communications*, 9(1):3888, 2018. doi:10.1038/s41467-018-06165-6.

Malay Mandal, Michael K. Okoreeh, Domenick E. Kennedy, Mark Maienschein-Cline, Junting Ai, Kaitlin C. McLean, Natalya Kaverina, Margaret Veselits, Iannis Aifantis, Fotini Gounari, and Marcus R. Clark. CXCR4 signaling directs Igk recombination and the molecular mechanisms of late B lymphopoiesis. *Nature Immunology*, 20(10):1393–1403, 2019. doi:10.1038/s41590-019-0468-0.

Malay Mandal, Mark Maienschein-Cline, Yeguang Hu, Azam Mohsin, Margaret L. Veselits, Nathaniel E. Wright, Michael K. Okoreeh, Young me Yoon, Jacob Veselits, Katia Georgopoulos, and Marcus R. Clark. BRWD1 orchestrates small pre-B cell chromatin topology by converting static to dynamic cohesin. *Nature Immunology*, 25(1):129–141, 2024. doi:10.1038/s41590-023-01666-z.

Nimitha R. Mathew, Jayalal K. Jayanthan, Ilya V. Smirnov, Jonathan L. Robinson, Hannes Axelsson, Sravya S. Nakka, Aikaterini Emmanouilidi, Paulo Czarnewski, William T. Yewdell, Karin Schön, Cristina Lebrero-Fernández, Valentina Bernasconi, William Rodin, Ali M. Harandi, Nils Lycke, Nicholas Borcherding, Jonathan W. Yewdell, Victor Greiff, Mats Bemark, and Davide Angeletti. Single-cell BCR and transcriptome analysis after influenza infection reveals spatiotemporal dynamics of antigen-specific B cells. *Cell Reports*, 35(12):109286, 2021. doi:10.1016/j.celrep.2021.109286.

Hanover Matz and Helen Dooley. 450 million years in the making: mapping the evolutionary foundations of germinal centers. *Frontiers in Immunology*, 14:1245704, 2023. doi:10.3389/fimmu.2023.1245704.

Hanover Matz, Richard S. Taylor, Anthony K. Redmond, Thomas M. Hill, Rose Ruiz Daniels, Mariana Beltran, Neil C. Henderson, Daniel J. Macqueen, and Helen Dooley. Organized B cell sites in cartilaginous fishes reveal the evolutionary foundation of germinal centers. *Cell Reports*, 42(7):112664, 2023. doi:10.1016/j.celrep.2023.112664.

Christian T. Mayer, Anna Gazumyan, Ervin E. Kara, Alexander D. Gitlin, Jovana Golijanin, Charlotte Viant, Joy Pai, Thiago Y. Oliveira, Qiao Wang, Amelia Escolano, Max Medina-Ramirez, Rogier W. Sanders, and Michel C. Nussenzweig. The microanatomic segregation of selection by apoptosis in the germinal center. *Science*, 358(6360):eaao2602, 2017. doi:10.1126/science.aao2602.

Kaitlin C. McLean and Malay Mandal. It takes three receptors to raise a B cell. *Trends in Immunology*, 41(7):629–642, 2020. doi:10.1016/j.it.2020.05.003.

Julia Merkenschlager, Shlomo Finkin, Victor Ramos, Julian Kraft, Melissa Cipolla, Carla R. Nowosad, Harald Hartweger, Wenzhu Zhang, Paul Dominic B. Olinares, Anna Gazumyan, Thiago Y. Oliveira, Brian T. Chait, and Michel C. Nussenzweig. Dynamic regulation of TFH selection during the germinal centre reaction. *Nature*, 591(7850):458–463, 2021. doi:10.1038/s41586-021-03187-x.

Pierre Milpied, Iñaki Cervera-Marzal, Marie-Laure Mollichella, Bruno Tesson, Gabriel Brisou, Alexandra Traverse-Glehen, Gilles Salles, Lionel Spinelli, and Bertrand Nadel. Human germinal center transcriptional programs are de-synchronized in B cell lymphoma. *Nature Immunology*, 19(9):1013–1024, 2018. doi:10.1038/s41590-018-0181-4.

Javier M. Di Noia and Michael S. Neuberger. Molecular mechanisms of antibody somatic hypermutation. *Annual Review of Biochemistry*, 76(1):1–22, 2007. doi:10.1146/annurev.biochem.76.061705.090740.

Elphège P. Nora, Laura Caccianini, Geoffrey Fudenberg, Kevin So, Vasumathi Kameswaran, Abigail Nagle, Alec Uebersohn, Bassam Hajj, Agnès Le Saux, Antoine Coulon, Leonid A. Mirny, Katherine S. Pollard, Maxime Dahan, and Benoit G. Bruneau. Molecular basis of CTCF binding polarity in genome folding. *Nature Communications*, 11(1):5612, 2020. doi:10.1038/s41467-020-19283-x.

Kyoko Ochiai, Mark Maienschein-Cline, Giorgia Simonetti, Jianjun Chen, Rebecca Rosenthal, Robert Brink, Anita S. Chong, Ulf Klein, Aaron R. Dinner, Harinder Singh, and Roger Sciammas. Transcriptional regulation of germinal center B and plasma cell fates by dynamical control of IRF4. *Immunity*, 38(5):918–929, 2013. doi:10.1016/j.immuni.2013.04.009.

Takaharu Okada, Mark J. Miller, Ian Parker, Matthew F. Krummel, Margaret Neighbors, Suzanne B. Hartley, Anne O'Garra, Michael D. Cahalan, and Jason G. Cyster. Antigen-engaged B cells undergo chemotaxis toward the T zone and form motile conjugates with helper T cells. *PLoS Biology*, 3(6):e150, 2005. doi:10.1371/journal.pbio.0030150.

Michael K. Okoreeh, Domenick E. Kennedy, Akinola Olumide Emmanuel, Margaret Veselits, Azam Moshin, Robert H. Ladd, Steven Erickson, Kaitlin C. McLean, Brianna Madrigal, David Nemazee, Mark Maienschein-Cline, Malay Mandal, and Marcus R. Clark. Asymmetrical forward and reverse developmental trajectories determine molecular programs of B cell antigen receptor editing. *Science Immunology*, 7(74):eabm1664, 2022. doi:10.1126/sciimmunol.abm1664.

Ana Ortega-Molina, Isaac W. Boss, Andres Canela, Heng Pan, Yanwen Jiang, Chunying Zhao, Man Jiang, Deqing Hu, Xabier Agirre, Itamar Niesvizky, Ji-Eun Lee, Hua-Tang Chen, Daisuke Ennishi, David W. Scott, Anja Mottok, Christoffer Hother, Shichong Liu, Xing-Jun Cao, Wayne Tam, Rita Shaknovich, Benjamin A. Garcia, Randy D. Gascoyne, Kai Ge, Ali Shilatifard, Olivier Elemento, Andre Nussenzweig, Ari M. Melnick, and Hans-Guido Wendel. The histone lysine methyltransferase KMT2D sustains a gene expression program that represses B cell lymphoma development. *Nature Medicine*, 21(10):1199–1208, 2015. doi:10.1038/nm.3943.

Marius Pachitariu and Carsen Stringer. Cellpose 2.0: how to train your own model. *Nature Methods*, 19(12):1634–1641, 2022. doi:10.1038/s41592-022-01663-4.

Juhee Pae, Jonatan Ersching, Tiago B.R. Castro, Marta Schips, Luka Mesin, Samuel J. Allon, Jose Ordovas-Montanes, Coraline Mlynarczyk, Ari Melnick, Alejo Efeyan, Alex K. Shalek, Michael Meyer-Hermann, and Gabriel D. Victora. Cyclin D3 drives inertial cell cycling in dark zone germinal center B cells. *Journal of Experimental Medicine*, 218(4): e20201699, 2020. doi:10.1084/jem.20201699.

Zeev Pancer, Chris T. Amemiya, Götz R. A. Ehrhardt, Jill Ceitlin, G. Larry Gartland, and Max D. Cooper. Somatic diversification of variable lymphocyte receptors in the agnathan sea lamprey. *Nature*, 430(6996):174–180, 2004. doi:10.1038/nature02740.

Antonin Papin, Ethel Cesarman, and Ari Melnick. 3D chromosomal architecture in germinal center B cells and its alterations in lymphomagenesis. *Current Opinion in Genetics & Development*, 74:101915, 2022. doi:10.1016/j.gde.2022.101915.

Thomas Perlot, Frederick W. Alt, Craig H. Bassing, Heikyung Suh, and Eric Pinaud. Elucidation of IgH intronic enhancer functions via germ-line deletion. *Proceedings of the National Academy of Sciences*, 102(40):14362–14367, 2005. doi:10.1073/pnas.0507090102.

Douglas H. Phanstiel, Alan P. Boyle, Carlos L. Araya, and Michael P. Snyder. Sushi.R: flexible, quantitative and integrative genomic visualizations for publication-quality multi-panel figures. *Bioinformatics*, 30(19):2808–2810, 2014. doi:10.1093/bioinformatics/btu379.

Natalia B. Pikor, Urs Mörbe, Mechthild Lütge, Cristina Gil-Cruz, Christian Perez-Shibayama, Mario Novkovic, Hung-Wei Cheng, César Nombela-Arrieta, Takashi Nagasawa, Michelle A. Linterman, Lucas Onder, and Burkhard Ludewig. Remodeling of light and dark zone follicular dendritic cells governs germinal center responses. *Nature Immunology*, 21(6):649–659, 2020. doi:10.1038/s41590-020-0672-y.

Eric Pinaud, Ahmed Amine Khamlichi, Caroline Le Morvan, Mireille Drouet, Valérie Nalesso, Marc Le Bert, and Michel Cogné. Localization of the 3' IgH locus elements that effect long-distance regulation of class switch recombination. *Immunity*, 15(2):187–199, 2001. doi:10.1016/s1074-7613(01)00181-9.

Aaron R. Quinlan and Ira M. Hall. BEDTools: a flexible suite of utilities for comparing genomic features. *Bioinformatics*, 26(6):841–842, 2010. doi:10.1093/bioinformatics/btq033.

Alvaro Rada-Iglesias, Ruchi Bajpai, Tomek Swigut, Samantha A. Brugmann, Ryan A. Flynn, and Joanna Wysocka. A unique chromatin signature uncovers early developmental enhancers in humans. *Nature*, 470(7333):279–283, 2011. doi:10.1038/nature09692.

Ziaur S. M. Rahman. Impaired clearance of apoptotic cells in germinal centers: implications for loss of B cell tolerance and induction of autoimmunity. *Immunologic Research*, 51(2-3): 125–133, 2011. doi:10.1007/s12026-011-8248-4.

Parham Ramezani-Rad, Cindi Chen, Zilu Zhu, and Robert C. Rickert. Cyclin D3 governs clonal expansion of dark zone germinal Ccenter B cells. *Cell Reports*, 33(7):108403, 2020. doi:10.1016/j.celrep.2020.108403.

Martín A. Rivas, Cem Meydan, Christopher R. Chin, Matt F. Challman, Daleum Kim, Bhavneet Bhinder, Andreas Kloetgen, Aaron D. Viny, Matt R. Teater, Dylan R. McNally, Ashley S. Doane, Wendy Béguelin, María Teresa Calvo Fernández, Hao Shen, Xiang Wang, Ross L. Levine, Zhengming Chen, Aristotelis Tsirigos, Olivier Elemento, Christopher E. Mason, and Ari M. Melnick. Smc3 dosage regulates B cell transit through germinal centers and restricts their malignant transformation. *Nature Immunology*, 22(2):240–253, 2021. doi:10.1038/s41590-020-00827-8.

James T. Robinson, Douglass Turner, Neva C. Durand, Helga Thorvaldsdóttir, Jill P. Mesirov, and Erez Lieberman Aiden. Juicebox.js provides a cloud-based visualization system for Hi-C data. *Cell Systems*, 6(2):256–258.e1, 2018. doi:10.1016/j.cels.2018.01.001.

Marcus James Robinson, Zhoujie Ding, Catherine Pitt, Erica Janet Brodie, Isaak Quast, David Mathew Tarlinton, and Dimitra Zotos. The amount of BCL6 in B cells shortly after antigen engagement determines their representation in subsequent germinal centers. *Cell Reports*, 30(5):1530–1541.e4, 2020. doi:10.1016/j.celrep.2020.01.009.

Mark D. Robinson, Davis J. McCarthy, and Gordon K. Smyth. edgeR: a Bioconductor package for differential expression analysis of digital gene expression data. *Bioinformatics*, 26(1):139–140, 2010. doi:10.1093/bioinformatics/btp616.

Jonathan A. Roco, Luka Mesin, Sebastian C. Binder, Christian Nefzger, Paula Gonzalez-Figueroa, Pablo F. Canete, Julia Ellyard, Qian Shen, Philippe A. Robert, Jean Cappello, Harpreet Vohra, Yang Zhang, Carla R. Nowosad, Arien Schiepers, Lynn M. Corcoran, Kai-Michael Toellner, Jose M. Polo, Michael Meyer-Hermann, Gabriel Victora, and Carola G. Vinuesa. Class-switch recombination occurs infrequently in germinal centers. *Immunity*, 51(2):337–350.e7, 2019. doi:10.1016/j.immuni.2019.07.001.

Alexis Saintamand, Christelle Vincent-Fabert, Armand Garot, Pauline Rouaud, Zeliha Oruc, Virginie Magnone, Michel Cogné, and Yves Denizot. Deciphering the importance of the palindromic architecture of the immunoglobulin heavy-chain 3' regulatory region. *Nature Communications*, 7(1):10730, 2016. doi:10.1038/ncomms10730.

Johannes Schindelin, Ignacio Arganda-Carreras, Erwin Frise, Verena Kaynig, Mark Longair, Tobias Pietzsch, Stephan Preibisch, Curtis Rueden, Stephan Saalfeld, Benjamin Schmid, Jean-Yves Tinevez, Daniel James White, Volker Hartenstein, Kevin Eliceiri, Pavel Tomancak, and Albert Cardona. Fiji: an open-source platform for biological-image analysis. *Nature Methods*, 9(7):676–682, 2012. doi:10.1038/nmeth.2019.

Rona S. Scott, Eileen J. McMahon, Shannon M. Pop, Elizabeth A. Reap, Roberto Caricchio, Philip L. Cohen, H. Shelton Earp, and Glenn K. Matsushima. Phagocytosis and clearance of apoptotic cells is mediated by MER. *Nature*, 411(6834):207–211, 2001. doi:10.1038/35075603.

George Sharbeen, Christine W.Y. Yee, Adrian L. Smith, and Christopher J. Jolly. Ectopic restriction of DNA repair reveals that UNG2 excises AID-induced uracils predominantly or exclusively during G1 phase. *Journal of Experimental Medicine*, 209(5):965–974, 2012. doi:10.1084/jem.20112379.

Nilushi S. De Silva and Ulf Klein. Dynamics of B cells in germinal centres. *Nature Reviews Immunology*, 15(3):137–148, 2015. doi:10.1038/nri3804.

Mandeep Singh, Katherine J.L. Jackson, Jing J. Wang, Peter Schofield, Matt A. Field, David Koppstein, Timothy J. Peters, Deborah L. Burnett, Simone Rizzetto, Damien Nevoltris,

Etienne Masle-Farquhar, Megan L. Faulks, Amanda Russell, Divya Gokal, Asami Hanioka, Keisuke Horikawa, Alexander D. Colella, Timothy K. Chataway, James Blackburn, Tim R. Mercer, David B. Langley, D. Margaret Goodall, Roy Jefferis, Muralikrishna Gangadharan Komala, Anthony D. Kelleher, Dan Suan, Maureen Rischmueller, Daniel Christ, Robert Brink, Fabio Luciani, Tom P. Gordon, Christopher C. Goodnow, and Joanne H. Reed. Lymphoma driver mutations in the pathogenic evolution of an iconic human autoantibody. *Cell*, 180(5):878–894.e19, 2020. doi:10.1016/j.cell.2020.01.029.

Shuang Song, Chun Cao, Mohamed-Amin Choukrallah, Fengyuan Tang, Gerhard Christofori, Hubertus Kohler, Fabian Wu, Barna D. Fodor, Mathias Frederiksen, Simon N. Willis, Jacob T. Jackson, Stephen L. Nutt, Stefan Dirnhofer, Michael B. Stadler, and Patrick Matthias. OBF1 and Oct factors control the germinal center transcriptional program. *Blood*, 137(21):2920–2934, 2021. doi:10.1182/blood.2020010175.

John C. Stansfield, Kellen G. Cresswell, Vladimir I. Vladimirov, and Mikhail G. Dozmorov. HiCcompare: an R-package for joint normalization and comparison of HI-C datasets. *BMC Bioinformatics*, 19(1):279, 2018. doi:10.1186/s12859-018-2288-x.

Isabelle Stewart, Daniel Radtke, Bethan Phillips, Simon J. McGowan, and Oliver Bannard. Germinal center B cells replace their antigen receptors in dark zones and fail light zone entry when immunoglobulin gene mutations are damaging. *Immunity*, 49(3):477–489.e7, 2018. doi:10.1016/j.immuni.2018.08.025.

Dan Suan, Nike J. Kräutler, Jesper L.V. Maag, Danyal Butt, Katherine Bourne, Jana R. Hermes, Danielle T. Avery, Clara Young, Aaron Statham, Michael Elliott, Marcel E. Dinger, Antony Basten, Stuart G. Tangye, and Robert Brink. CCR6 defines memory B cell precursors in mouse and human germinal centers, revealing light-zone location and predominant low antigen affinity. *Immunity*, 47(6):1142–1153.e4, 2017. doi:10.1016/j.immuni.2017.11.022.

Aravind Subramanian, Pablo Tamayo, Vamsi K. Mootha, Sayan Mukherjee, Benjamin L. Ebert, Michael A. Gillette, Amanda Paulovich, Scott L. Pomeroy, Todd R. Golub, Eric S. Lander, and Jill P. Mesirov. Gene set enrichment analysis: A knowledge-based approach for interpreting genome-wide expression profiles. *Proceedings of the National Academy of Sciences*, 102(43):15545–15550, 2005. doi:10.1073/pnas.0506580102.

Alex Sunshine, David Goich, Alifa Stith, Katherine Sortino, Justin Dalton, Sarah Metcalfe, Eric C. Svensson, and Lee Ann Garrett-Sinha. Ets1 controls the development of B cell autoimmune responses in a cell-intrinsic manner. *ImmunoHorizons*, 3(7):331–340, 2019. doi:10.4049/immunohorizons.1900033.

Justin J. Taylor, Kathryn A. Pape, and Marc K. Jenkins. A germinal center–independent pathway generates unswitched memory B cells early in the primary response. *The Journal of Experimental Medicine*, 209(3):597–606, 2012. doi:10.1084/jem.20111696.

Michiel J. Thiecke, Gordana Wutz, Matthias Muhar, Wen Tang, Stephen Bevan, Valeriya Malysheva, Roman Stocsits, Tobias Neumann, Johannes Zuber, Peter Fraser, Stefan Schoenfelder, Jan-Michael Peters, and Mikhail Spivakov. Cohesin-dependent and -independent mechanisms mediate chromosomal contacts between promoters and enhancers. *Cell Reports*, 32(3):107929, 2020. doi:10.1016/j.celrep.2020.107929.

Laura Vian, Aleksandra Pękowska, Suhas S.P. Rao, Kyong-Rim Kieffer-Kwon, Seolkyoung Jung, Laura Baranello, Su-Chen Huang, Laila El Khattabi, Marei Dose, Nathanael Pruett, Adrian L. Sanborn, Andres Canela, Yaakov Maman, Anna Oksanen, Wolfgang Resch, Xingwang Li, Byoungkoo Lee, Alexander L. Kovalchuk, Zhonghui Tang, Steevenson Nelson, Michele Di Pierro, Ryan R. Cheng, Ido Machol, Brian Glenn St Hilaire, Neva C. Durand, Muhammad S. Shamim, Elena K. Stamenova, José N. Onuchic, Yijun Ruan, Andre Nussenzweig, David Levens, Erez Lieberman Aiden, and Rafael Casellas. The energetics and physiological impact of cohesin extrusion. *Cell*, 173(5):1165–1178.e20, 2018. doi:10.1016/j.cell.2018.03.072.

Charlotte Viant, Tobias Wirthmiller, Mohamed A. ElTanbouly, Spencer T. Chen, Melissa Cipolla, Victor Ramos, Thiago Y. Oliveira, Leonidas Stamatatos, and Michel C. Nussenzweig. Germinal center–dependent and –independent memory B cells produced throughout the immune response. *Journal of Experimental Medicine*, 218(8):e20202489, 2021. doi:10.1084/jem.20202489.

Gabriel D. Victora and Michel C. Nussenzweig. Germinal centers. *Annual Review of Immunology*, 40(1):413–442, 2022. doi:10.1146/annurev-immunol-120419-022408.

Roser Vilarrasa-Blasi, Paula Soler-Vila, Núria Verdaguer-Dot, Núria Russiñol, Marco Di Stefano, Vicente Chapaprieta, Guillem Clot, Irene Farabella, Pol Cuscó, Marta Kulis, Xabier Agirre, Felipe Prosper, Renée Beekman, Silvia Beà, Dolors Colomer, Hendrik G. Stunnenberg, Ivo Gut, Elias Campo, Marc A. Marti-Renom, and José Ignacio Martin-Subero. Dynamics of genome architecture and chromatin function during human B cell differentiation and neoplastic transformation. *Nature Communications*, 12(1):651, 2021. doi:10.1038/s41467-020-20849-y.

Christelle Vincent-Fabert, Remi Fiancette, Eric Pinaud, Véronique Truffinet, Nadine Cogné, Michel Cogné, and Yves Denizot. Genomic deletion of the whole IgH 3' regulatory region (hs3a, hs1,2, hs3b, and hs4) dramatically affects class switch recombination and Ig secretion to all isotypes. *Blood*, 116(11):1895–1898, 2010. doi:10.1182/blood-2010-01-264689.

Stéfan van der Walt, Johannes L Schönberger, Juan Nunez-Iglesias, François Boulogne, Joshua D Warner, Neil Yager, Emmanuelle Gouillart, Tony Yu, and scikit-image contributors. scikit-image: image processing in Python. *PeerJ*, 2:e453, 2014. doi:10.7717/peerj.453.

Qiao Wang, Kyong-Rim Kieffer-Kwon, Thiago Y. Oliveira, Christian T. Mayer, Kaihui Yao, Joy Pai, Zhen Cao, Marei Dose, Rafael Casellas, Mila Jankovic, Michel C. Nussenzweig,

and Davide F. Robbiani. The cell cycle restricts activation-induced cytidine deaminase activity to early G1. *The Journal of Experimental Medicine*, 214(1):49–58, 2017. doi:10.1084/jem.20161649.

Florian J. Weisel, Griselda V. Zuccarino-Catania, Maria Chikina, and Mark J. Shlomchik. A temporal switch in the germinal center determines differential output of memory B and plasma cells. *Immunity*, 44(1):116–130, 2016. doi:10.1016/j.immuni.2015.12.004.

Armin A. Weiser, Nicole Wittenbrink, Lei Zhang, Andrej I. Schmelzer, Atijeh Valai, and Michal Or-Guil. Affinity maturation of B cells involves not only a few but a whole spectrum of relevant mutations. *International Immunology*, 23(5):345–356, 2011. doi:10.1093/intimm/dxr018.

Simon N. Willis, Julie Tellier, Yang Liao, Stephanie Trezise, Amanda Light, Kristy O'Donnell, Lee Ann Garrett-Sinha, Wei Shi, David M. Tarlinton, and Stephen L. Nutt. Environmental sensing by mature B cells is controlled by the transcription factors PU.1 and SpiB. *Nature Communications*, 8(1):1426, 2017. doi:10.1038/s41467-017-01605-1.

Nathaniel E. Wright, Malay Mandal, and Marcus R. Clark. Molecular mechanisms insulating proliferation from genotoxic stress in B lymphocytes. *Trends in Immunology*, 44(9):668–677, 2023. doi:10.1016/j.it.2023.06.010.

Robert Wuerffel, Lili Wang, Fernando Grigera, John Manis, Erik Selsing, Thomas Perlot, Frederick W. Alt, Michel Cogne, Eric Pinaud, and Amy L. Kenter. S-S synapsis during class switch recombination is promoted by distantly located transcriptional elements and activation-induced deaminase. *Immunity*, 27(5):711–722, 2007. doi:10.1016/j.immuni.2007.09.007.

Heping Xu, Virendra K Chaudhri, Zhiguo Wu, Konstantinos Biliouris, Krista Dienger-Stambaugh, Yrina Rochman, and Harinder Singh. Regulation of bifurcating B cell trajectories by mutual antagonism between transcription factors IRF4 and IRF8. *Nature Immunology*, 16(12):1274–1281, 2015. doi:10.1038/ni.3287.

Nevin Yusufova, Andreas Kloetgen, Matt Teater, Adewola Osunsade, Jeannie M. Camarillo, Christopher R. Chin, Ashley S. Doane, Bryan J. Venters, Stephanie Portillo-Ledesma, Joseph Conway, Jude M. Phillip, Olivier Elemento, David W. Scott, Wendy Béguelin, Jonathan D. Licht, Neil L. Kelleher, Louis M. Staudt, Arthur I. Skoultchi, Michael-Christopher Keogh, Effie Apostolou, Christopher E. Mason, Marcin Imielinski, Tamar Schlick, Yael David, Aristotelis Tsirigos, C. David Allis, Alexey A. Soshnev, Ethel Cesarman, and Ari M. Melnick. Histone H1 loss drives lymphoma by disrupting 3D chromatin architecture. *Nature*, 589(7841):299–305, 2021. doi:10.1038/s41586-020-3017-y.

Jiyuan Zhang, David Dominguez-Sola, Shafinaz Hussein, Ji-Eun Lee, Antony B Holmes, Mukesh Bansal, Sofija Vlasevska, Tongwei Mo, Hongyan Tang, Katia Basso, Kai Ge, Riccardo Dalla-Favera, and Laura Pasqualucci. Disruption of KMT2D perturbs germinal center B cell development and promotes lymphomagenesis. *Nature Medicine*, 21(10):1190–1198, 2015. doi:10.1038/nm.3940.

Jiyuan Zhang, Sofija Vlasevska, Victoria A. Wells, Sarah Nataraj, Antony B. Holmes, Romain Duval, Stefanie N. Meyer, Tongwei Mo, Katia Basso, Paul K. Brindle, Shafinaz Hussein, Riccardo Dalla-Favera, and Laura Pasqualucci. The CREBBP acetyltransferase is a haploinsufficient tumor suppressor in B-cell lymphoma. *Cancer Discovery*, 7(3):322–337, 2017a. doi:10.1158/2159-8290.cd-16-1417.

Li Zhang, Taylor L. Reynolds, Xiaochuan Shan, and Stephen Desiderio. Coupling of V(D)J recombination to the cell cycle suppresses genomic instability and lymphoid tumorigenesis. *Immunity*, 34(2):163–174, 2011. doi:10.1016/j.immuni.2011.02.003.

Ting-ting Zhang, David G. Gonzalez, Christine M. Cote, Steven M. Kerfoot, Shaoli Deng, Yuqing Cheng, Masaki Magari, and Ann M. Haberman. Germinal center B cell development has distinctly regulated stages completed by disengagement from T cell help. *eLife*, 6:e19552, 2017b. doi:10.7554/elife.19552.

Xuefei Zhang, Yu Zhang, Zhaoqing Ba, Nia Kyritsis, Rafael Casellas, and Frederick W. Alt. Fundamental roles of chromatin loop extrusion in antibody class switching. *Nature*, 575 (7782):385–389, 2019a. doi:10.1038/s41586-019-1723-0.

Yong Zhang, Tao Liu, Clifford A. Meyer, Jérôme Eeckhoute, David S. Johnson, Bradley E. Bernstein, Chad Nusbaum, Richard M. Myers, Myles Brown, Wei Li, and X Shirley Liu. Model-based analysis of ChIP-seq (MACS). *Genome Biology*, 9(9):R137, 2008. doi:10.1186/gb-2008-9-9-r137.

Yu Zhang, Xuefei Zhang, Zhaoqing Ba, Zhuoyi Liang, Edward W. Dring, Hongli Hu, Jiangman Lou, Nia Kyritsis, Jeffrey Zurita, Muhammad S. Shamim, Aviva Presser Aiden, Erez Lieberman Aiden, and Frederick W. Alt. The fundamental role of chromatin loop extrusion in physiological V(D)J recombination. *Nature*, 573(7775):600–604, 2019b. doi:10.1038/s41586-019-1547-y.

Yu Zhang, Xuefei Zhang, Hai-Qiang Dai, Hongli Hu, and Frederick W. Alt. The role of chromatin loop extrusion in antibody diversification. *Nature Reviews Immunology*, 22(9): 550–566, 2022. doi:10.1038/s41577-022-00679-3.

Yingyao Zhou, Bin Zhou, Lars Pache, Max Chang, Alireza Hadj Khodabakhshi, Olga Tanaseichuk, Christopher Benner, and Sumit K. Chanda. Metascape provides a biologist-oriented resource for the analysis of systems-level datasets. *Nature Communications*, 10(1):1523, 2019. doi:10.1038/s41467-019-09234-6.

Dimitra Zotos, Isaak Quast, Connie S. N. Li-Wai-Suen, Craig I. McKenzie, Marcus J. Robinson, Andrey Kan, Gordon K. Smyth, Philip D. Hodgkin, and David M. Tarlinton. The concerted change in the distribution of cell cycle phases and zone composition in germinal centers is regulated by IL-21. *Nature Communications*, 12(1):7160, 2021. doi:10.1038/s41467-021-27477-0.

Griselda V. Zuccarino-Catania, Saheli Sadanand, Florian J. Weisel, Mary M. Tomayko, Hailong Meng, Steven H. Kleinstein, Kim L. Good-Jacobson, and Mark J. Shlomchik.

CD80 and PD-L2 define functionally distinct memory B cell subsets that are independent of antibody isotype. *Nature Immunology*, 15(7):631–637, 2014. doi:10.1038/ni.2914.